5-18-2015

# Laser scanning aggregates for real-time property identification

Andrew Branin

# LASER SCANNING AGGREGATES FOR REAL-TIME PROPERTY IDENTIFICATION

by
Andrew Matheson Branin

A Thesis

Submitted to the
Department of Civil Engineering
College of Engineering
In partial fulfillment of the requirements
For the degree of
Master of Science in Civil Engineering
at
Rowan University
April 17, 2015

Thesis Chair: Beena Sukumaran, Ph.D.

## Dedications

*I would like to dedicate this thesis to my grandparents; Jack Sr. and Ritva Ellen Branin, and James and Arlene Hughes.*

**Acknowledgements**

I would like to thank Dr. Beena Sukumaran; chair of the Rowan University Civil Engineering Department and my advisor, for the opportunity to work on this project, her continued support and advice, and for her unwavering desire to see her students and advisees succeed in both their education and professional careers. I would also like to thank Dr. Ravi Ramachandran from the Rowan University Electrical and Computer Engineering Department and Dr. Michael Lim from the Rowan University Physics Department for their time, support, and assistance in making this research possible.

I would like to thank my family and friends for their continuous support throughout this research. I would like to thank all of the undergraduate students who worked alongside me toward the completion of this research, and wish them all luck with future phases of this research and in all of their future endeavors. I would also like to extend a special thanks to Bless Ann Varghese for her continual support and assistance during the latter half of this research, and wish her luck with her future work with this project and with her graduate studies.

Finally, I would like to thank the New Jersey Department of Transportation for their continued support, assistance, and for the research grant which made this research possible. I would also like to thank the University Transportation Research Center (UTRC) for their support throughout this research.

## Abstract

Andrew Matheson Branin
LASER SCANNING AGGREGATES FOR REAL-TIME PROPERTY IDENTIFICATION
2014/15
Beena Sukumaran, Ph.D.
Master of Science in Civil Engineering

The strength of concrete and asphalt is provided by the aggregate stone within it, and as such maintaining a high standard for these materials is crucial in ensuring that these materials meet their projected design lives. One key factor to consider for an aggregate's long-term strength is its mineralogy, which can affect the strength and long-term performance of these materials. Conventional chemical testing techniques and petrographic examination methods presently exist which can be used to identify and/or quantify problematic minerals, however these tests are typically costly, time consuming, and/or require significant sample preparation and a controlled lab environment.

The purpose of this study is to develop a portable, reliable system to determine traits of aggregate stone in the field and compare the results to New Jersey state standards as a means of quality control. This research presently focuses on quantifying the chemical composition and mineralogy of aggregates, with focus on minerals such as mica and limestone which can cause rapid degradation of aggregate stone in asphalt and concrete. Chemical composition testing is performed via Laser-Induced Breakdown Spectroscopy (LIBS), which involves firing a laser pulse at a sample and predicting its composition based on the spectrum of light emitted by the resulting plasma. Predictive models are generated via Partial Least Squares Regression Analysis.

## Table of Contents

**Table of Contents (continued)**

**Table of Contents (continued)**

**Table of Contents (continued)**

**Table of Contents (continued)**

**Table of Contents (continued)**

## List of Figures

# Chapter 1

# Introduction

## 1.1 Problem Statement

Asphalt and concrete derive their strength from the aggregate stone within them. The mineralogy of aggregate stone is an important consideration; the presence of various types of minerals in the stone can have detrimental effects on the integrity and long term performance of the materials overall. Minerals such as mica in fine aggregate can make the material susceptible to weathering and weaken the binder, limestone can cause aggregates in asphalt surface course to polish smooth over time when exposed to water and wheel loads, reactive silica can cause damaging expansion of aggregate stone, and so forth. Various techniques are presently employed to test the composition of aggregate stone samples; however these methods have a number of shortcomings. Techniques such as titration and precipitate analyses require the use of potentially caustic chemicals, while techniques such as X-ray fluorescence and Electron Microprobe Analysis require significant testing periods and cumbersome equipment. Physical examinations of aggregates, such as petrographic examinations, are similarly time consuming. Most conventional techniques require significant sample preparation and a highly controlled lab environment, and so are generally unsuitable for testing in the field.

This research is intended to develop a system to determine aggregate traits such as aggregate mineralogy, in the field using laser scanning techniques. These tests can be conducted rapidly, in-situ, and with little to no sample preparation. Future phases of this

research will involve using various imaging techniques to determine aggregate morphology in the field.

### 1.2 Hypothesis

1. Laser-Induced Breakdown Spectroscopy (LIBS) can be used to rapidly and accurately analyze the composition of aggregate stone samples.
2. Partial Least Squares Regression Analysis (PLSR) can be used to develop accurate, quantitative models for predicting aggregate chemical composition, and these predictions can be used to determine aggregate traits such as mineralogy.
3. Other aggregate properties, such as predictions of outcomes of standard tests can be added to existing models with relative ease.
4. Such a system can be implemented for field use in a cost-, time-, and labor-effective way.

### 1.3 Significance of Research

The New Jersey Department of Transportation (NJDOT) and potentially other similar entities will benefit from the results of this study. While conventional testing techniques are reasonably reliable, they tend to require significant sample preparation, and utilize fixed equipment and/or miscellaneous, non-reusable supplies. The development of a reliable, portable system for analyzing aggregate chemical and morphological traits will provide an alternative to conventional testing techniques, and will allow testing to be conducted more easily in the field. By improving the speed and versatility of such testing, state standards for aggregate quality can be more easily enforced, with reduced impact on construction timelines. As standards will be easier to

maintain, New Jersey roadways will be less likely to experience premature failure due to aggregate deterioration; helping to reduce unnecessary expenditures and to improve driver safety. The results and associated techniques used in this research can also easily be applied by other entities for similar applications, thus benefitting other regions.

### 1.4 Study Objectives

This study will focus on the development of an alternative means of in-situ quality control for aggregate stone through the use of laser analysis; namely through a technique called Laser-Induced Breakdown Spectroscopy. The primary objectives of this study are as follows:

- Laser-Induced Breakdown Spectroscopy is utilized to obtain characteristic data sets from a variety of aggregate stone samples, which are used to develop predictive models for aggregate chemical composition through a linear analysis technique known as Partial Least Squares Regression Analysis.
- The accuracy of each model's predictions is determined by comparing them to the results of X-ray Fluorescence testing on similar aggregate samples, and the optimal model calibration strategy is selected.
- Detrimental minerals will be identified and quantified based on the predicted chemical compositions (this will be completed in a future phase of this research).
- Models are adjusted to be effective when utilizing a portable LIBS system and/or commercially available systems, if necessary, so as to make the finished product more versatile and compatible with varying system hardware (this step will be completed once a field setup has been completed).

- User-friendly software is developed and a standardized, streamlined testing and analysis procedure is developed.

## 1.5 Research Approach

This section will provide an overview of the research process used to achieve the above goals. This research included a thorough review of past work and literature and selection of a testing and analysis method, followed by collection of data via LIBS, the development of predictive models, and analysis of model performance.

**1.5.1 Literature review.** Background information into various detrimental minerals of concern to the NJDOT were reviewed during the literature review stage, along with conventional methods for measuring chemical and mineralogical traits of aggregate stone. The Laser-Induced Breakdown Spectroscopy technique and applications were also researched, with particular emphasis on previous applications involving the identification and quantification of aggregate stone traits. Various methods for developing predictive models using LIBS data were then considered. As Partial Least Squares Regression Analysis was eventually selected, this technique was reviewed in greater detail. The overall goals of the literature review were to:

1. Understand the negative effects of detrimental minerals and the present need for a portable system to detect and quantify them.
2. Understand the concept of Laser-Induced Breakdown Spectroscopy as a testing methodology and examine the range of possible applications for this technique.
3. Evaluate the effectiveness of using LIBS for geological applications.

4. Consider various data analysis methods for developing predictive models from data collected via LIBS, and evaluate the effectiveness of each.

**1.5.2 Data acquisition.** Unique data sets; namely light spectra, corresponding to each type of aggregate stone in this study were collected via Laser-Induced Breakdown Spectroscopy. Each of these output spectra represents the sum of the emissions of all elemental components of the stone sample. The composition of each type of stone was be determined via X-Ray Fluorescence Spectrometry (XRF) to provide a set of known data for model calibration.

**1.5.3 Model development.**

***1.5.3.1 Model generation.*** The information obtained through the literature review and the data collected via LIBS and XRF analyses made it possible to generate a predictive model. Various models were developed via PLSR and using varying data pre-processing methods, including but not limited to: center clipping, spectral normalization, spectral amplitude adjustments, baseline subtraction and noise cancellation, and so forth.

***1.5.3.2 Model validation.*** The accuracy and reliability of predictive models were determined by comparing the predicted chemical composition obtained via the developed models to the corresponding results of XRF testing. The overall deviation from the accepted ‘true’ values obtained via XRF analyses was determined, and the optimal pre-processing strategy was selected based on which method produced the least deviatory model while maintaining reasonable reproducibility.

**1.5.4 Results analysis.** Once the optimal calibration strategy and predictive model had been selected, LIBS tests were performed on aggregate samples which were not used in the model calibration. XRF testing was then performed on these same samples, and the results compared to the composition predicted by each model. A useable range of samples was determined, and additional samples may be obtained to further calibrate the model in the event that the present model is not sufficiently versatile for its intended use.

## 1.6 Thesis Structure

The collected information and results described above are detailed in the next several chapters. Chapter 2 of this thesis consists of a comprehensive literature review and background pertaining to this research. The purpose of this chapter is to provide sufficient background knowledge for one to understand the research herein. The chapter begins with a review of several detrimental minerals which may be found in aggregate stone, and the negative effects each has on the stone or aggregate-binder mixture. Next, the chapter will include a brief overview of several conventional methods for quantifying aggregate stone traits, including their strengths and shortcomings. The chapter will then review the concept of Laser-Induced Breakdown Spectroscopy, and why this method shows promise as a means of aggregate quality control. Finally, this chapter will provide an overview of various data analysis methods for generating a predictive model based on the results of LIBS testing.

Next, Chapter 3 will outline the experimental setups and methods employed to collect data and to produce predictive models and compare predictions to accepted

values. Chapter 4 discusses the results of each set of model calibration and testing, the optimization of the predictive model calibration strategy, and discusses the feasibility of using such a model and technique as a means of quality control. Chapter 5 will discuss all conclusions which can be drawn from this research, and makes recommendations for further development and/or improvement of such methods and models.

# Chapter 2

# Literature Review

## 2.1 Aggregate Mineralogy

While a number of factors affect the performance of asphalt and concrete pavements, a major component of the material's integrity and durability is the quality of aggregate stone used in it. The aggregate stone provides the strength of the material and the bulk of the friction present on a road surface. As such, maintaining a high quality standard for this component is of high priority. Aggregate performance is linked to such factors as particle size and shape; collectively the morphology, and factors such as overall strength and durability, which are partially related to the mineralogical composition of the stone. This research focuses on maintaining high standards of aggregate mineralogy via rapid in-situ chemical analyses, while a future phase of the project will focus on performing in-situ analyses of aggregate morphology. The following section reviews several mineralogical features which should be considered. As this research was done on behalf of the New Jersey Department of Transportation (NJDOT), the following sections are primarily concerned with controls set in place by NJDOT, however many of the principles used in this research can be easily applied to similar applications.

## 2.2 Detrimental Minerals in Aggregate Stone

The New Jersey Department of Transportation imposes limits pertaining to the mineralogical qualities of aggregate stone to be used in asphalt and concrete applications. While this is primarily intended for roadway quality control, the presence of most of these qualities can be detrimental in any aggregate-binder mixture. Some studies suggest

that aggregate mineralogical deficiencies may actually have a larger effect on cement concrete mixes than asphalt mixes [1]. The mineralogical qualities monitored by the New Jersey Department of Transportation are listed below.

**2.2.1 Limestone/carbonate rock and acid soluble material.** Carbonate rocks (aka calcareous rocks); or stone containing more than trace amounts of calcium carbonate, such as calcite or dolomite which form in limestones [1], are not to be used in surface course for Hot Mix Asphalt (HMA) roadways, except in shoulder areas, parking areas, or driveways, in the state of New Jersey [2]. The LA abrasion test for softer carbonate rocks such as some limestones can result in 60% or more passing the #12 sieve following a test; demonstrating the rock's innate weakness to friction and abrasion. While these rocks often perform well in field applications despite this, this tendency can cause a large amount of dust to form in the aggregate blend during aggregate processing, which can become a secondary detriment to HMA performance by increasing the dust to binder ratio (see Section 2.2.3 for a more detailed description of this effect and its implications) [1].

Because of this weakness to abrasion, these carbonate rocks tend to polish and become smooth over time when subjected to weathering and wheel loads, causing a loss of skid resistance on the roadway's surface and potential loss of inter-aggregate friction; presenting a safety hazard and weakness in the roadway. While a variety of testing methods, such as the acid insoluble residue test (ASTM D3042), polishing tests (ASTM D3319 or E660 and E303), or petrographic examinations (ASTM C295), are used to identify these rocks and quantify or predict the likelihood of polishing in such rocks, it is a significant consideration to most highways agencies [1]. Diringer's 1990 study found

that substantial variability in polishing resistance can be found in limestone and carbonate aggregates [3]. For this reason, a conservative roadway design should not include limestone or carbonate rock in the wearing surface, and it is therefore important to be able to identify carbonate rocks, which can be estimated based on a stone's calcium content.

While no required standard is explicitly stated in the NJDOT requirements, in most applications, one should make an effort to minimize the amount of Acid Soluble Material (ASM) in fine aggregate, particularly in surface course for roadways. Acid Soluble Material, such as limestone, is the material in an aggregate sample which is dissolved when placed in a hot hydrochloric acid solution, while Acid Insoluble Residue (AIR), such as grains of quartz and mica, are not dissolved. Fine aggregates low in ASM are less subject to weathering effects and experience less damage due to exposure to acidic rain. Materials high in ASM are conversely more likely to wear due to weathering and polish smooth [4]. Aggregates with high ASM are typically carbonate rocks, which should not be used in surface course regardless, as previously noted.

**2.2.2 Mica.** Mica is a brittle, sheet-like mineral containing weak shear planes. The mica content of an aggregate blend in New Jersey is limited to no more than 2% weight in fine aggregate, as determined by standard NJDOT testing method A-2 [2]. While a mechanically weak mineral, mica particles are commonly found as fines released as rock such as granite is crushed, and the shear planes themselves are therefore not the major source of deterioration, though the brittleness of the material causes a larger representation in the fine fraction [5]. Rather, the specific surface area of these fine particles and the presence of intra-crystalline cavities in the particles cause the mineral to

be highly absorptive, which can increase a road's susceptibility to frost weathering in both bound and unbound layers. This effect in turn causes the roadways to deteriorate more rapidly [6]. Previous research has determined that the detrimental effects of mica in the fine fraction become most evident around 2.5% by weight, or 30-35% by volume, beyond which it will have significant detrimental effects on various aggregate blend properties, and on the tensile strength of the pavement, partly due to the increase in the dust to asphalt ratio. Fine mica particles were also found to prefer to orient themselves around course aggregates, likely due to the typical method of compaction, which further promotes issues pertaining to the mineral's adsorptive properties [5]. For these reasons, it is important for a system to be able to detect mica in coarse or fine aggregate and fines, and ideally determine when measures should be taken to remove such material from an aggregate stockpile.

**2.2.3 Clay content/deleterious materials.** Clay and clay lumps are limited to no more than 5% by weight, as determined via AASHTO method T88 [2], although this is above average. Clay materials and other fines form a coating on the surface of aggregate stones which prevent binder material from properly adhering to it, resulting in spalling, raveling, stripping, and general weakness in a roadway. Excess clay can also reduce the drainage characteristics of unbound base or sub-base layers due to its absorptive and expansive behavior [7]. Additionally, clay lumps surviving HMA material processing may cause pitting and surface deterioration to rapidly form over the roadway's lifetime, as clay lumps near the surface break down as they are exposed to rolling and wheel loadings [1]. Excessive clay in a mixture can also increase the dust-to-binder ratio of an HMA mixture, resulting in an unintentionally stiff asphalt pavement. While a

certain dust-to-binder ratio (typically 0.6 to 1.6 by weight depending on the case) is desirable to stiffen the binder so as to improve permanent deformation resistance, the presence of larger quantities of clay or other deleterious, absorptive materials result in excessive loss of pavement ductility, causing it to be more prone to cracking, particularly at low temperatures [8]. For these reasons, it is important to consider the amount of deleterious material in an aggregate blend. While LIBS; the testing method used herein, is not exceptionally well suited to quantifying the amount of deleterious material in an aggregate blend, it can be used to detect such materials as a surface contaminant on aggregate samples. A future phase of this project will partially consider an alternate means of quantifying the amount of fines in an aggregate blend.

**2.2.4 Expansive quartz.** Poorly crystalized, porous, and less dense species of quartz, such as volcanic glass, cristobalite, or opal, are more permeable than other, more dense varieties of silica to alkaline hydroxide solutions that form in Portland Cement Concrete (PCC), and are therefore more susceptible to experiencing alkali-silica reactions. The solubility of amorphous silica increases rapidly in highly basic environments, causing such reactions, which produce expansive silica gels on and in the aggregates in which expansive minerals are found, which will in turn induce stresses in concrete media, leading to cracking of binder and aggregate fracturing, and causing deterioration of the materials over time [9]. While less of a concern in asphalt mixtures given its less rigid binder, this factor should still be considered. Unfortunately, while structurally distinct, amorphous silica is chemically identical to better crystalized species, and so one would intuitively not expect it to produce distinct spectral patterns during LIBS testing. This stated, the varying structure may allow amorphous silica to ablate

more or less readily than crystalline silica during LIBS testing, and may result in varying intensities of light emission corresponding to siliceous compounds, or these materials may actually produce distinct spectral patterns due to chemical matrix effects (see Section 2.5.1.7). While this hypothesis is not explored in this research, previous work using LIBS by the Texas Department of Transportation suggests that it is possible to use LIBS models to effectively quantify amorphous silicates in aggregate stone (see Section 2.4.7.3) [10].

## 2.3 Chemical Analyses of Geological Materials

Before a method can be developed for determining the chemical composition of, and eventually the presence and quantity of detrimental minerals in aggregates, one must first consider the methods currently employed to chemically analyze stone samples. Once a reliable technique for quantifying the chemical composition of a stone has been selected, one can interpret the results so as to determine or predict the presence and quantity of target minerals.

**2.3.1 Traditional chemical analysis methods.** A number of methods presently exist for quantifying the chemical composition of stone samples. The most commonly used methods include, but are not limited to, wet chemical analyses, Inductively Coupled Plasma Mass Spectrometry (ICP-MS), X-Ray Fluorescence Spectrometry (XRF), and Electron Microprobe Analysis (EMPA) [11].

***2.3.1.1 Wet chemical analyses.*** Wet chemical analyses involve dissolving a powdered sample in an acid solution, and include gravimetric, volumetric, and colorimetric analyses. In gravimetric analyses, a sample's composition is determined by

inducing a chemical reaction in the solution and measuring the mass of a precipitate produced. Volumetric analyses involve using titration to determine the amount of a chemical component based on the amount of another chemical which must be added for the solution to react to completion. Colorimetric analyses involve making inferences about a sample's composition based on changes in solution color following a chemical reaction [11]. Each of these methods requires significant sample preparation, testing time, and non-reusable reactants, and are inconvenient for field use.

***2.3.1.2 Inductively coupled plasma mass spectrometry (ICP-MS).*** Inductively-coupled plasma-mass spectrometry involves injecting an aerosolized sample into Argon plasma to break the dissolved sample into separate ions, which are then extracted into a mass spectrometer in a vacuum, which separates the particles according to their mass to charge ratio. The results are determined relative to standard solutions with known concentrations. Alternatively, a small portion of the sample material may be ablated via laser before injecting it into the Argon plasma [12]. Regardless, this type of analysis involves significant testing time and sample preparation, and requires equipment which cannot be easily used in the field.

***2.3.1.3 X-ray fluorescence spectrometry (XRF).*** X-ray fluorescence spectrometry (XRF) is often used in the analysis of stone samples, but typically involves testing on a compressed or vitrified, powdered sample in solid form [11]. This analysis is performed by focusing an incident X-ray beam at a sample to induce dissociation of inner shell electrons. As outer shell electrons drop to the inner shell, X-rays of characteristic wavelengths are emitted and collected by a variety of sensors [13]. The intensities of a given emission wavelength can be correlated to concentrations; however a large number

of separate standards are required to determine and account for all of the interfering effects [11]. While generally not suitable for field use due to required sample preparation, testing time, and cumbersome equipment, this type of analysis generally produces accurate, reproducible results, and as such was used during the course of this research to determine ground truth chemical compositions of aggregate stone samples for use in calibrating predictive models. These analyses were almost exclusively conducted by the NJDOT, which uses this method as their primary chemical analysis technique for aggregate stone. An overview of the XRF testing procedure is provided in Chapter 3.

***2.3.1.4 Electron microprobe analysis (EMPA).*** Electron Microprobe Analysis operates on the same principle as X-ray fluorescence, but uses a focused electron beam rather than X-rays to induce electron dissociation, considers emitted electrons as well as X-rays, and requires different sample preparation. Electron Microprobe analysis is generally used for very small points on samples, rather than a broad sample area [14]. While this method also tends to produce accurate results, it may be less useful for samples with non-uniform composition, requires significant sample preparation, testing time, and bulky equipment, and is therefore not suitable for field use.

**2.3.2 Laser-Induced Breakdown Spectroscopy (LIBS).** An alternative testing method to those discussed above is Laser-Induced Breakdown Spectroscopy (LIBS); which uses pulses of focused light to induce fluorescence in the visible light range of wavelengths which can then be used to determine a sample's composition. This research utilized this technique to develop a versatile, portable system capable of measuring the chemical composition of aggregate stone rapidly in the field, thereby overcoming the common limitations of conventional testing methods. While this technology does not

intend to replace traditional testing methods outright, it is intended to be utilized to obtain reasonably accurate estimates of aggregate properties as a means of in-situ quality control. However, developing a predictive model for such a system required reliable, accepted data from a variety of samples. Such 'known' data on stone composition was provided by the New Jersey Department of Transportation (NJDOT), and was obtained via XRF analysis of several types of stone obtained from a variety of quarries and sources in New Jersey and surrounding areas.

Laser-Induced Breakdown Spectroscopy (LIBS) was used to conduct all experiments performed during the course of this research. LIBS is a laser analysis technique wherein a high energy laser is fired at a sample; in this case a sample of aggregate stone. This focused light strikes the sample, ablating some of the material, rapidly heating some of the matter and exciting the particles, breaking the compounds into individual atoms. These atoms are rapidly ionized by the energy in the laser pulse; forming a small plume of plasma wherein all elements and ion species emit photons of characteristic wavelengths, which can be collected and used to infer the sample's composition [15]. Studies have shown that LIBS can be used to obtain rapid, complete results, and portable LIBS systems are now commercially available [16]. However, while these commercially available systems are capable of qualitatively identifying elements, and in some cases performing rough quantitative analyses on simple samples, application-specific models must be developed for more accurate quantitative analyses, or for predicting sample traits other than chemical composition [17].

***2.3.2.1 Laser emission.*** Any test using LIBS begins when a pulse laser is fired. Upon being activated, an ultraviolet flash lamp, excites the particles in the gain medium, which in this case is a $Nd^{+}$ doped Yttrium Aluminum Garnet rod (a Nd:YAG crystal). Stimulated emission then occurs in the gain medium, wherein a photon spontaneously emitted as an excited particle returns to a lower energy state can stimulate other excited particles to emit identical photons in the same direction as similar light passes through the gain medium. Light emitted reflects between a mirror and a second partially reflecting mirror to continue stimulated emission while allowing a portion of light to be emitted as a beam of light [18]. Some lasers, such as the one used throughout testing, utilize a Q-Switch; or Quality Switch. A laser's Q-Switch blocks light emitted by the gain medium for a set period of time after some trigger, such as when the flash lamp emits a burst of ultraviolet light, preventing light from reaching the partial mirror. This allows energy to build up in the gain medium to a maximum amount until the gain medium is said to be saturated, and energy begins to dissipate due to spontaneous emission of photons. Stimulated emission does not occur to the degree observed in a non-Q-Switched laser because this phenomenon is partially dependent on light re-entering the gain medium. With correct timing, allowing light to pass as the gain medium is saturated allows for a more intense, shorter laser pulse, however this device may also be used with a longer delay to allow energy to dissipate prior to laser emission; reducing the laser pulse energy, as is done throughout this research [19]. A simple diagram of a Q-Switched laser is shown in Figure 2.1 below.

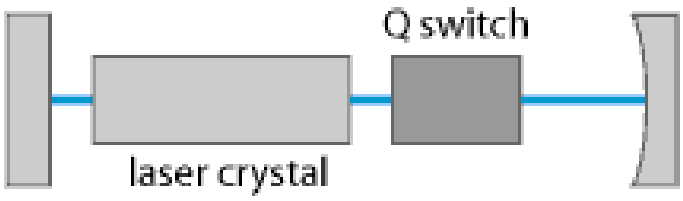


*Figure 2.1.* Laser Schematic [20]

***2.3.2.2 Sample ablation and light collection.*** The light emitted by the laser is then directed onto a sample. The focused light energy ablates some of the matter, vaporizing and exciting the then dissociated elements. Over the course of several microseconds, this energy dissipates, and electrons recombine with positive ions and return to lower energy states. As electrons return to lower energy states, photons in the visible range of wavelengths characteristic to the atom or ion species are emitted. This emitted light can be sampled and separated via an optical spectrometer into a set of intensities of light emitted at various wavelengths within an observed range, to form a resultant light spectrum. Such a light spectrum is composed of the sum of the light emitted from a sample; representing all components in the sample, assuming that the range of wavelengths observed is sufficiently broad. Light is sampled a set period of time after the Q-Switch allows the laser to emit light. If this spectrometer delay is not sufficient, light emitted by the laser itself may be represented in the collected light spectrum, and a large proportion of the collected light will be from ion species, while if the delay is excessive, the plasma plume may have cooled such that very little light can be collected. It is therefore important to determine an appropriate spectrometer delay time for the application in question [15]. As the spectrometer used throughout this research was not sensitive to the emitted 1064 nm wavelength, light from the laser pulse was not a

concern. Light emitted by an ablated sample decreases rapidly over time, as shown in Figure 2.2 below, and as such accurate timing is very important for obtaining accurate results.

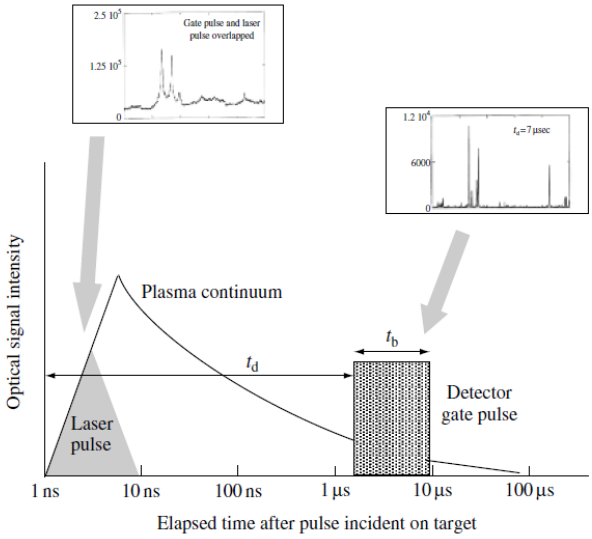


*Figure 2.2.* Energy Graph [15]

The resulting light spectrum can be considered to be analogous to a ‘fingerprint’ for the sample in question; providing a set of peaks and light intensities unique to the sample. The relative quantities of each element can be determined based on the intensities of light at each wavelength, as well as the distribution of neutral atoms and ion species, as determined by various parameters unique to each element, such as the ease of which an element will ionize and the rate at which it will re-accept electrons once ionized [21]. As modeling and predictions throughout this research were based on pattern recognition

techniques and known samples, the distribution of ions and neutral particles was not considered.

## 2.4 Previous Applications of LIBS

Laser-Induced Breakdown Spectroscopy has been successfully applied in a variety of fields. A series of previous applications of LIBS are briefly described in the following sections. Note that LIBS is a very versatile technique and this list should not be considered to be exhaustive.

**2.4.1 Analysis of metals.** LIBS is often used to analyze metal alloys, such as steel alloys. Various studies have shown that trace elements can be accurately quantified using LIBS, but some have shown that using a double or even triple laser pulse configurations (see Section 2.5.2.1) may be useful in identifying and quantifying more trace components. Studies have also shown that the Limit of Detection of trace elements can be improved by applying inter-elemental corrections to account for chemical matrix effects caused by the original chemical structure (see Section 2.5.1.7). Some studies achieved a limit of detection of a few parts per million, or even less [22].

**2.4.2 Environmental applications.** LIBS has been employed as a means to analyze soil and water contamination, and to observe contamination seepage patterns. Due to the varied testing mediums, chemical matrix effects (see Section 2.5.1.7) presented a source of interference in making accurate measurements of contaminants, however by using various internal standards and alternate calibration techniques, model accuracy was improved, but in some cases this improvement was not sufficient for accurate detection and quantification of some trace compounds [22].

**2.4.3 Archeological applications.** LIBS has previously been used as a minimally destructive means to quantify contamination of recovered artifacts, and to identify pigments and binding agents for art restoration purposes. While studies used LIBS to measure the depths of encrustations without damaging underlying layers or to identify unknown chemicals, such principles can easily be applied to other applications [22].

**2.4.4 Medical and pharmaceutical applications.** LIBS has previously been used as a means of quality control for liquid and tablet medications, a means of analyzing concentrations of minerals in bone samples, and one study used LIBS to differentiate between benign and malignant tumors [22].

**2.4.5 Analysis of aerosols.** LIBS can be used to analyze any state of matter including aerosols, and so has been previously used in to analyze and classify aerosolized samples [22].

**2.4.6 Military and forensic applications.** LIBS analyses can be conducted at a distance, and so this technique has been used in the remote detection of explosive substances [23]. LIBS has also been used to detect Barium and Lead residue; which are by-products of firearm discharge, for purposes of identifying suspects in crimes [22].

**2.4.7 Applications of LIBS for analysis of geologic samples.** LIBS has also been used as an effective tool for analyzing traits of aggregate stone in the past, namely by a variety of State Departments of Transportation. The sections below describe some past applications of LIBS for classifying aggregate stones and for quantifying various aggregate traits.

***2.4.7.1 New York State Department of Transportation research.*** New York State DOT Materials Method 28 limits the use of carbonate rock to be used in asphalt and concrete. More specifically, it requires any aggregate blend to contain at least 20% Acid Insoluble Residue (AIR). Two models were developed; one which accurately predicted the amount of AIR in a particular sample, while the other predicted the amount of AIR in an aggregate blend, based on the results of tests on a variety of samples from a given stockpile. Both models were produced via Partial Least Squares Regression (PLSR); using samples with known AIR obtained via typical testing procedures to develop predictive models which accurately predicted the amount of AIR in homogenous aggregate samples and aggregate blends based solely on the light emitted during LIBS testing. Figure 2.3 below shows the relative accuracy of values predicted through these analyses compared to known values. Note that the New York Department of Transportation used relatively large data sets to calibrate and test their predictive models [10].

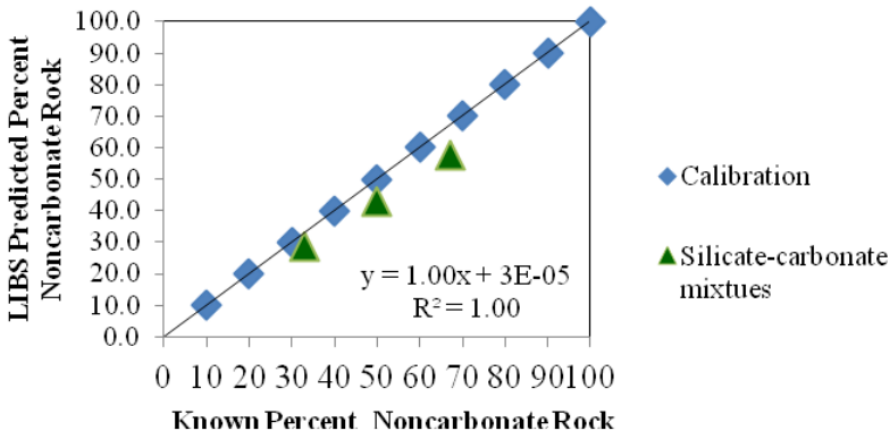


*Figure 2.3.* NYDOT Predictive Model Results for AIR in Aggregate Blends [10]

***2.4.7.2 Kansas Department of Transportation research.*** The Kansas Department of Transportation (KSDOT) used LIBS to develop and test two predictive models; one to predict the likelihood of D-Cracking failures in aggregate stone, while the other was used to determine the source bed or quarry of a tested aggregate sample. D-Cracking is a fracturing and breakdown of aggregate stone, believed to be caused by freeze-thaw conditions. The KTMR-21 and KTMR-22 testing procedures are used in Kansas to analyze the likelihood of such failures in an aggregate blend. A model was generated to predict whether a given aggregate would pass or fail this standard test [10].

PLSR was used to generate this model based on a series of samples tested via the conventional procedures, assigning a 1 to a passing stone and a 0 to a failing one, and then determining a Value of Apparent Distinction based on the predicted values; between 0 and 1 and generally about 0.5. The high accuracy of this model suggests that D-Cracking is strongly linked to the stone's chemical and/or mineral composition. The second model was developed using Principle Component Analysis (PCA) to develop a branching tree algorithm by which the source bed of a particular aggregate could be determined with a high degree of accuracy [10].

***2.4.7.3 Texas Department of Transportation research.*** The Texas Department of Transportation (TXDOT) limits the amount of Alkali Silica Reactive Aggregates to be used in various applications. These aggregates, caused by a mineral known as chert; a type of amorphous silica, may react with Portland cement binder, forming expansive silica gels, which exert stress in the concrete and cause cracking, as described in Section 2.2.4. Three predictive models were developed; one to quantify the amount of chert in an

aggregate sample, one to predict the result of state testing procedures, and one to differentiate between different varieties of chert [10].

The first model was achieved a very high degree of accuracy in predicting the quantity of chert present in a sample, as shown in Figure 2.4 below, and was developed via PLSR on a series of samples with known quantities of chert, as determined by standard testing procedures. The second model was developed using a similar technique to the Kansas DOT's pass/fail model; using a 1/0 as a pass/fail representation, and determining a Value of Apparent Distinction from the predictions between 0 and 1, to accurately predict whether an unknown sample would pass or fail the standard test. The final model used PCA to differentiate between different types of chert which may be present in a sample [10].

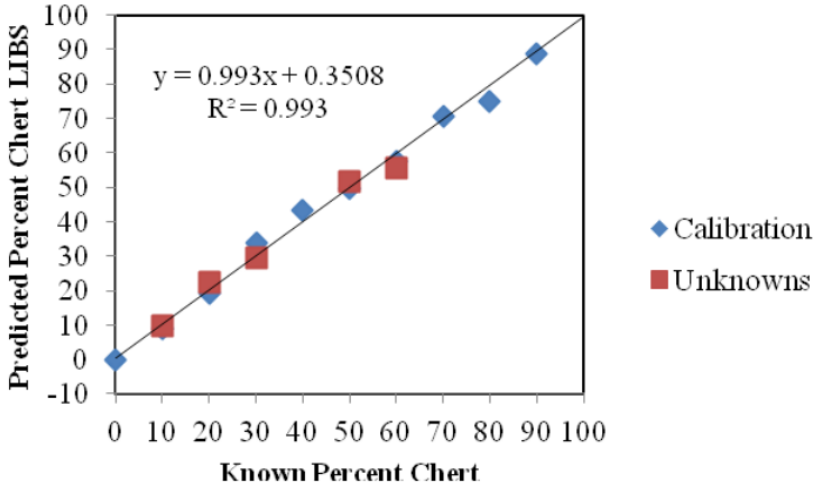


*Figure 2.4.* Texas DOT Predictive Model Results for Chert in Aggregate Stone [10]

**2.4.8 Other noteworthy applications of LIBS.** LIBS has shown to also be useful for concrete quality control. LIBS has been used as an alternative means of determining the depth profile of chloride and sulfur contamination in concrete, so as to mitigate unnecessary destruction of material during concrete remediation [24]. LIBS has further been used to produce models for determining the concentration of calcium, silicon, potassium, magnesium, aluminum, sodium, titanium, manganese, and strontium in cement powder to aid in quality control [25]. LIBS has been shown to show promise for screening recycled concrete by monitoring waste streams for both chemical and bulky contaminants [26]. While these sub-fields are certainly worth exploring further, this study will focus only on quality control of aggregate stone.

## 2.5 Development of LIBS Testing

Laser-Induced Breakdown Spectroscopy has developed over the past several decades, and has relatively recently emerged as a versatile testing method for a variety of applications. Throughout its development, a number of studies have been conducted to examine sources of interference and various methods of improving results, some of which will be briefly discussed in the sections below.

**2.5.1 Sources of interference and error.** As LIBS has developed over time, patterns have been observed and interfering effects and phenomena have become better observed and understood. This section will briefly discuss various common sources of error and interference encountered during LIBS testing, as well as methods used to account for and mitigate the effects of these errors on results.

***2.5.1.1 Plasma opacity.*** Following a laser pulse, a small plume of plasma is produced which emits light that can be sampled and used to determine the original material's composition. However, this plasma plume is not completely transparent, and may partially shield light emitted by material closer to the center of the plasma plume, particularly immediately following ablation; when the plasma is most dense. The plasma plume may also shield the sample from some of the initial laser pulse energy. Depending on the material tested, these effects can result in skewed results. The impact of this phenomenon can be mitigated through the use of short laser pulses (typically nano- or femto-seconds in lengths), and through use of accurate predictive models or standards [15]. Due to hardware limitations, the pulse duration was not varied in this research.

***2.5.1.2 Atmospheric plasma.*** Unless LIBS testing is conducted in a vacuum, the laser pulse will cause plasma to form in the atmosphere immediately adjacent to where the laser strikes the sample. Over the course of a laser pulse's duration, the resulting plasma plume can grow toward the laser pulse due to the aforementioned effects of the plasma plume's inherent opacity, producing additional atmospheric plasma. The light given off by atmospheric elements will be represented in the resulting light spectrum, and will result in erroneously high peaks corresponding to said elements, such as nitrogen and oxygen if conducted in air. While testing in a vacuum is an option, it is typically more time effective to simply apply the same methods as to account for plasma opacity; utilizing an accurate model calibrated from data collected under similar conditions, and using a short laser pulse [15]. As in-situ testing will be most conveniently conducted without adjusting the atmospheric conditions in the sample chamber, models in this study were developed based on results from tests conducted in air.

***2.5.1.3 Incomplete vaporization.*** Plasma opacity, combined with the tendency for certain materials to ablate more readily than others may cause some material to be left behind as a residue after a laser pulse. This will cause inconsistency between subsequent pulses on a single sample location. Completely vaporized particles will also produce higher light intensities than would otherwise be observed [15]. As in-situ applications may not be able to test on powdered samples, sufficient sampling sizes will be used with short laser pulses to mitigate the impact of incomplete vaporization on the results.

***2.5.1.4 Baseline light.*** While background light will be represented in a resulting light spectrum, this can be eliminated by simply testing in a dark chamber. While some baseline may continue to exist due to signal noise in the testing system, this can be subtracted from the output spectra through various methods. Additional light collected due to plasma forming in the atmosphere can similarly be removed from the spectra, if necessary for the given application [15]. In the case of the tests conducted throughout this study, baseline light was eventually determined to be insignificant, however early tests used center clipping in an attempt to remove baseline while mitigating signal noise.

***2.5.1.5 Stark widening.*** Local electric fields produced by the ionization of atoms in the plasma plume can result in increased variation in the wavelength of light emitted by a particular element as its electrons fall to lower energy states. In the resulting light spectrum, this causes the light emitted from a certain species to be a wider Gaussian distribution with respect to wavelength than would otherwise be observed. In such cases, the tails of these distributions are more likely to overlap and result in apparent elevated baseline within a range of wavelengths, which was encountered during the course of this research. The total light emitted by a certain species can be determined by integrating the

resulting light spectrum between the limiting wavelengths for said species. Alternatively, one can simply sample light relatively late in the plasma glow, thereby mitigating the presence of ions which produce the previously mentioned electric fields [15]. The latter option was used throughout this research for sake of simplicity.

***2.5.1.6 Accelerated ionization.*** The presence of free electrons can cause interactions in some particles which will increase their likelihood of ionization, which can skew the distribution of various species for a given element or all elements present [15]. By sampling light late in the plasma glow, one can assume that most light at that time is emitted by neutral particles, and the distribution of ions and neutral particles becomes largely irrelevant.

***2.5.1.7 Chemical matrix effects.*** Some elements ionize more readily than others, producing more free electrons to recombine with other elements, resulting in higher concentrations of neutral particles in other elements, which may interfere with results in studies where the distribution of ions and neutral particles is significant. As previously, collecting light from cooler plasma should mitigate such effects. Some studies suggest that the original molecular composition and arrangement can partially affect the wavelengths of the light produced by a given element, and while research on this phenomenon is still ongoing, the need for application-specific standards or models when using LIBS for quantitative analyses is often attributed to this [15]. While the distribution of ions and neutral particles was not considered during this research, distortion of emitted wavelengths due to the original material structure may explain some of the model performance behaviors observed throughout this research. Using properly calibrated models should mitigate the effects of this phenomenon on predictions.

***2.5.1.8 Surface conditions.*** The roughness and pitting of a sample, such as an aggregate, will affect the amount of material that is ablated by a laser pulse, which may skew results. A sufficiently large sample size should mitigate this effect. Dust or other surface contaminants may also be present on a sample, and the composition of said contaminants will be represented in the resulting light spectrum. If it is determined that this significantly affects the quality of the results, an appropriate testing procedure may include firing multiple pulses at a single point on each sample tested before collecting emitted light to ensure that the majority of surface contaminants are ablated away before collecting data [10].

**2.5.2 Potential improvements of LIBS technique.** Several studies over the course of the technique's development have found that modifications to the base concept of LIBS have yielded more accurate or more complete results. Some example techniques are discussed in the sections below.

***2.5.2.1 Multiple laser pulse configuration.*** A modification to the base LIBS method has been proposed by several studies, in which an initial laser pulse is used to heat a sample before analysis is performed based on the emission produced by a second pulse so as to ensure more complete and uniform vaporization of material. The initial pulse helps the system to achieve thermal equilibrium prior to taking an optical measurement, which allows for more uniform distribution of energy in the resulting plasma [27]. For simplicity, many studies simply assume that the system has reached local thermal equilibrium during LIBS testing, however some studied investigate the accuracy of these assumptions, and more accurate results have been obtained in cases where this assumption was not made or could not be made. Overall, using some variant

of a double pulse configurations has shown to improve results overall [22]. Due to hardware limitations, this study only considers systems with a single pulse configuration. As this study did not consider the physics of expanding or cooling plasma systems, local thermal equilibrium, or lack thereof, was not considered.

***2.5.2.2 Microwave assisted LIBS.*** While using a two-laser setup initially appears to be an attractive option, the addition of a second laser incurs significant additional costs and complicates the system as a whole. Research has been conducted into extending the useable plasma life through the use of radiations such as microwaves, and has found microwave stimulation to be an attractive alternative to a multi-laser system for LIBS analyses [28] and [29]. A variant of this method, using radiofrequency (RF) heating; which allows for the injection of energy deeper into dense plasma at earlier times in the plasma glow, potentially allowing for better control of plasma temperature, was explored during the course of this research to extend the life of the plasma glow and improve signal collection. These tests were inconclusive, so the conventional approach continued to be employed.

## 2.6 NJDOT Mineralogical Analyses

The NJDOT does not directly use chemical analysis results for aggregate quality control, however one of the goals of this research is to interpret predicted chemical composition so as to draw conclusions about the stone's mineralogy. Presently, the NJDOT uses qualitative lithographic examinations and, if necessary, closer inspections such as microscope point counts and petrographic examinations in the event field inspectors are suspicious that an aggregate stockpile does not meet quality control

standards. Microscope point counts are performed in the event excessive free mica is present in the mixture, while petrographic examinations and individual sample inspections can be used to determine the amount of weathered, or otherwise undesirable stone present in a sample. The combination of chemical data and morphological information as determined in a later phase of this research should help to reduce the need for such time consuming procedures. This thesis however, only considers the use of LIBS for determining the chemical composition of aggregate stone, which will later be interpreted for mineralogical information.

## 2.7 Data Processing and Analyses

The spectrum of light emitted by ablated material during LIBS testing is a pattern or signal unique to the sample in question, forming a sort of 'spectral fingerprint.' These unique patterns can be used to develop predictive models, wherein quantities of elements and compounds, or direct traits and other qualitative or quantitative information are inferred based on the spectrum features observed to represent said traits in other samples, as has been done in several previous applications, such as in the work conducted by the New York, Kansas, and Texas Departments of Transportation, as discussed in Section 2.4.7 above. A number of methods have been shown to be useful in producing such models, several of which will be considered in the section below. Each method is used to predict traits by recognizing patterns in signals corresponding to various known traits.

**2.7.1 Artificial Neural Networks (ANN).** Artificial Neural Networks present a versatile system for pattern recognition. The first, and simplest ANN was developed in 1958 by psychologist Frank Rosenblatt, and the technique has been further developed and

refined since [30]. These systems utilize a series of nodes, or neurons, to determine the correlation between a given input and a reference line, before assigning weights to various sections of the network to more easily identify and make predictions based on an input [31]. While entirely feasible for applications similar to those presently considered, other, simpler methods of pattern recognition are more commonly used, and this method was not selected for this research.

### 2.7.2 Principle Component Analyses (PCA) and Soft Independent Modeling of Class Analogies (SIMCA).

Principle Component Analysis; invented in 1901 by Karl Pearson and independently developed and named by Harold Hotelling in the early 1930s [32] and [33], is a pattern recognition technique which can be used to reduce data projections using linear algebraic techniques, so as to visually determine whether samples can be differentiated based on various sample data features. The Kansas and Texas Departments of Transportation effectively used this method to differentiate between different samples based on spectral data features collected from each sample [10].

Soft Independent Modeling of Class Analogies, or SIMCA, is an additional technique applied after PCA which allows samples to be classified into multiple categories simultaneously, and develop confidence regions for each classification [34]. As this research does not intend to develop models for classification purposes, these techniques will not be explored in detail, however these methods may be used in the event that the scope of the research is expanded in the future.

**2.7.3 Partial Least Squares Regression analysis (PLSR).** Partial Least Squares Regression Analysis is another linear analysis technique which can be used to produce various data projections, however this type of model can be used to produce quantitative predictions of multiple sample traits simultaneously. PLSR was developed by Swedish statistician Herman Wold, and the method was developed through collaboration with his son, Svante [35]. Predictions are made from PLS models in a manner similar to in Multiple Linear Regression, however in the case of PLS, predictive model coefficients are determined by maximizing the covariance between collected independent variables; in this case light intensities at various wavelengths, and known dependent variables; in this case the known mineral concentrations of samples used to calibrate the model. This method was used by the previously discussed Departments of Transportation to produce very accurate predictive models [10].

PLSR may refer to one of two separate algorithms; PLS1 or PLS2. PLS1 calibrates a predictive model which is designed to predict a single value or factor, while PLS2 is used to develop models which predict multiple factors concurrently. Research by Tucker et. al. determined that the two algorithms produce similar results; as separate models or a single more versatile one, except in cases where there is a high degree of inter-correlation between various dependent variables, in which case PLS2 tended to perform marginally better for applications such as the one considered herein [36]. This technique was selected for this research given its versatility, relative simplicity and speed in making predictions from an established model, previous successes using this method for similar research, and the ability to improve or expand on existing models with only superficial changes to the calibration procedure. A pre-made PLSR algorithm was used

throughout this research, and an explanation of each step and a simplified example are provided in Appendix A to demonstrate how predictive models are developed and used.

# Chapter 3

## Equipment and Experimental Procedure

### 3.1 Testing Setups and Procedures

For this research study, Laser-Induced Breakdown Spectroscopy was used to obtain unique spectra of light emitted by a variety of stone samples so as to develop and test predictive models for aggregate stone chemical composition, and eventually mineralogy. This chapter will review the development of the various testing setups utilized throughout the research, as well as the various model calibration and testing techniques utilized to develop, refine, and test the predictive models.

**3.1.1 Preliminary lab setup.** The first LIBS testing setup was only used for preliminary tests and primarily qualitative analyses which were used to evaluate the effectiveness of the testing method. The laser used was a Quantel Brilliant B laser, with a $Nd^{+}$ doped Yttrium Aluminum Garnet crystal gain medium (Nd:YAG), capable of firing at a rate of 10 Hz, and set to emit a wavelength of 1,064 nm over a 4.96 ns pulse duration. This initial setup had a variety of shortcomings, such as an inability to easily test on non-flat samples, and as these preliminary tests were of little consequence to the overall result, it will not be discussed in detail.

**3.1.2 Secondary lab setup.** Following the earliest, largely qualitative tests, a second experimental setup was constructed which was more conducive to testing on irregularly shaped samples, such as aggregates. This secondary setup is shown in Figures 3.1 and 3.2 below. The same Quantel Brilliant B laser as in the preliminary setup was used for this new station, however all other components were replaced. Rather than

impeding directly on a sample after firing, the emitted light was relayed and focused, impinging on the sample at nearly vertical beam orientation. A horizontal sample stage with adjustable height was used. A sample tray was fixed in place on the sample stage, and the location of the center of the tray was placed such that it was horizontally in line with the focal point of the laser and plasma light collection paths. A simple instrument was constructed and installed to identify the vertical location of the focal point so that the sample stage could be appropriately adjusted for samples of varying sizes and shapes. This instrument was also set to rotate into place over the horizontal location of the focus as an additional measure to ensure that the sample was placed correctly. All sample testing took place in a newly constructed testing chamber, which was darkened (with the exception of a laser light entry hole) to prevent external light contamination in the collected light spectra.

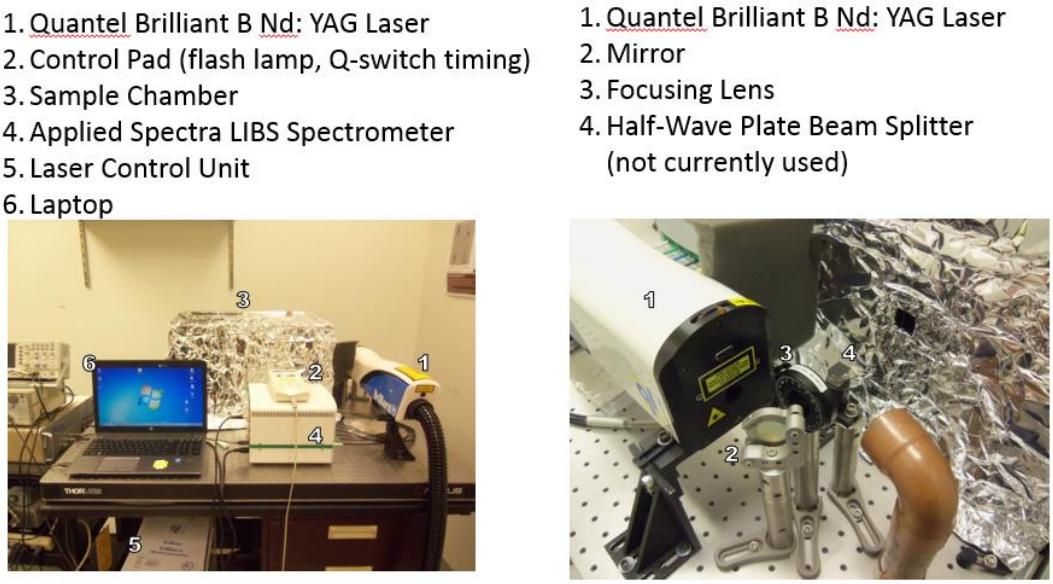


*Figure 3.1.* Secondary Experimental Setup

1. Adjustable Sample Stage
2. Off-Axis Hyperbolic Reflectors
3. Sample Tray
4. Focal Point Indicator

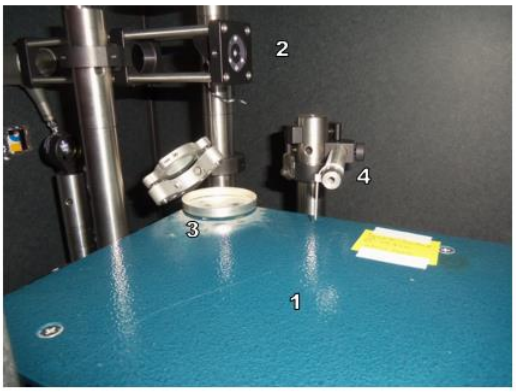


*Figure 3.2.* Secondary Setup Sample Chamber

This setup utilized an Applied Spectra, 6-channel Aurora LIBS spectrometer. Light emitted by plasma plumes was collected and re-imaged by two off-axis hyperbolic reflectors onto a fiber optic bundle, which then splits into 6 individual fiber optics; each feeding into one of the spectrometer's channels. This new spectrometer would be used for further testing. Some testing included the use of a beam splitter. During such tests, a higher intensity laser pulse energy was used, and a half-wave plate beam splitter at a $54^{O}$ angle split approximately 95% of the laser energy off and directed it to a light sink while the remaining light proceeded to the sample. This was used in an attempt to reduce variation in collected light intensity caused by variation in emitted laser pulse intensity caused by the means by which energy emission was controlled, however it was later determined that the beam splitter tended to split off the more focused component of the emitted laser light, resulting in less focused light striking the sample, and this addition

was eventually abandoned. Various system timing combinations were used throughout testing, and the optimal set of timing delays was determined. While earlier tests collected spectral data as the emission resulting from individual laser shots, the procedure was eventually modified such that the data collected was the accumulated light emission resulting from 100 laser shots so as to minimize the effect of intermittent low-emission tests on the output data. This procedure change was found to be effective and continued to be used.

In each test, the following standard procedure was observed: First, the laser's control unit was activated, and the coolant fluid was allowed to heat to the appropriate temperature. The laser was unable to fire until an optimal temperature was reached, due to a built-in interlock in the laser system. Before activating the flashlamp, all connections were checked and communication between the spectrometer and the corresponding computer software was established. The laser's flashlamp-Q-switch delay and the Q-switch-spectrometer delay were then set to appropriate timing. When the sample chamber was closed to minimize external light contamination, any windows were shielded with a dark, non-reflective screen, and all individuals present put on protective eyewear designed to block most of the 1,064 nm wavelength light scattered during the course of a test. When all safety precautions had been enforced, the laser's flashlamp was activated, and after waiting the required 8 seconds for the laser energy to stabilize, the laser was fired, and the resulting plasma light emission was sampled. This was repeated an appropriate number of times for the test in question.

As mentioned in Section 2.5.2.2, a radiofrequency system was briefly used in an attempt to prolong the useful plasma life through a mechanism similar to previous

microwave enhancement systems. The research team designed and constructed an ancillary module to the original LIBS system, capable of generating high-power RF (727 MHz) at the sample volume location. The module consisted of a voltage-controlled oscillator, variable attenuators, a pre-amp, a high-power (50 W) amplifier, and a custom-built, impedance-matched magnetic field resonator. The research team intended to systematically vary the applied RF power, duration, and point of application in an attempt to enhance LIBS signal collection, however collected results were eventually found to be excessively variable and the system was eventually rejected on the ground that the equipment addition would have been cumbersome and produced negligible, if any improvement in the effectiveness of the overall testing system. As these tests were conducted only briefly and were of negligible consequence, they will not be discussed in detail.

**3.1.3 Field setup.** At the time of writing, a third setup intended for field use is being constructed. This setup utilizes a more compact Quantel Ultra laser capable of firing at 20 Hz, but will otherwise be similar to the previous experimental setup in most ways. The laser beam path will be simplified; using fewer optics, and the sample stage will be replaced with one which can be repositioned to the system focal point automatically. This setup will be used for both lab and field testing, and to ensure that developed predictive models will be compatible with the field system.

**3.1.4 X-Ray Fluorescence testing.** All ‘known’ chemical composition data was collected via XRF testing. While the results used to generate predictive models were obtained by the New Jersey Department of Transportation, some testing was performed by the research team to confirm the accuracy and reproducibility of the provided results.

The testing unit used by the Rowan University research team was a Rigaku ZSX Primus II X-Ray Fluorescence Spectrometer, and the research team tested solid samples while the NJDOT tested on powdered samples, which were expected to be more reliable because the powdered samples were more homogeneous. Regardless, for each test conducted by the research team, each solid aggregate sample was first rinsed with water and dried completely so that surface dust would not damage the testing apparatus and the presence of water would not skew results. Each clean, dry sample was placed in the center of a standard sample container, which was securely sealed and arranged such that a surface of the aggregate would be approximately flush with the test opening. As a safety precaution, the sealed sample stage was placed beneath a simple measuring fixture to ensure that the stage sections were screwed together correctly. The sample container was then placed in the XRF spectrometer and the chamber was closed. A dedicated computer was used to inform the system of the size of the sample opening and its location in the chamber. A simplified, built-in testing procedure was used for completeness of results. The system was run, and the XRF unit automatically moved the sample container to the appropriate testing location, the chamber depressurized to near-vacuum, and the test was conducted automatically. Results were reported as percent composition by mass. Note that lighter elements (such as lighter than fluorine) may have been misrepresented due to interfering effects innate to the technique, and therefore were not considered. Chemical composition results were most conveniently reported assuming all elements to be bound in oxides, independent of the accuracy of this assumption.

### 3.2 Development of a LIBS Analysis Procedure

Once a complete set of data had been collected, the next step was to calibrate a predictive model based on the collected spectral data and known chemical compositions, as determined via XRF analysis. While a variety of pre-processing methods were used, all models were calibrated via PLSR.

A number of pre-processing steps were performed on the raw light spectra data prior to calibrating and testing models. This section will describe each method used throughout this research.

- Removal of baseline light: It was determined during this research that baseline or background light was insignificant in the collected data overall given the dark sample chamber, however this was not immediately apparent, and earlier tests attempted to remove baseline light. This was done manually in the case of the preliminary setup by simply subtracting an apparent baseline threshold from each light intensity value in the resultant data. Additional manual attempts to remove remaining baseline caused by signal noise were attempted throughout much of this research (see below), however it was determined that this does not significantly improve the accuracy of models and this practice ceased following a change to collecting data as the sum of the emissions of 100 laser shots.
- Discarding test results with exceptionally poor fluorescence: Due to innate randomness caused by variability of sample composition from location to location, variability in actual laser emission compared to nominal emission, etc., there is a possibility that no appreciable quantity of plasma light, or such a small

amount is collected by the spectrometer that the majority of the typical spectral peaks cannot be discerned. In earlier tests which collected spectral data resulting from individual laser shots as opposed to the sum of many subsequent laser pulses, these low emission shots would have significantly skewed the attempts to calibrate predictive models and so were manually removed from the data sets as they were observed during testing. By considering the sum of the emissions produced following many laser pulses, occasional low-emission tests trend to having negligible effects on the overall results due to individual normalization of spectra; and as such it is unnecessary to manually remove erroneous data which clearly does not represent the sample in question.

- Reduction of spectral amplitudes: In later tests which collected data as the sum of the emissions caused by 100 laser pulses, each resulting total spectrum amplitude was reduced by a factor of 100 to convert each to the average emission caused by 100 laser shots. While not necessary in cases where spectra were normalized to total light emission, this practice was continued for sake of consistency so as to more easily compare the performance of various models and in cases where this normalization technique was not used.
- Removing variation along baseline or negative values caused by signal noise: A method called center clipping, wherein all light intensity data below a certain threshold was assumed to be noise and was set to 0, was used to remove variation caused by noise along the spectral baselines. While it was suspected that this caused loss of useful data, neglecting this step was initially found to have adverse effects on model accuracy. However, following the procedure change to the

accumulated data method, baseline variation began to largely cancel to approximately 0 when one summed the emissions caused by many laser shots, and as such this method was rendered largely unnecessary. This pre-processing step is currently employed with a threshold of 0 light intensity to remove remaining negative values from the results, but is otherwise no longer used.

- Normalizing spectra to total light emission: To account for random variation in the overall intensity of light emitted by a plasma plume and collected by the spectrometer during a test, each light intensity value in a given collected light spectrum is divided by the total light emission for the spectrum. While the total light emission was initially based on a point to point approximation of the area enclosed by the light spectrum, this was later changed to a straightforward normalization of all light intensity values collected, such that the sum of all normalized light intensity values in the given spectrum is unity. This was found to benefit the accuracy of the predictive models more than alternative methods and it was therefore continued except where specifically noted.

# Chapter 4

# Results and Model Analysis

## 4.1 Preliminary Setup Results

The preliminary testing setup was primarily used to conduct qualitative analyses and to calibrate a very simplified model for the sake of evaluating LIBS as a testing method and PLSR as a means to calibrate predictive models.

**4.1.1 Qualitative identification of elements.** The earliest LIBS tests were conducted on samples of pure metals; namely aluminum and copper, which were used to confirm the viability of qualitatively identifying elements present based on the light emitted by the plasma glow. The National Institute of Standards and Technology (NIST) Atomic Spectra database was used to identify typical locations of peaks for each element, and these wavelengths were compared to observed spectral peaks. In each case, observed emitted wavelengths corresponded to those identified in the database, confirming that LIBS could be used to qualitatively identify elements in samples. LIBS tests were then conducted on samples of limestone and mica; two of the minerals considered in this study, to obtain characteristic spectra for each, so that they could later be used to identify the presence of these minerals in unknown samples.

**4.1.2 Evaluation of PLSR for developing quantitative predictive models.** Following the above initial qualitative tests, PLSR was evaluated as a means of developing quantitative predictive models using spectral data collected via LIBS and known composition values. As a simplified case, LIBS tests were conducted on a series of pennies minted in various years with known elemental compositions; namely several

known blends of zinc and copper. Coins minted in 1953, 1980, and 2006 were tested, and the resulting predictive model was accurate for a randomly selected 1953 coin sample, demonstrating that the PLSR method is viable for generating predictive models, however this simplified case considered only two elements and tested a sample which was identical to a sample used in calibration, and more complex samples were not expected to produce as accurate models without additional analysis or pre-processing.

## 4.2 Secondary Setup Results

Following the testing of the simplified model described above, the setup was reconstructed into the secondary lab testing setup, which was used to conduct the majority of this research. The following sections will review the work conducted using this setup. All tests conducted using this secondary setup were on samples of aggregate stone provided by the New Jersey Department of Transportation. Samples' chemical composition were obtained via XRF analysis conducted by NJDOT as well. The known compositions provided are outlined in Appendix B.

**4.2.1 Early models.** The earliest predictive model for aggregate stone chemical composition was calibrated using data collected from just three types of stone. These stones were a Carbonate Dolomite from Carpentersville, NJ (referred to herein as Carbonate Dolomite), a Gneiss sample from Glen Mills, PA (Glen Mills Gneiss), and an Argillite sample from Plumstead Twp., PA (Plumstead Argillite 1). A fourth sample of Jurassic Diabase (a trap rock) from Haverstraw, NY (referred to as Diabase), was also initially provided, but did not have a known composition at the time and was used as a pure testing set sample. This model was developed using data collected from individual

laser shots, and low-emission shots were manually removed from the data sets, as discussed in Section 3.2. This step would not be necessary following the procedure change such that each collected spectrum would be the sum of the collected emissions from 100 laser shots; which thereby made the model more feasible for use. Despite varying numbers of low-emission shots between different stone types, these removed shots were not replaced for the earliest models, and as such, the amount out input data was not always consistent between different stone types. This error would be corrected in later models. Center clipping was used in an attempt to remove baseline and signal noise from the raw data sets at this phase, and spectra were normalized to an approximation of the area beneath the given spectrum as a metric of total light emission. Models were calibrated using 27 PLS components, which was determined to account for the majority of the variation in the known chemical compositions, but would later be found to over-calibrate the model. This model was tested using data from each of the four originally provided samples. To observe the effects of each case, testing inputs included both data which had been previously used to calibrate the model and data which had not. As in all other cases, testing data was adjusted in the same manner as calibration data.

The results of these tests showed a common trend in that any data matching data used to calibrate the model produced very accurate results, while any data from outside the calibration set produced much less accurate results. To observe the effect of adding an additional sample to the calibration set, a new model was developed which included the Diabase sample. All calibration methods and parameters were otherwise consistent with the first model. While the addition of the Diabase stone to the calibration set improved predictions for that type of stone, error in predictions continued to be significant. At this

phase, it was believed that these errors were caused by using an inappropriate number of PLS components, or due to lack of variability being represented in the calibration set.

**4.2.2 Parameter variation.** Following these initial, preliminary models, a simplified method of examining relative model performance was used. This method used L1 Error; which is the sum of the absolute values of each deviation from accepted values, as a metric of overall error in predictions. In an attempt to mitigate error caused by variability in the energy emitted by the laser, a new data set was collected using the half-wave plate beam splitter discussed in Chapter 3, and future analyses would use this newly collected data. The hypothesis that the error could be attributed to using an inappropriate number of PLS components to calibrate the model was examined first. Models were calibrated using varying numbers of PLS components, and each was tested using 10 independent spectra from inside and outside the calibration set to observe the performance of each. Each sample was considered independently to observe variability of the predictions.

The expected trends were observed when testing using samples within the calibration set; using fewer PLS components results in higher variability in the accuracy of predictions, while using more resulted in significantly less variability and a general improvement in overall accuracy. This however contrasted the results obtained for the data outside the calibration set. The testing data not used in the calibration sets did not follow the expected trend beyond approximately 10 to 13 PLS components. The use of further PLS components did not improve predictions, and in some cases error increased as more PLS components were used. This partially showed that the number of PLS

components used previously was excessive, but also shows that the majority of the error in the models was not caused by the number of PLS components used to calibrate it.

Following the above tests, two additional samples were provided; a second carbonate rock from Andreas, PA (Lehigh Carbonate; named after the source company), and an additional trap rock sample from Oldwick, NJ (Oldwick Trap Rock 1). The addition of these samples slightly improved the model accuracy, and models moving forward included these samples. The next set of models used 90% of collected data for calibration, and the remaining 10% for testing.

It was then considered that the error in the models may have been caused by using an inappropriate center clipping threshold. The minimum threshold considered was 200 arbitrary light intensity units because there was very little if any data below this point. A threshold above 370 was found to remove an excessive amount of data, and the PLSR algorithm was unable to regress a model given the amount of zeroes in the overall data set. The results of these tests suggested that a threshold of 330 light intensity units would be optimal overall.

**4.2.3 Other data adjustment methods.** Following the previous model tests, it was observed that several of the test spectra included very significant, broad light intensity ranges as opposed to the more distinct peaks otherwise observed. As normalization of spectra was achieved through an approximation of the area beneath the spectrum, these broad areas significantly affected this approximation, potentially skewing the normalized data used to calibrate the models. These areas generally occurred between about 545 nm and 560 nm wavelengths, typically peaking around 551 nm. While a

variety of methods were attempted to remove or otherwise account for this area, none were particularly effective, and the presence of this broadened area was later mitigated by adjusting system timing during future LIBS tests. It was eventually concluded that this uplifted spectrum area was caused by several broadened peaks with overlapping tails; caused by an inappropriate LIBS system timing.

Additional models were tested which involved another step in the calibration process. Prior to calibrating a model, data from shots corresponding to a particular stone sample were averaged, and these averaged data sets were used to generate predictive models. This was the first attempt at using averaged data sets. Models were developed after applying this averaging before and after the data sets were normalized to total light emission, however neither of these measures significantly improved model accuracy and was omitted from model calibration until much later attempts. Each of these models maintained the established 330 center clipping threshold.

During this period, the research team attempted to use the RF enhancement system described in Chapter 3 to prolong the measureable plasma glow, however the results were found to be excessively variable and this addition was not ultimately used. The preliminary testing results obtained during these attempts were not used to calibrate or test models.

**4.2.4 New data sets.** At this point in time, it was considered possible that the data set itself was the source of the error in the models. To test this hypothesis, an entire new set of data was collected for future models. The averaged data set testing was repeated on this new data, and returning to the original center clipping threshold of 200,

however as before, results were inconsistent and in most cases did not outperform the original calibration technique or data set, however the new data collected continued to be used moving forward.

These results led the research team to the conclusion that this error was caused by excessive variation in spectrum data. Future models utilized data collected using the modified procedure; such that the output spectrum would be the sum of the emissions resulting from 100 shots, and used results collected from testing on multiple locations per sample, which would reduce the effects of test to test variation on the overall results, as discussed in Chapter 3. Visually abnormal resultant spectra continued to be manually removed immediately following this adjustment, but only until it became apparent that this was no longer necessary. Once new data had been collected using this new procedure, new models were developed. These models continued to use a center clipping threshold of 200 light intensity units.

**4.2.5 Additional model refinement.** A new normalization technique was attempted which normalized spectral amplitude to the maximum light intensity for that spectrum; however this was rejected almost immediately, as predictions were found to be unreasonable. The area normalization method continued to be used. Models were then generated using data obtained by averaging the spectra collected for various locations on a particular sample, however the un-averaged models were found to perform marginally better; likely due to the larger calibration set size, and the previous method of center clipping and area normalization continued to be used. It was also found that models performed slightly better without removing visually abnormal data, such as collected from low-emission tests, and manual data filtering was no longer employed.

The next model tests examined the performance of models which used varying sized calibration sets, first calibrating models using 50 PLS components (with the exception of the 30 data point test, which used 25 because 50 would be above the maximum), then using the maximum number of PLS components, and finally using a number of PLS components equal to 20% of the total sample size. This was done to determine what size calibration set was optimal, or how large it should be for this purpose before addition of more data began to yield significantly depreciating returns in model accuracy. Only data from outside of the calibration set was used for testing moving forward because testing using calibration data consistently yielded high accuracy regardless of the actual reliability of the model. As expected, model accuracy generally improved as more calibration data was used in each of the three cases, however the behavior was semi-random due to high variability in predictions, which the research team attempted to account for in the future by using larger testing sets.

At this time, it was considered that model inaccuracy was caused primarily by inaccuracy in accepted values used to calibrate the model. To ensure that the provided XRF data, and thereby the accepted values, were reproducible, additional XRF tests were performed by both the Rowan research team and NJDOT staff. The Rowan research team tested on solid samples while the NJDOT staff tested on powdered samples. Given this difference in procedure, it was expected that the Rowan research team's results would be less consistent, as these tests examined various points on an inherently inhomogeneous sample, whereas the NJDOT staff's powdered samples were expected to produce more consistent results given the fact that the samples effectively blended the solid samples into a more homogeneous mass. As previously, XRF results were reported assuming all

elements to be bound in oxides, regardless of the accuracy of this assumption. While the independently performed XRF tests produced somewhat comparable results, the NJDOT results were significantly more reproducible, and future models continued to use the provided NJDOT results. Future models would also be calibrated using larger calibration sets in an attempt to provide more reliable models. Note that XRF results for the Oldwick Trap Rock 1 sample were found to be very variable for the NJDOT results and were suspected to be inaccurate. As the accuracy of these results could not be verified at the time, this sample was not used to calibrate future models.

**4.2.6 Finalizing system timing and procedure.** Following these tests, an inspection of the testing equipment found a previously unconsidered problem in that dust from the aggregate samples which had been ejected during testing had begun to collect on the system's optics, potentially reducing the amount of energy reaching the samples, which may have affected testing results. The optics were cleaned, realigned, and a new series of tests were conducted. These tests no longer used the half-wave plate beam splitter; as the loss of beam focus caused by this method had become apparent by this time. These tests used a flashlamp-Q-Switch delay time of 400 μs, with a total spectrometer delay of 6.3 μs; including the 1.3 μs timing offset. This was done to mitigate the widened peaks previously described, and to better mimic the conditions which would be present with a portable system used for field testing. Testing was conducted on a total of 14 types of stone, but samples without reliable known compositions were only used for testing purposes. The 8 new samples provided since the previous tests included two additional Argillite samples from Plumstead Twp., PA (Plumstead Argillite 2 and 3), each with slightly differing chemical composition, a

sample of quartzite from Paupack Twp., PA (Atkinson Quartzite after the providing company; Atkinson Materials), a carbonate rock sample from Woodsboro, MD (Woodsboro Carbonate), a Gneiss sample from Hamburg, NJ (EI Gneiss after the providing Eastern Concrete Materials, aka Eastern Industries), another Gneiss sample from Bechtelsville, PA (Bechtelsville Gneiss), and two additional Oldwick Trap Rock samples (Oldwick Trap Rock 2 and 3). For the calibration samples, 5 locations were tested for each of 10 samples, resulting in 50 resulting spectra per stone type. For a testing set, an additional 2 samples were tested (10 data points total) for each type of stone. This testing set size would later be expanded to 5 samples for purposes of determining an optimal testing sample size. Additionally, the sample tray was cleaned with a damp cloth before changing the type of stone being tested as an additional measure to ensure dust and fines from previous samples would not contaminate the surface of subsequent samples.

Once a complete new data set had been collected, a series of models were developed and tested using this expanded calibration set and a series of pre-processing techniques; some which had been attempted previously, others of which were new. These models no longer used L1 error as a metric of overall model performance, as this did not provide sufficient information as to which compounds were being predicted inaccurately. During calibration, each model began using the sum of the light intensity values as a simplified metric of total light emission, which did not affect results because the wavelength interval between adjacent light measurements was constant across the light spectrum. Each of these models also used a better optimized number of PLS components to calibrate them, as determined via the algorithm's built-in cross-validation function. In

most cases, using more PLS components yielded consistently depreciating returns in the amount of variation in the set of known values which was explained by the model, and so in general a number of PLS components was used past which adding more would explain less than another 1% of the variation. While the actual amount of this variation which was explained varies depending on the pre-processing technique used, the number of PLS components used was typically about 5 to 10.

**4.2.7 Model optimization.** The system timing using a 400 µs flashlamp-Q-switch delay and a 6.3 µs spectrometer delay yielded very consistent results with little, if any peak widening or distortion. Due to inhomogeneity and the possibility of sample contamination caused by some individual stones of another type being included in a particular provided sampling, occasional spectra were distinct among other tests from the same stone type; however these results were comparatively rare. As more reliable test results were finally obtained, efforts shifted toward producing a more optimized predictive model. Additional past research was reviewed in an attempt to determine how best to optimize the model. While PLSR as a pattern recognition technique appeared to be sound, some data pre-processing techniques had not been attempted, and additional pre-processing variations were considered.

***4.2.7.1 Base model.*** Before any alternative pre-processing options were explored, a Base Model was developed for sake of comparison. In the Base Model, the 100 shot total spectra were reduced in amplitude by a factor of 100, negative values caused by signal noise were removed through applying center clipping with a 0 threshold, and spectra were normalized to a metric of total light emission; namely the sum of the light intensity values for each. In each of the Figures below, the X-axis displays the XRF

results; or the ‘known’ percentage of a given compound, while the Y-axis shows the average of 25 predictions for each of the 10 stone types with known composition. Only the 5 most significant compounds are reported for sake of simplicity. Each prediction is compared to a ‘Perfect’ line indicating the data point placement in the event the average prediction perfectly matched the XRF data. Unless otherwise noted, each method below includes the previously stated pre-processing steps before applying others. The results of the Base Model are shown in Figures 4.1 through 4.5.

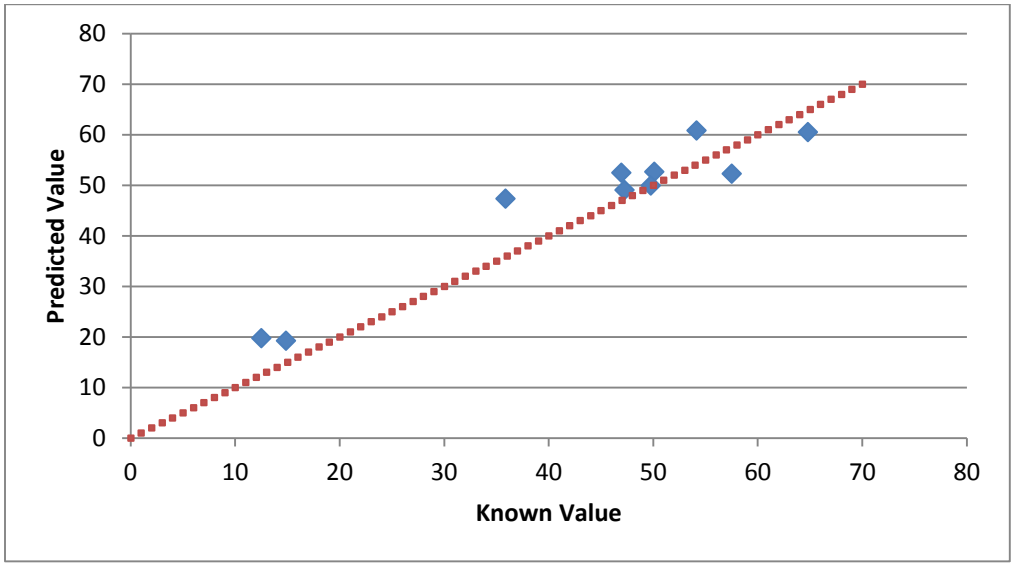


*Figure 4.1.* $SiO_2$ Base Model Predictions

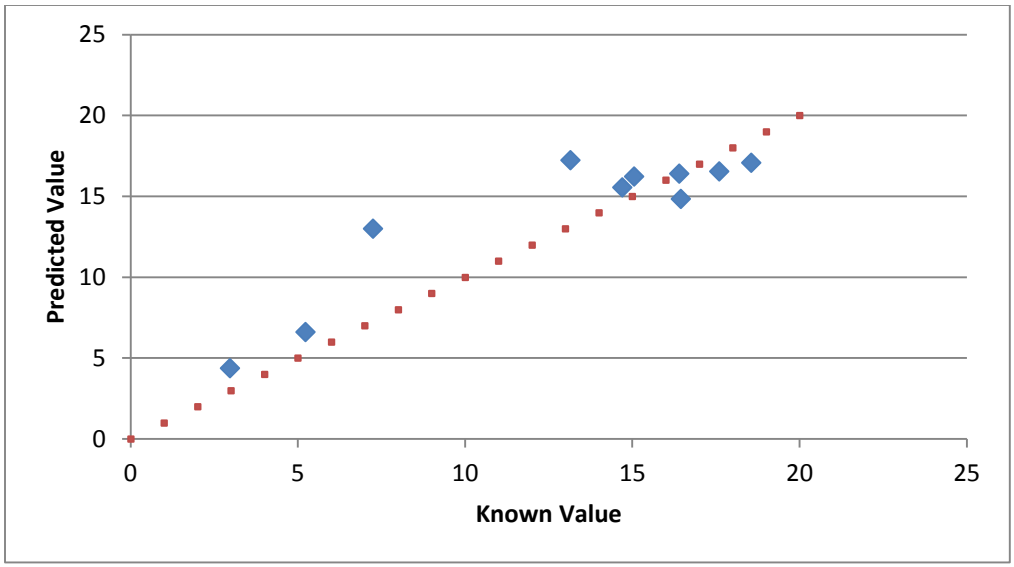


*Figure 4.2.* $Al_2O_3$ Base Model Predictions

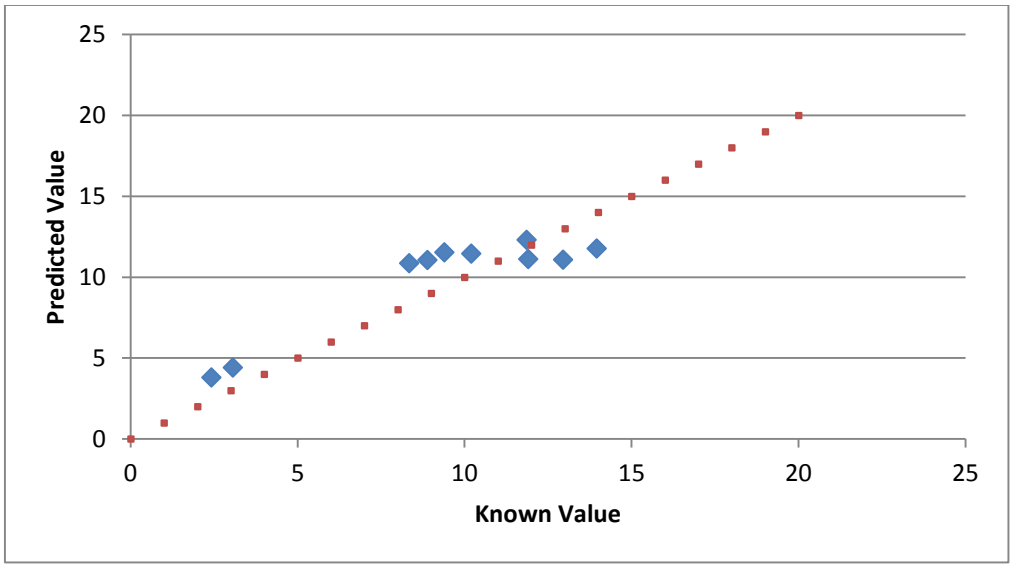


*Figure 4.3.* $Fe_2O_3$ Base Model Predictions

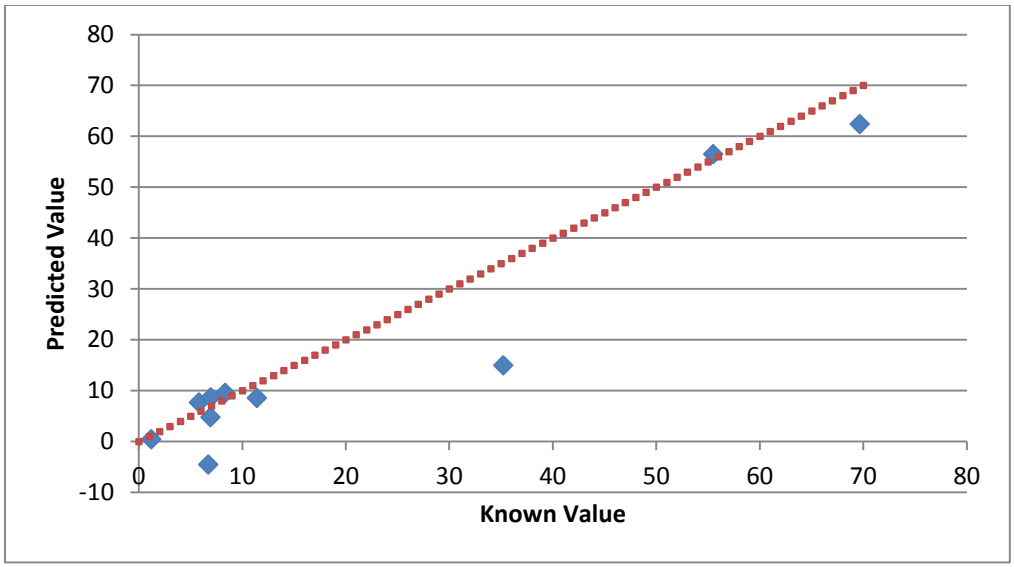


*Figure 4.4.* CaO Base Model Predictions

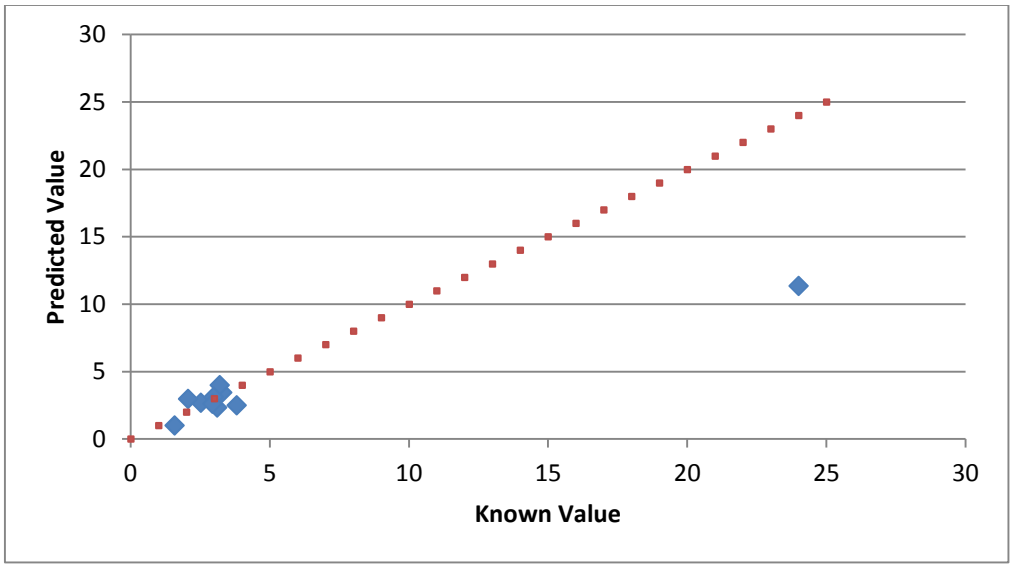


*Figure 4.5.* MgO Base Model Predictions

While some predictions using the Base Model produced large errors, the majority of predictions can be considered to be at least reasonable. However, to be accepted as a reliable predictive model, the predictions must be accurate for all samples, and the alternative pre-processing methods described below were used in attempts to improve on this base case. Note that the Magnesium predictions for the original Carbonate Dolomite sample were expected to be outliers in each case because the proportion of magnesium in this sample was much larger than any other sample used to calibrate the models.

***4.2.7.2 Y-scaling.*** While researching additional methods of optimizing PLS models, the research team found a publication by Tucker et. al. (2010), which used various methods for optimizing a PLS model for predicting the chemical composition of various types of igneous rocks. While the scope of the research varies from that herein, its relevance could not be overlooked, and some of the pre-processing techniques attempted in Tucker et. al.'s work were emulated for this research. One method explored in Tucker et. al.'s work is scaling the Y-variables, which forces the PLSR algorithm to consider the concentrations of all compounds equally rather than prioritizing compounds with high variability in the calibration set. This is done in three ways. One method was to divide the value of each concentration by the maximum for that compound in the calibration set, thereby reducing each Y matrix value to between the ratio of the smallest to the largest value, to 1 for each compound being considered. The second method involves first subtracting the minimum value for each case before dividing all remainders by the range for that compound, thereby reducing each to a value between 0 and 1. Tucker et. al.'s work explored a third method; in which values were scaled relative to the standard deviation of each Y variable, however, this method required the distribution of

each variable to be approximately Gaussian, which could not be assumed for the available samples, and this third method was not considered in this research. Regardless of which method is used, the reverse adjustments must be applied to predicted values to convert them to actual predictions [36]. The average composition predictions for each case are shown below in Figures 4.6 through 4.10. The ratio:1 Y-Scaling produced very inaccurate and typically unreasonable predictions, however the 0:1 Y-Scaling method, while moderately variable, generally produced results comparable to the Base Model overall. Note that the ratio:1 model results were dissimilar to future attempts at using this method, and these poor results may have been the result of an error in data processing.

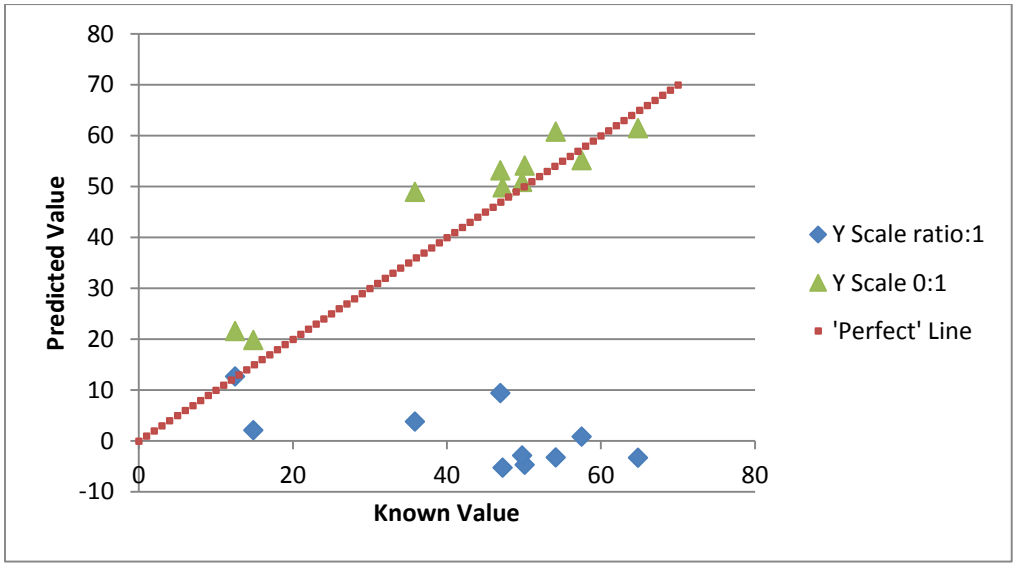


*Figure 4.6.* $SiO_2$ Y-Scaling Model Predictions

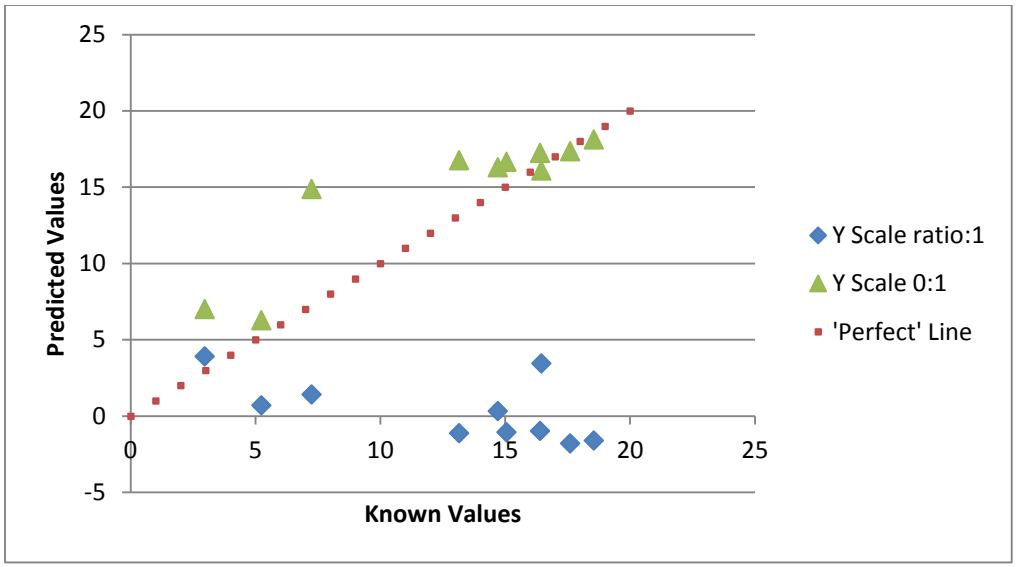


*Figure 4.7.* $Al_2O_3$ Y-Scaling Model Predictions

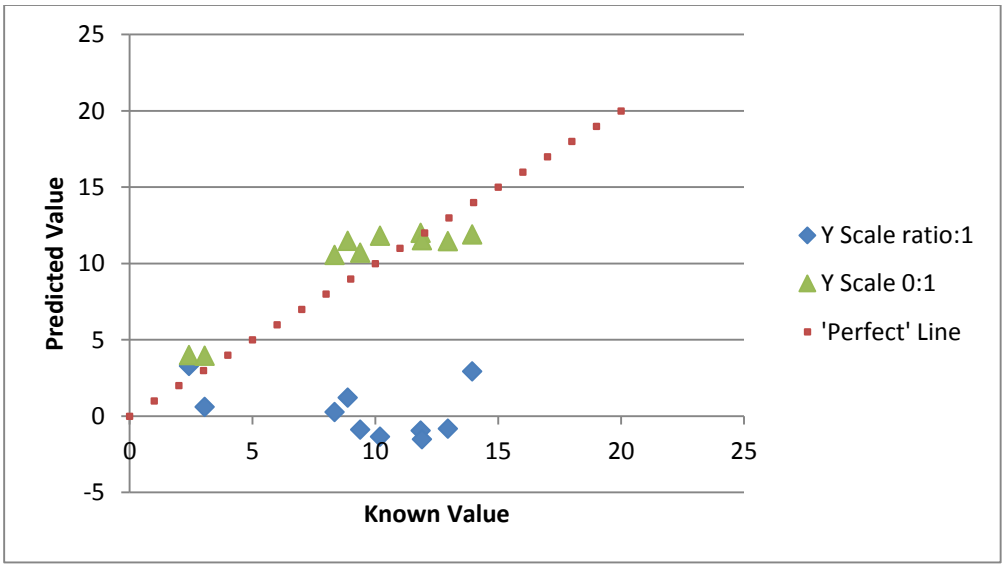


*Figure 4.8.* $Fe_2O_3$ Y-Scaling Model Predictions

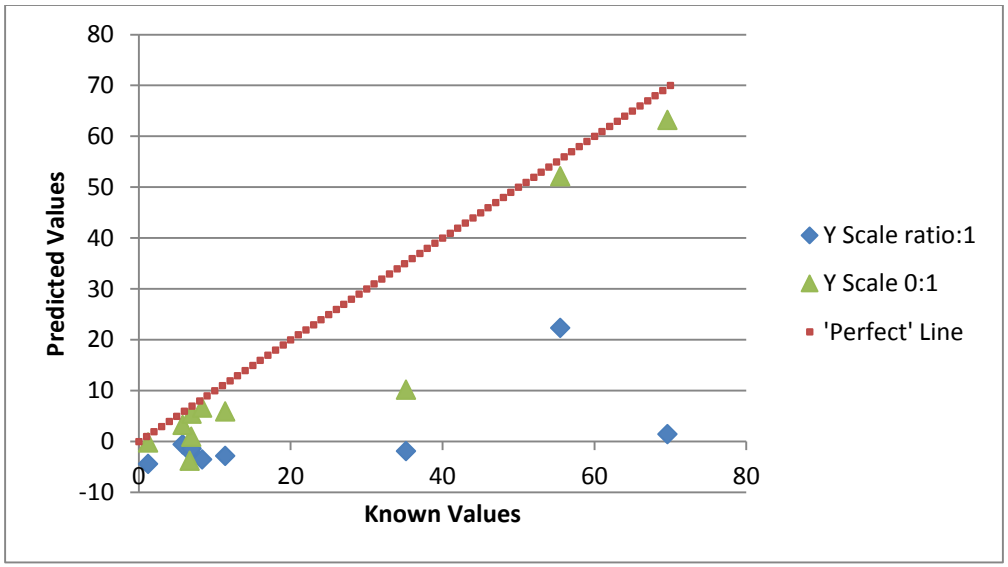


*Figure 4.9.* CaO Y-Scaling Model Predictions

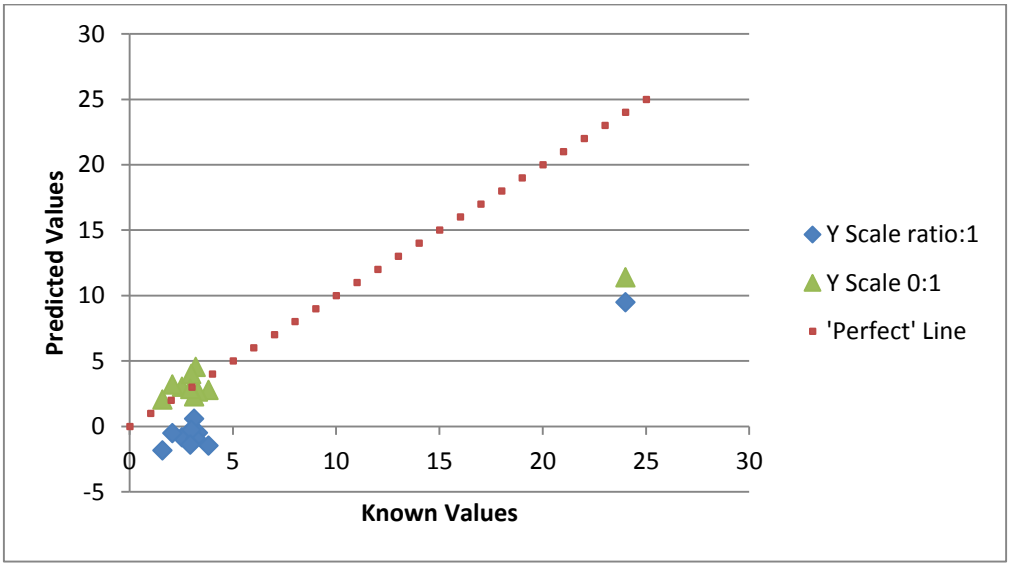


*Figure 4.10.* MgO Y-Scaling Model Predictions

***4.2.7.3 Averaged calibration set.*** The next method considered averaging the calibration data corresponding to a particular type of stone before calibrating a model; similar to previous attempts. All data for a given type of stone was reduced to a single effective data set prior to any other pre-processing steps being applied. This model was then tested using both individual testing spectra ('Averaged' points), and test spectra averaged as with the calibration set, which results in a single prediction rather than several somewhat variable independent predictions ('Averaged Both' points). The results are shown in Figures 4.11 through 4.15 below. This model was generally less accurate than the Base Model, with the exception of the silica prediction, and variability in predictions was somewhat greater, as was expected given the reduction in calibration data. Using the averaged testing sets as well generally produced marginally more accurate results.

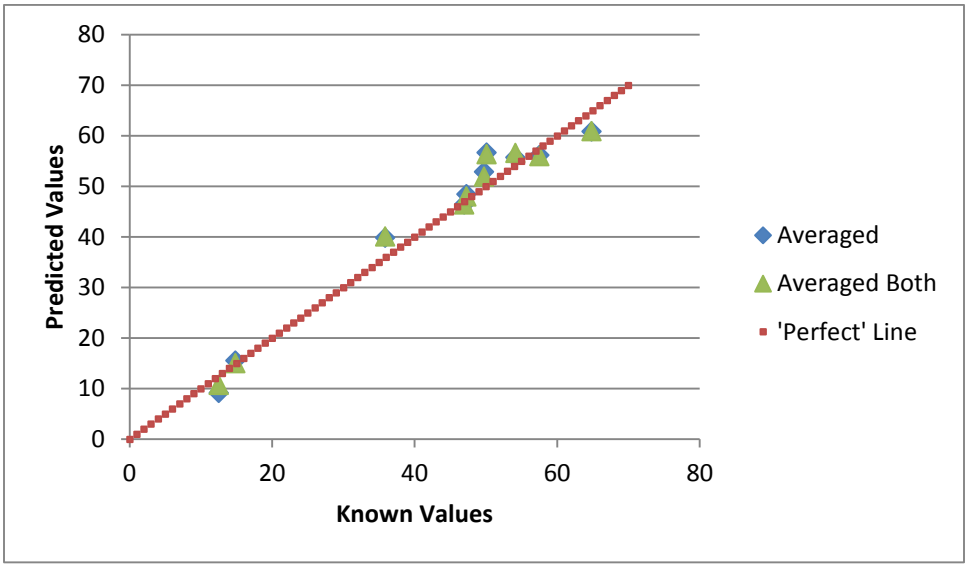


*Figure 4.11.* $SiO_2$ Averaged Model Predictions

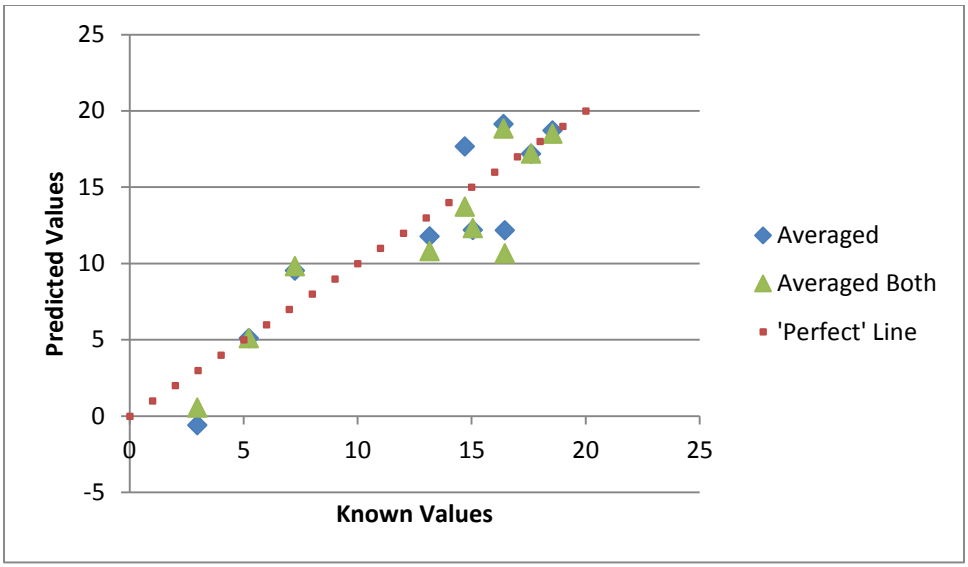


*Figure 4.12.* $Al_2O_3$ Averaged Model Predictions

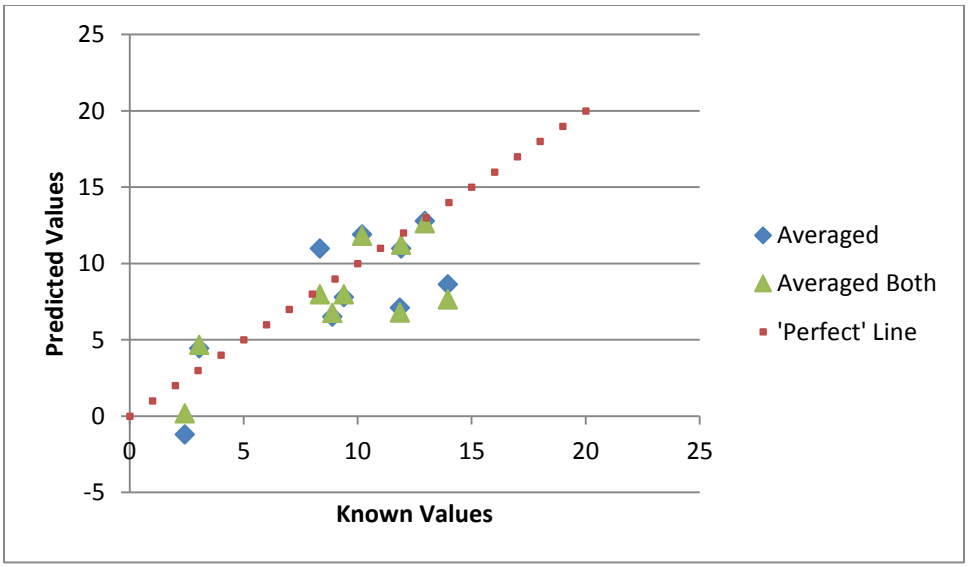


*Figure 4.13.* $Fe_2O_3$ Averaged Model Predictions

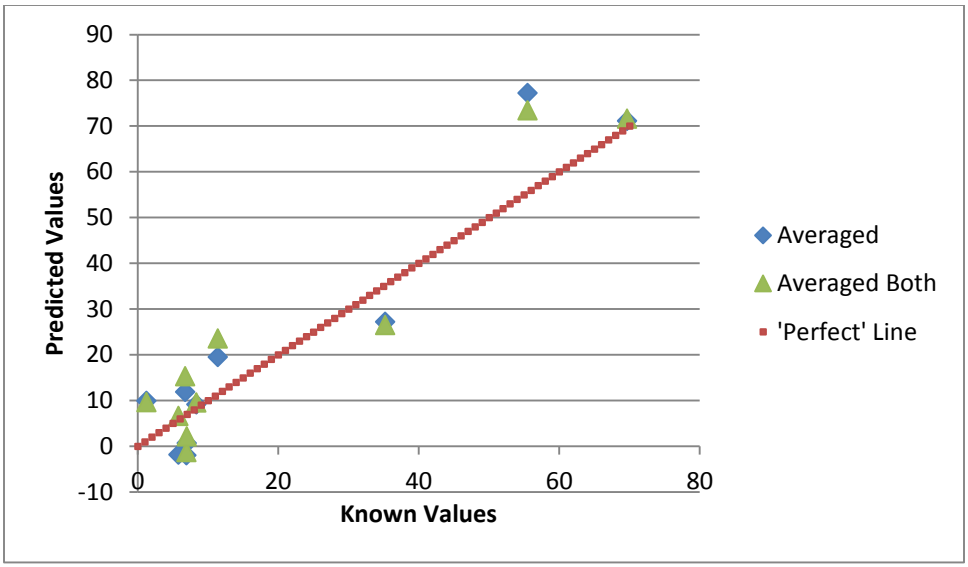


*Figure 4.14.* CaO Averaged Model Predictions

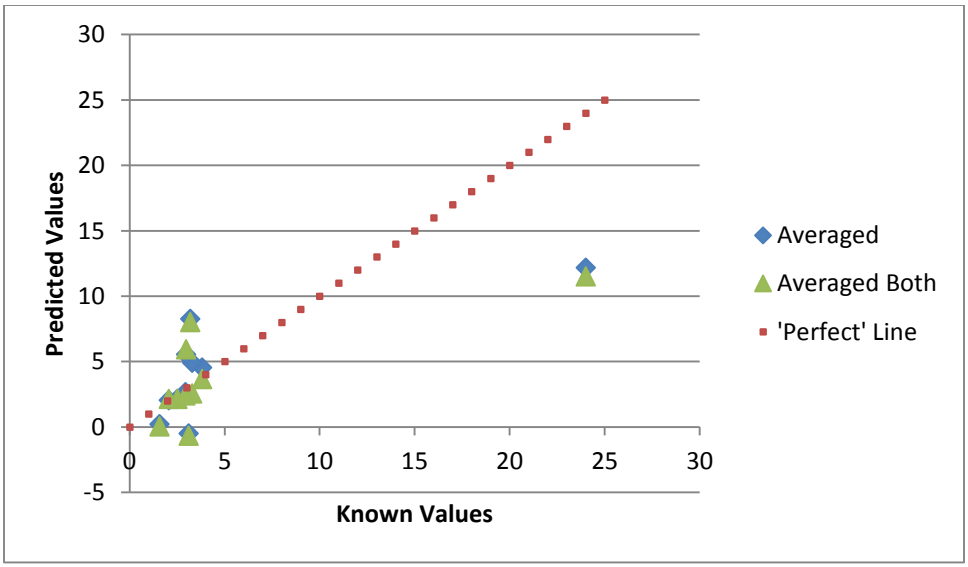


*Figure 4.15.* MgO Averaged Model Predictions

***4.2.7.4 Amplitude scaling.*** The next method involved an alternative means of normalization, in which the amplitudes of spectra were scaled relative to the average amplitude for that type of stone. This attempts to adjust the amplitude of spectra for each stone type independently to mitigate the effects of variability in emissions between testing locations, while preserving the information present in amplitude differences between different types of stone. Model testing was performed using unadjusted testing spectra ('Amp Scale' points), and testing spectra which had been independently scaled as in the calibration set ('Amp Scale Both' points). Spectra were not normalized to total light emission in this case. The results of this method are shown in Figures 4.16 through 4.20 below. While the independently scaled testing data was less variable than the unadjusted sets, both produced highly variable predictions and both methods were inaccurate, and so this method was rejected.

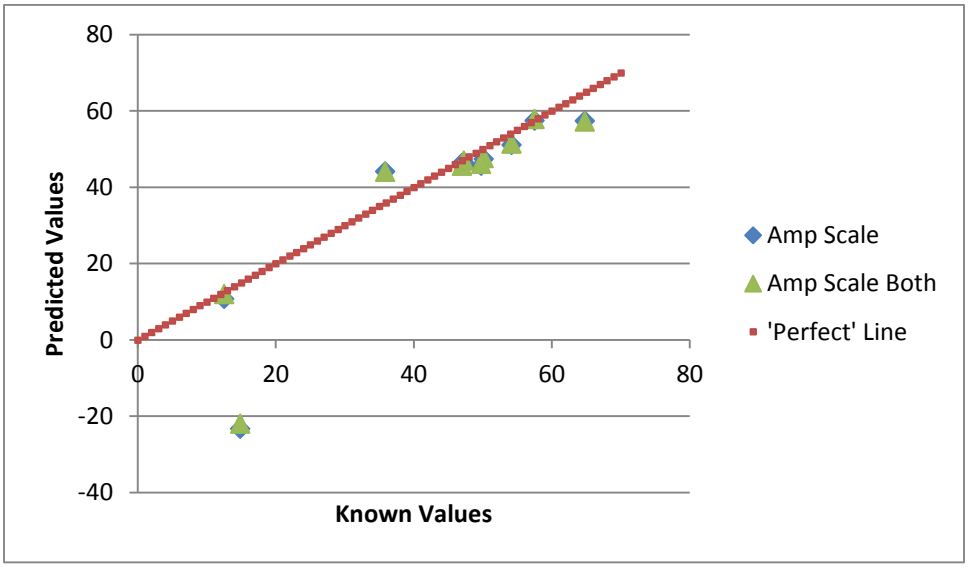


*Figure 4.16.* $SiO_2$ Amplitude Scaling Model Predictions

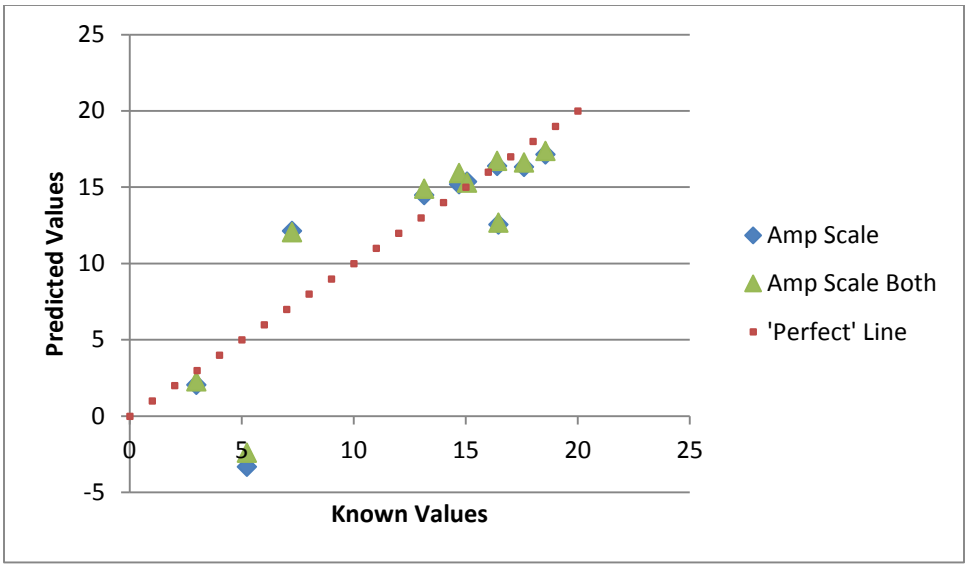


*Figure 4.17.* $Al_2O_3$ Amplitude Scaling Model Predictions

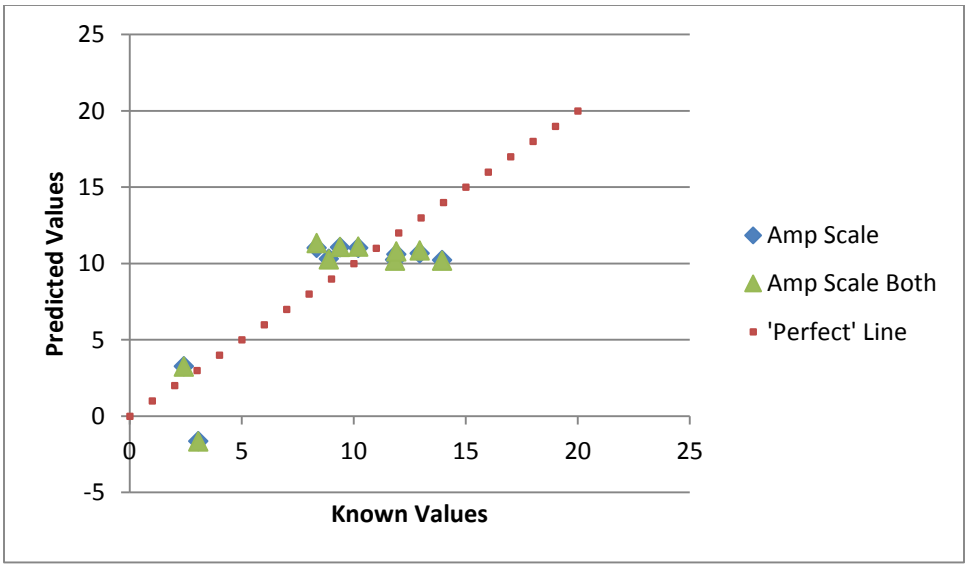


*Figure 4.18.* $Fe_2O_3$ Amplitude Scaling Model Predictions

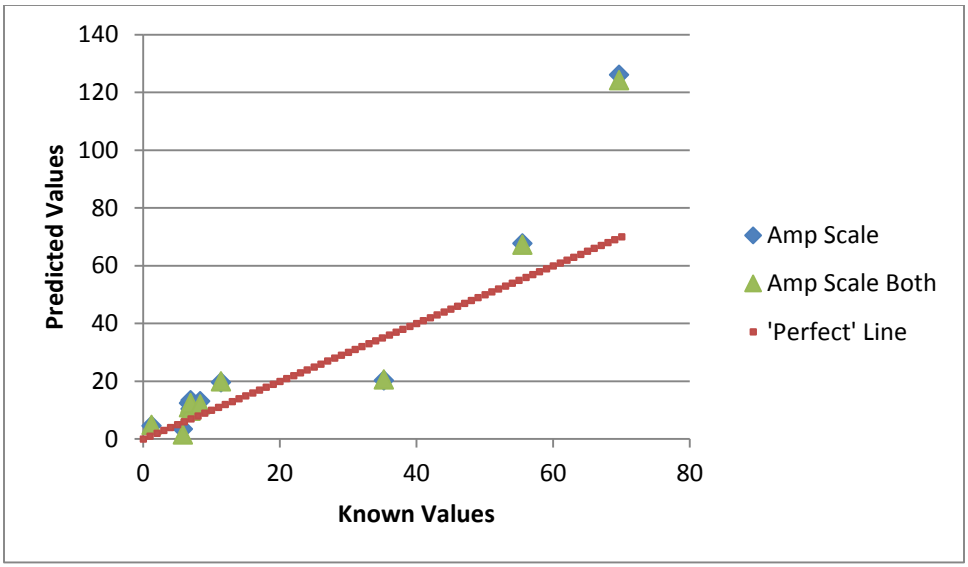


*Figure 4.19.* CaO Amplitude Scaling Model Predictions

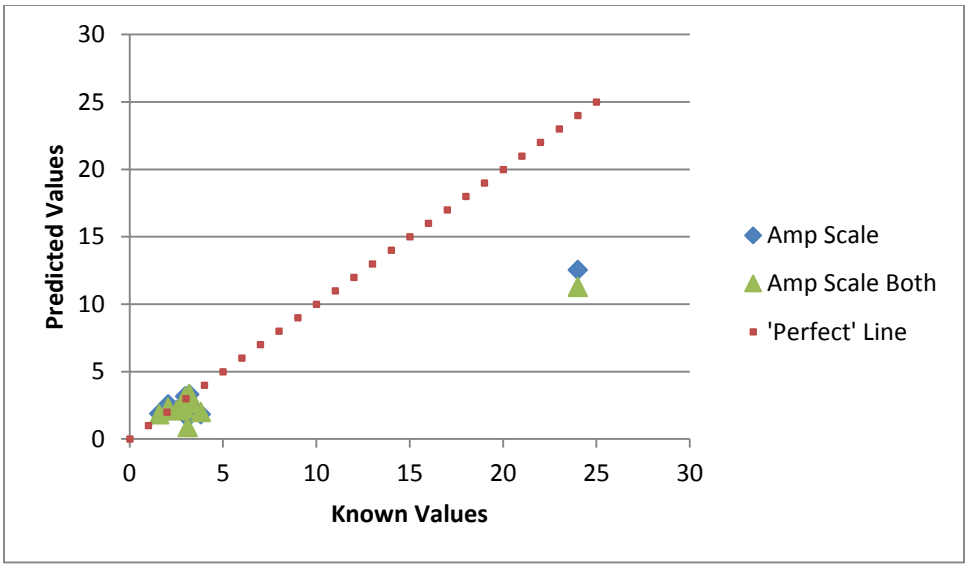


*Figure 4.20.* MgO Amplitude Scaling Model Predictions

***4.2.7.5 Spectral derivatives.*** The next method involved using an approximation of the derivative of each spectrum for calibration and testing instead of the spectrum itself, so as to use slope trends rather than light intensity values to predict composition, as inspired by Tucker et. al.'s work [36]. A point to point slope for each subsequent light intensity value for each spectrum was determined and used as an alternate X data set with one less variable than the original. Negative values were not removed, nor were the spectra normalized to the total light emission in this case. The results of this method are shown in Figures 4.21 through 4.25 below. In nearly all cases, the predictions using this method were less accurate and more variable than the Base Model, and this method was rejected.

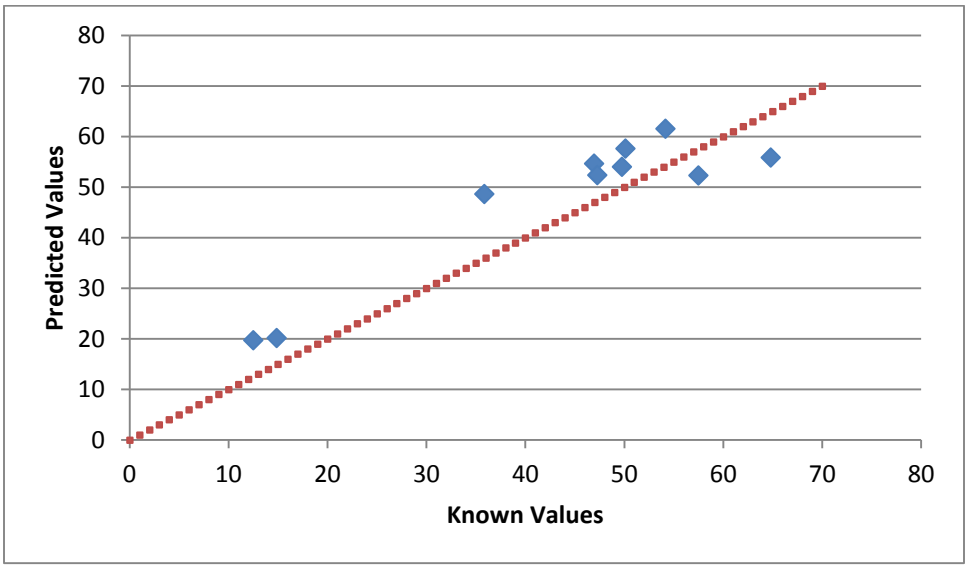


*Figure 4.21.* $SiO_2$ Derivative Model Predictions

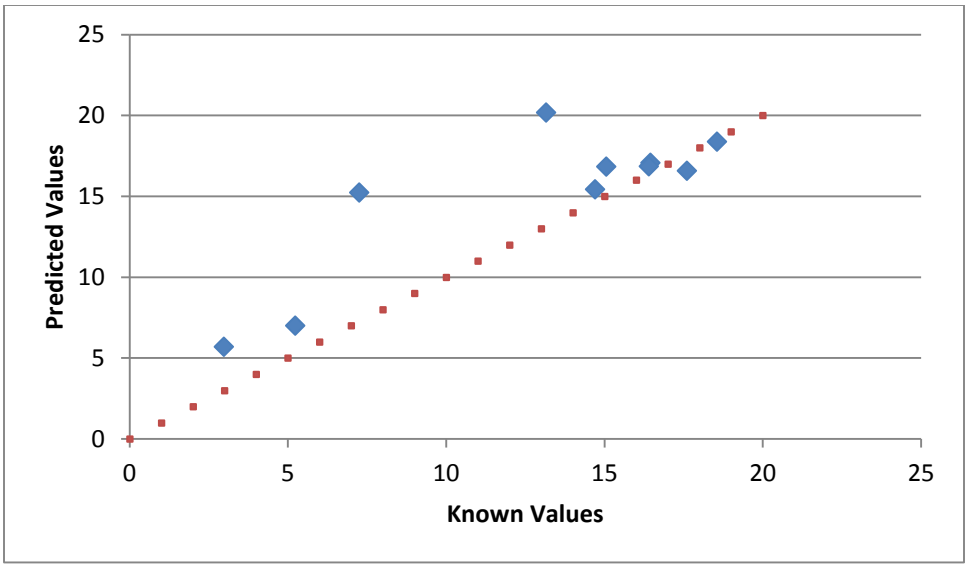


*Figure 4.22.* $Al_2O_3$ Derivative Model Predictions

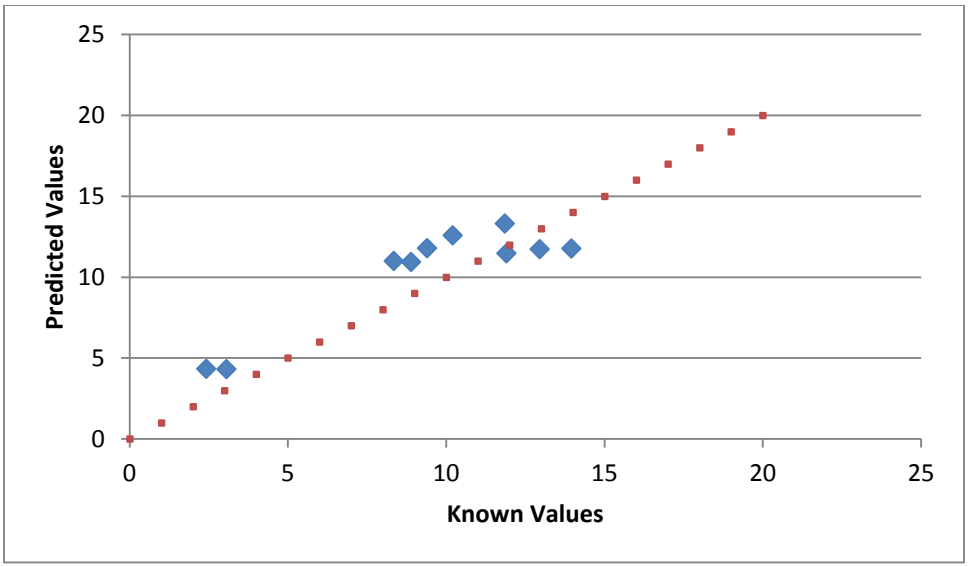


*Figure 4.23.* $Fe_2O_3$ Derivative Model Predictions

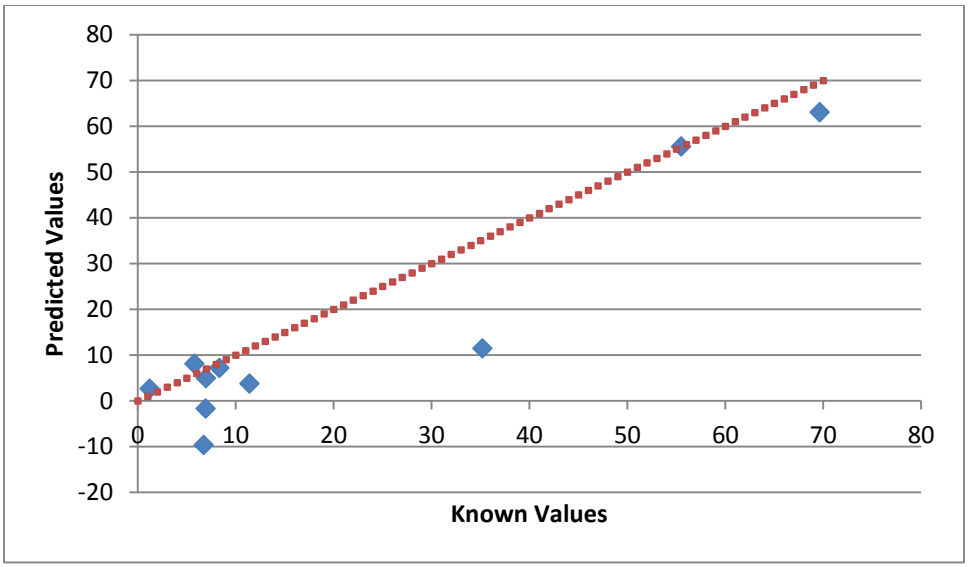


*Figure 4.24.* CaO Derivative Model Predictions

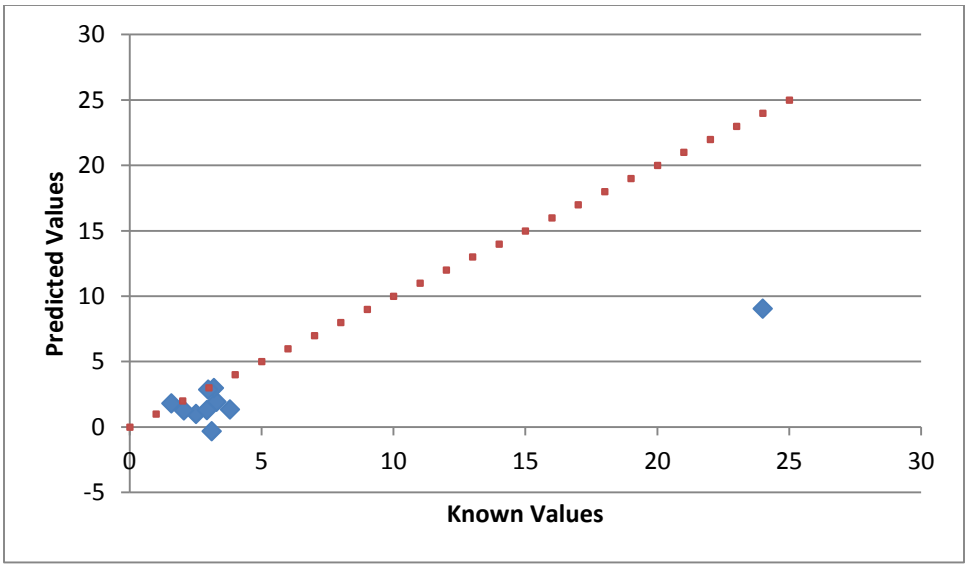


*Figure 4.25.* MgO Derivative Model Predictions

***4.2.7.6 Split training set.*** The final method explored was also partially inspired by the work by Tucker et al. This technique involved reducing the range of values present in the calibration set by calibrating two or more separate models as opposed to a broad base one. Tucker et al. suggested that by applying a broad base model to obtain a 'first guess' of a stone's composition, and then applying an appropriate, more specialized model for a more precise prediction, individual models can become more accurate because they consider a more narrow range of possibilities [36]. In this case, samples were divided into carbonate and non-carbonate rocks for the sake of providing an intuitive classification of samples. The models were otherwise calibrated similar to the Base Model. Figures 4.26 through 4.30 show the results for the model corresponding to the stone's classification; carbonate or non-carbonate.

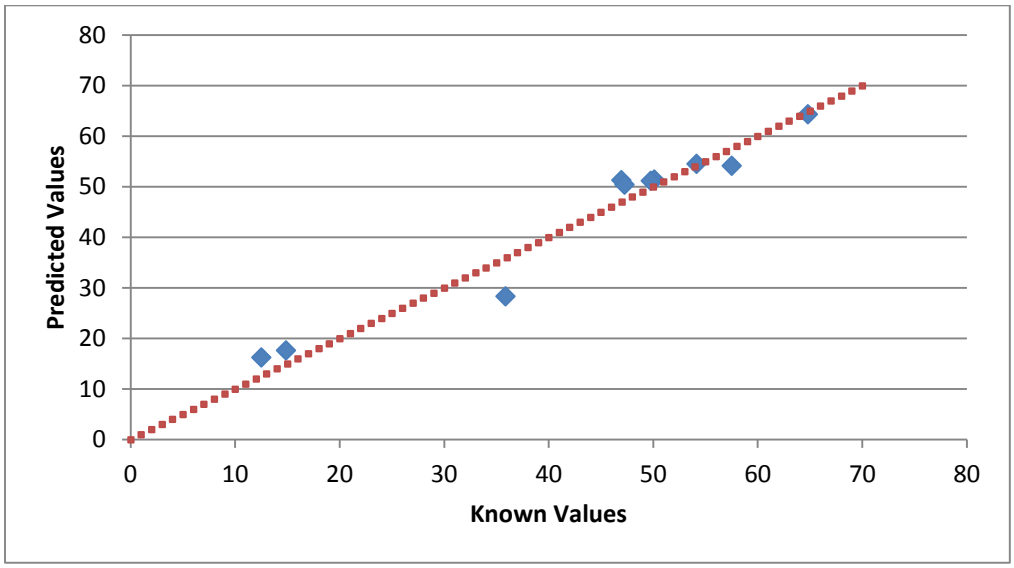


*Figure 4.26.* $SiO_2$ Split Training Model Predictions

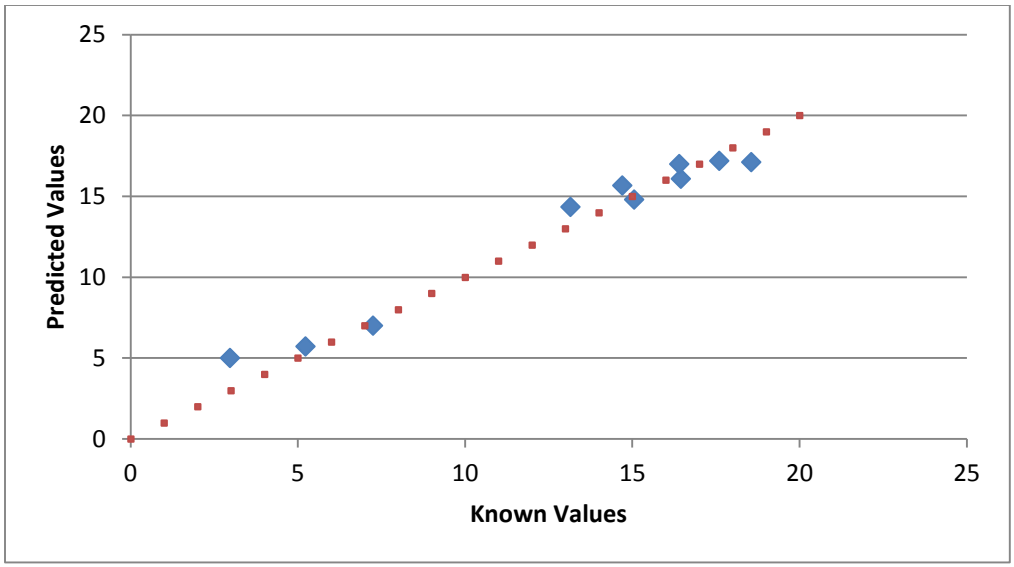


*Figure 4.27.* $Al_2O_3$ Split Training Model Predictions

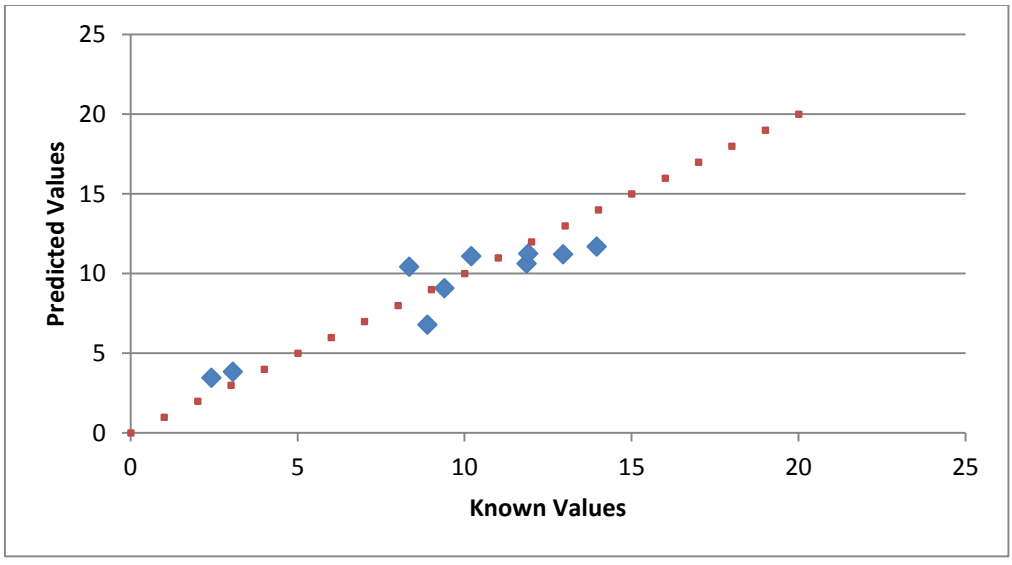


*Figure 4.28.* $Fe_2O_3$ Split Training Model Predictions

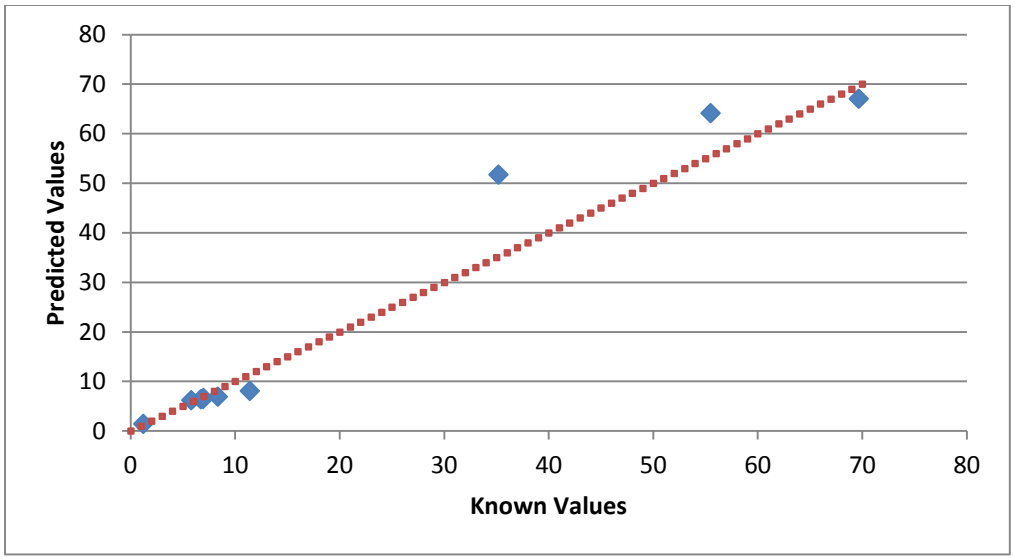


*Figure 4.29.* CaO Split Training Model Predictions

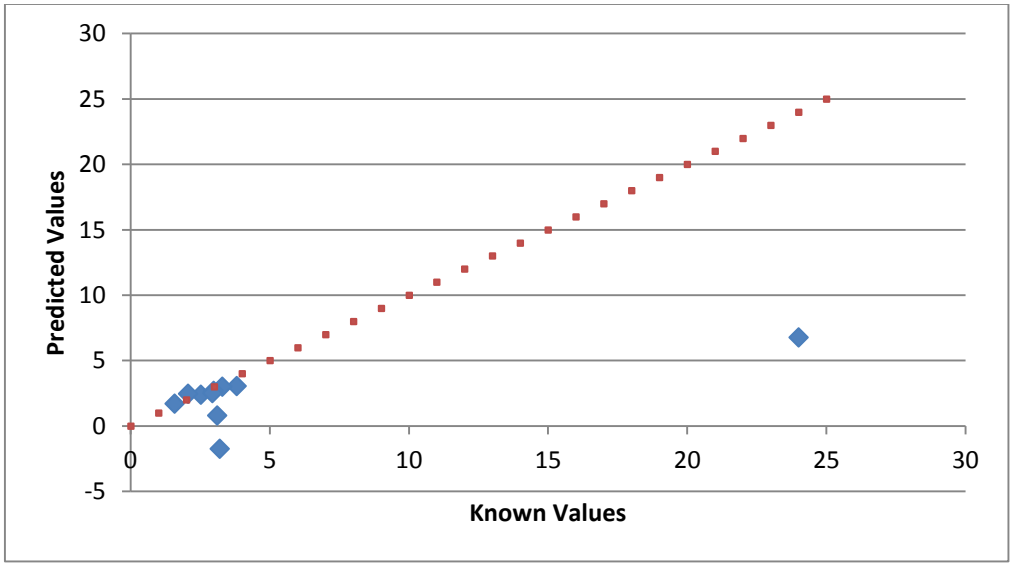


*Figure 4.30.* MgO Split Training Model Predictions

While imperfect, this method showed promise; typically yielding more accurate and more consistent results, likely due in part to reducing variability caused by chemical matrix effects within each model. The remaining error, particularly in the carbonate stone model, was likely caused primarily by a lack of calibration data. Calibrating each model using data collected from additional stone types would be expected to improve their accuracy. Regardless, the performance of these split models is generally an improvement over the Base Model, and further models were calibrated building on this method.

**4.2.8 Combined method models.** To observe the full effects of dividing the training data set, a series of models were developed and tested which used the split training method in combination with the other techniques. In each case, two separate models were developed using the previous pre-processing techniques, and testing data was applied to the corresponding model for its classification.

***4.2.8.1 Split Y-scaling model.*** The results of using Y-Scaling in combination with a split training set are shown in Figures 4.31 through 4.35. Each produced similar results, suggesting that the previous failures of the ratio:1 scaling may have been caused by the variability of the samples, or through an error during analysis. Regardless, this method produces accurate, reproducible results, and the Y-Scaling from 0:1 with split training was selected for final use.

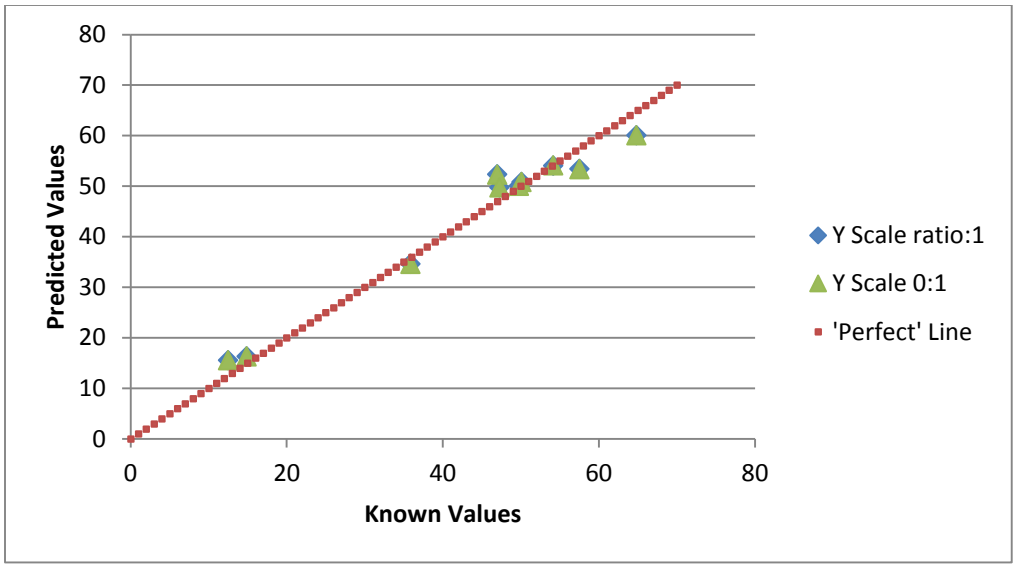


*Figure 4.31.* $SiO_2$ Split Training, Y-Scaling Model Predictions

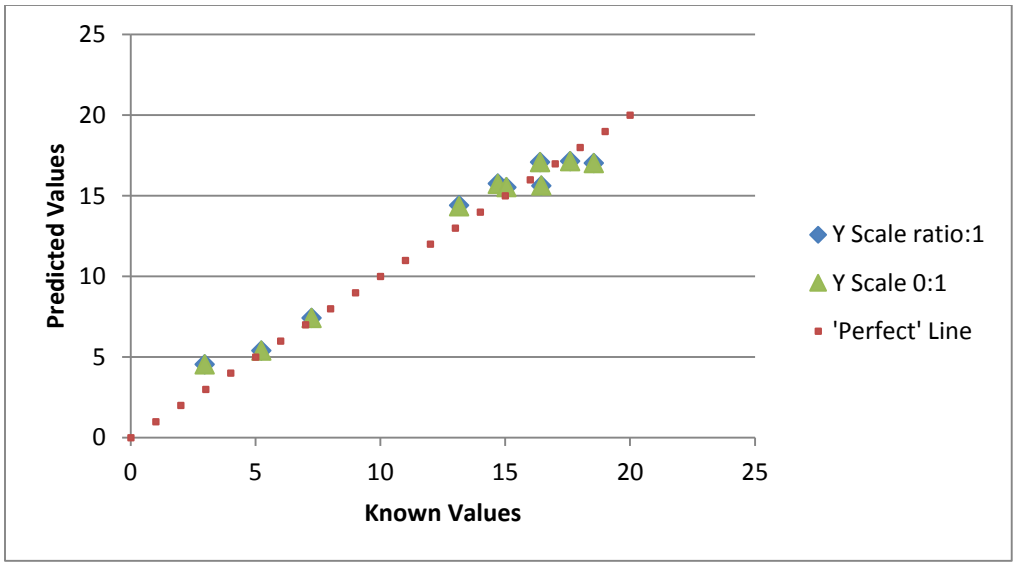


*Figure 4.32.* $Al_2O_3$ Split Training, Y-Scaling Model Predictions

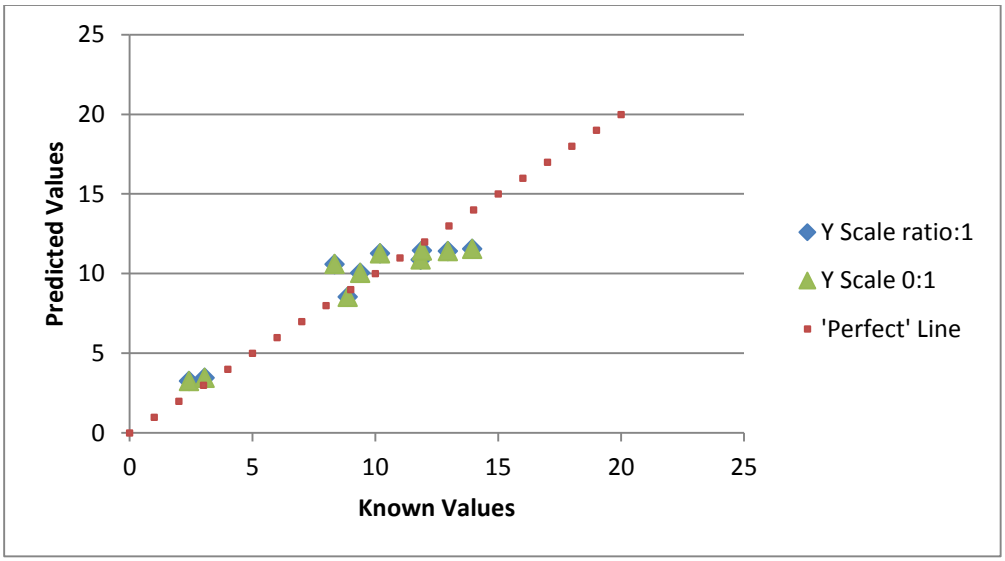


*Figure 4.33.* $Fe_2O_3$ Split Training, Y-Scaling Model Predictions

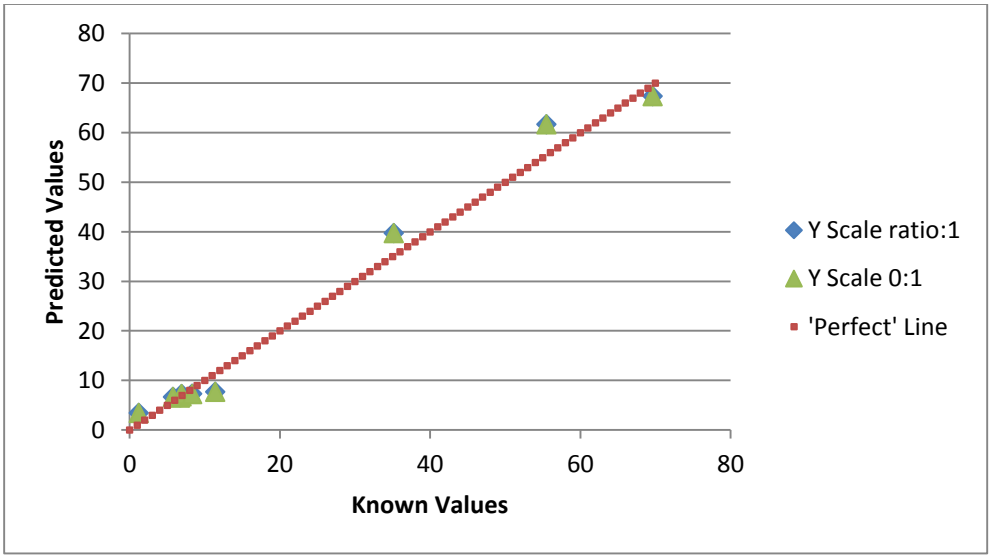


*Figure 4.34.* CaO Split Training, Y-Scaling Model Predictions

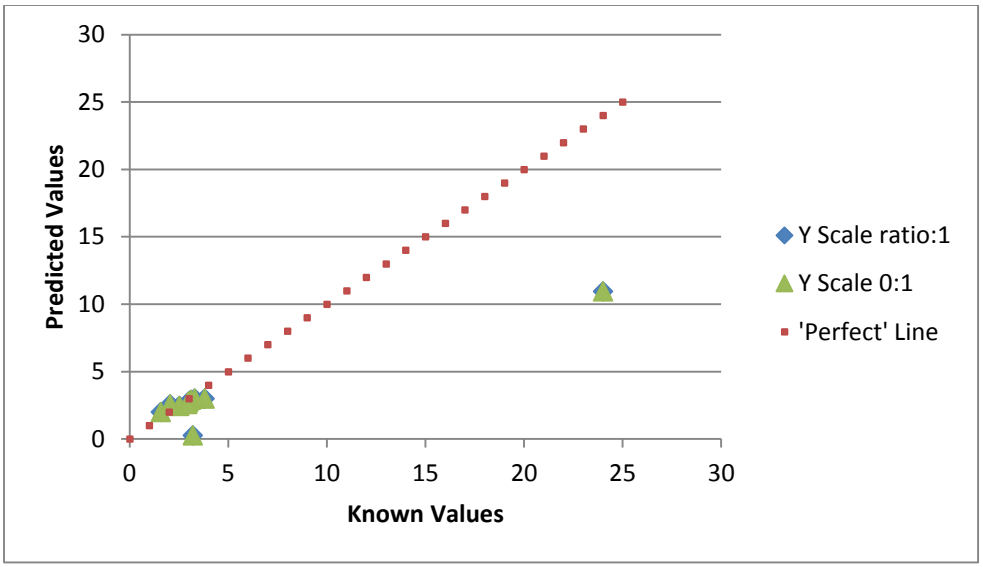


*Figure 4.35.* MgO Split Training, Y-Scaling Model Predictions

***4.2.8.2 Split averaged models.*** Figures 4.36 through 4.40 below show the results of averaging data sets for the separate carbonate and non-carbonate models. While a significant improvement over the original averaged data set model, this did not outperform the Y-Scaling with split training model, and so it was not selected for final use.

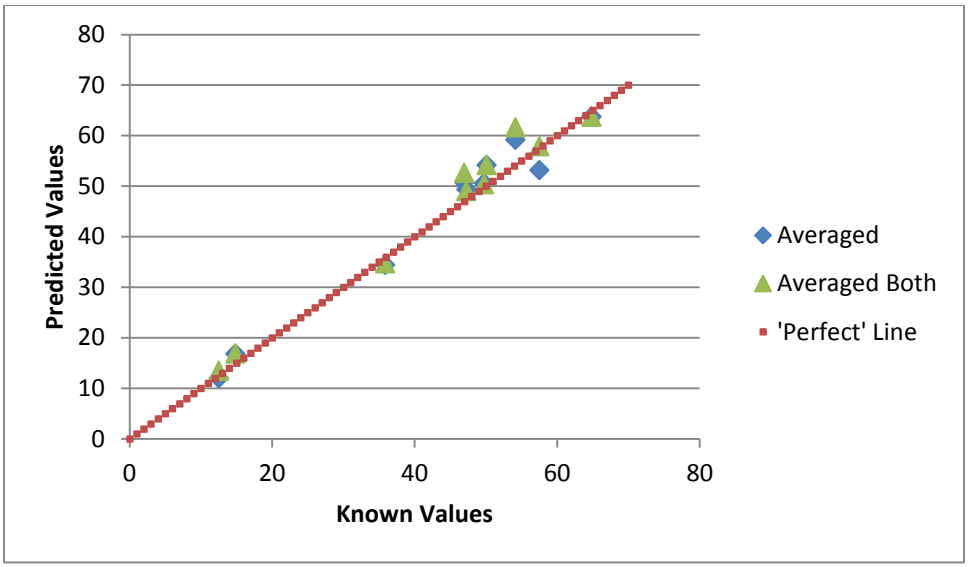


*Figure 4.36.* $SiO_2$ Split Training, Averaged Model Predictions

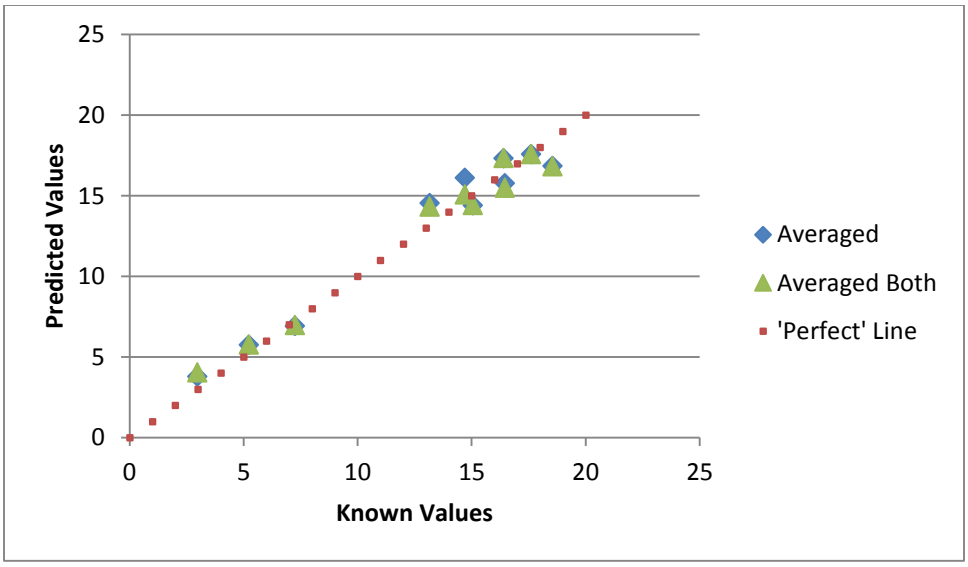


*Figure 4.37.* $Al_2O_3$ Split Training, Averaged Model Predictions

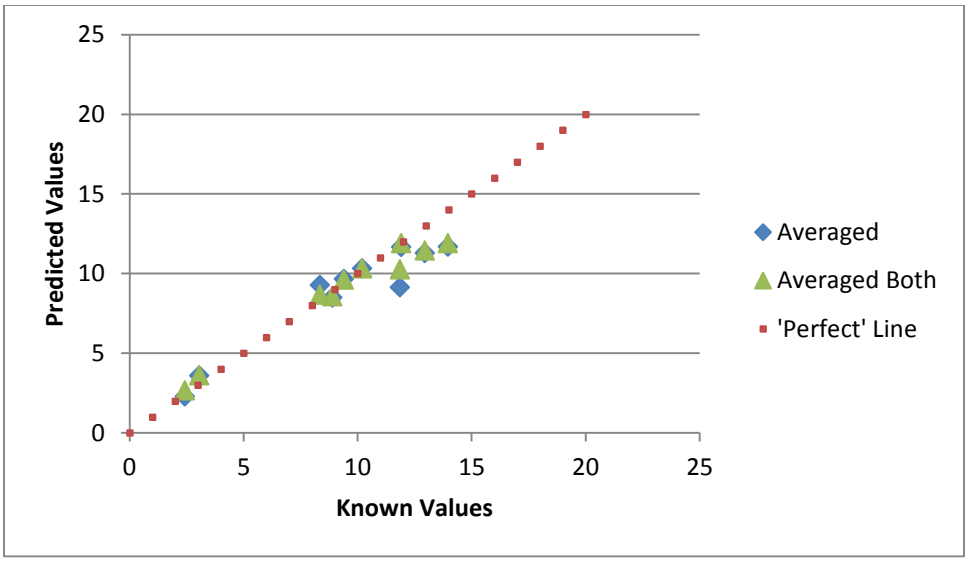


*Figure 4.38.* $Fe_2O_3$ Split Training, Averaged Model Predictions

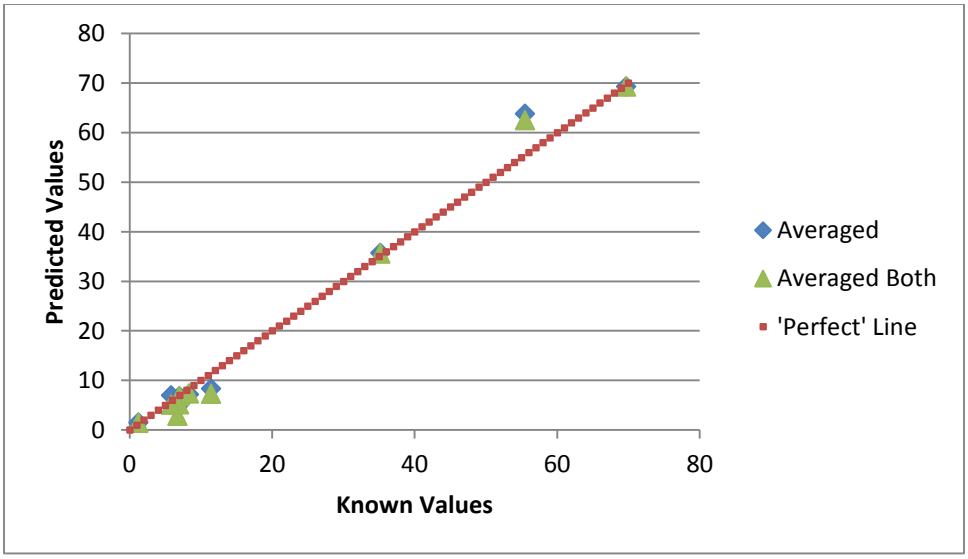


*Figure 4.39.* CaO Split Training, Averaged Model Predictions

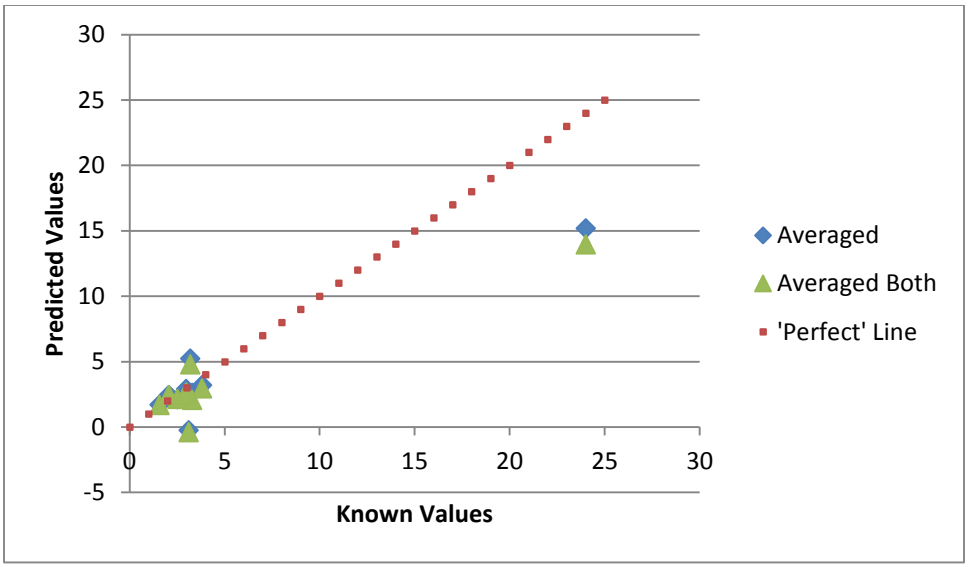


*Figure 4.40.* MgO Split Training, Averaged Model Predictions

***4.2.8.3 Split amplitude scaling.*** Figures 4.41 through 4.45 show the results of using the previous amplitude scaling on a split training set. While an improvement over using amplitude scaling alone, results continued to be variable and less accurate than other methods, and this technique was no longer used.

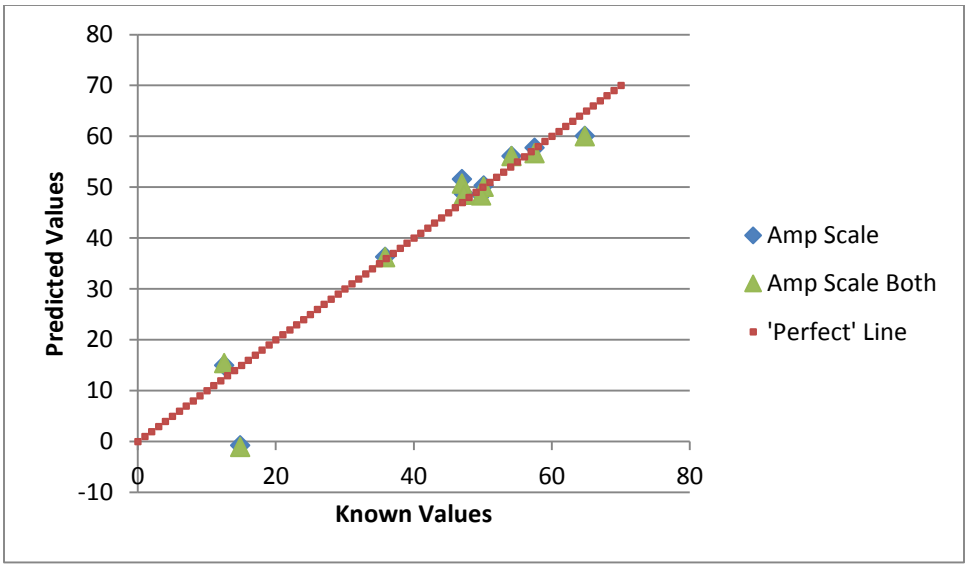


*Figure 4.41.* $SiO_2$ Split Training, Amplitude Scaling Model Predictions

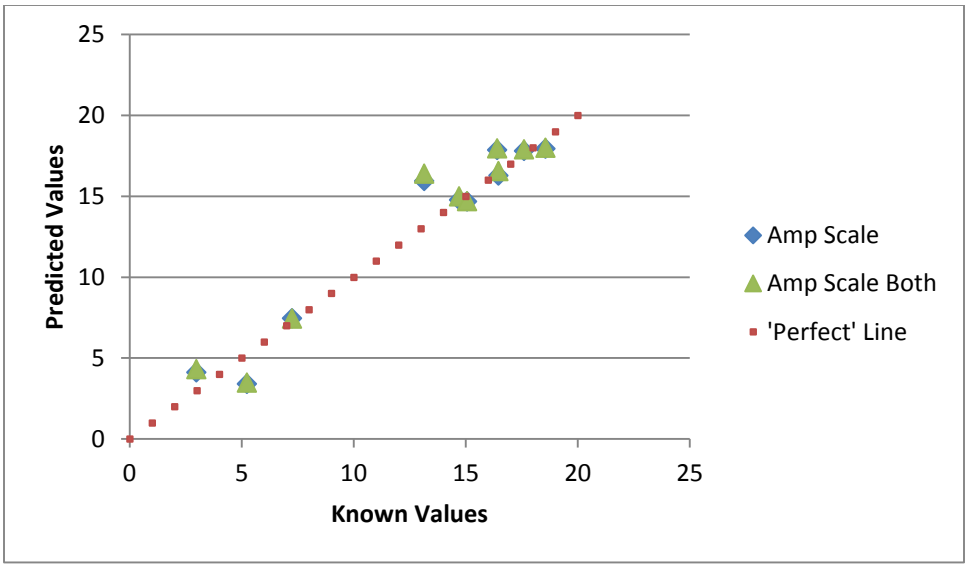


*Figure 4.42.* $Al_2O_3$ Split Training, Amplitude Scaling Model Predictions

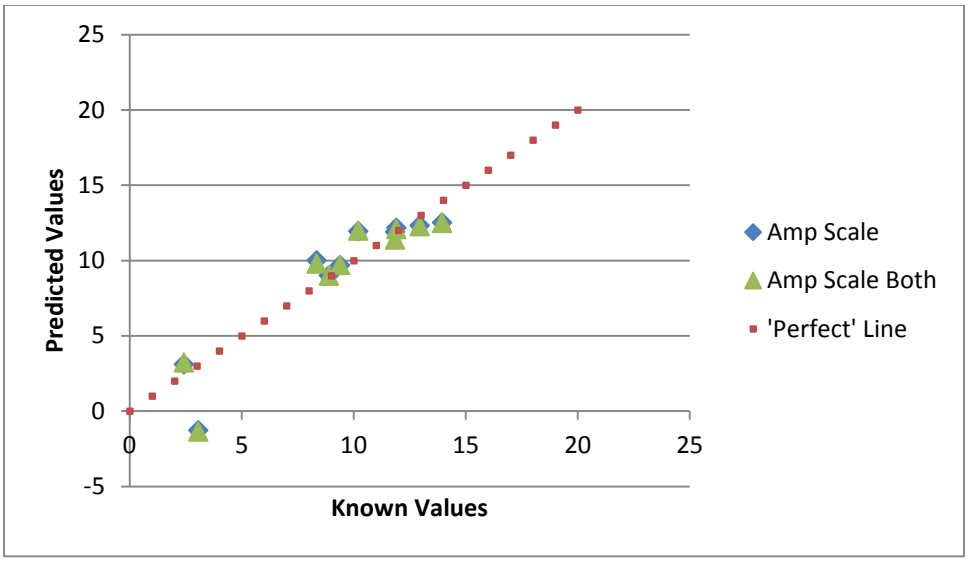


*Figure 4.43.* $Fe_2O_3$ Split Training, Amplitude Scaling Model Predictions

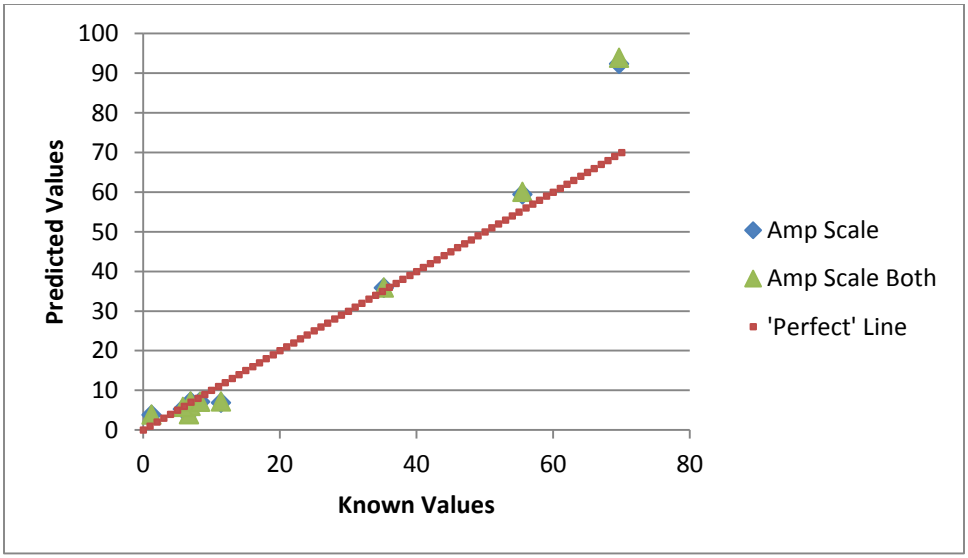


*Figure 4.44.* CaO Split Training, Amplitude Scaling Model Predictions

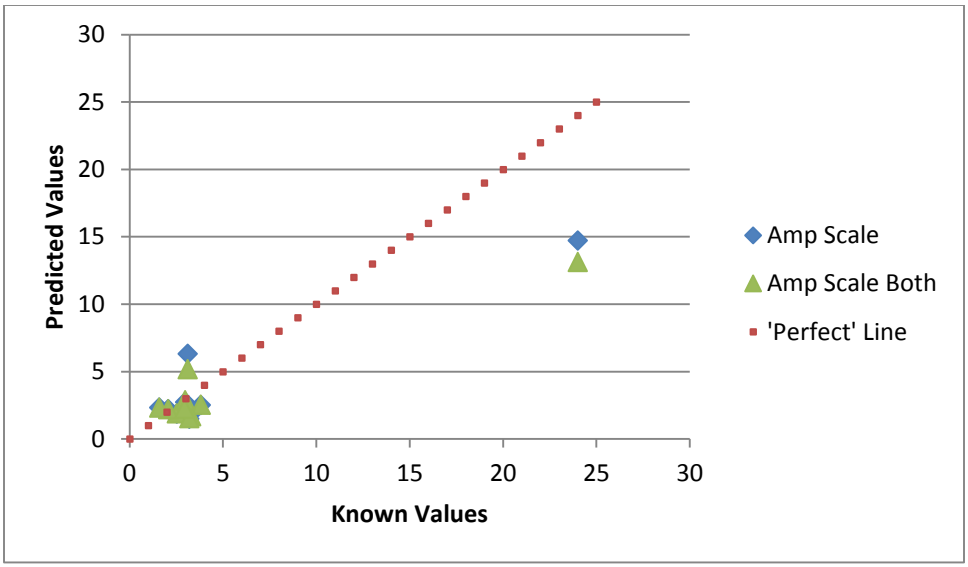


*Figure 4.45.* MgO Split Training, Amplitude Scaling Model Predictions

***4.2.8.4 Split derivative model.*** Figures 4.46 through 4.50 below show the results of using the derivative spectra method on the split training sets. Again, while it is an improvement over the broad base derivative model, there are more accurate and more reproducible alternatives, and this method was not used moving forward.

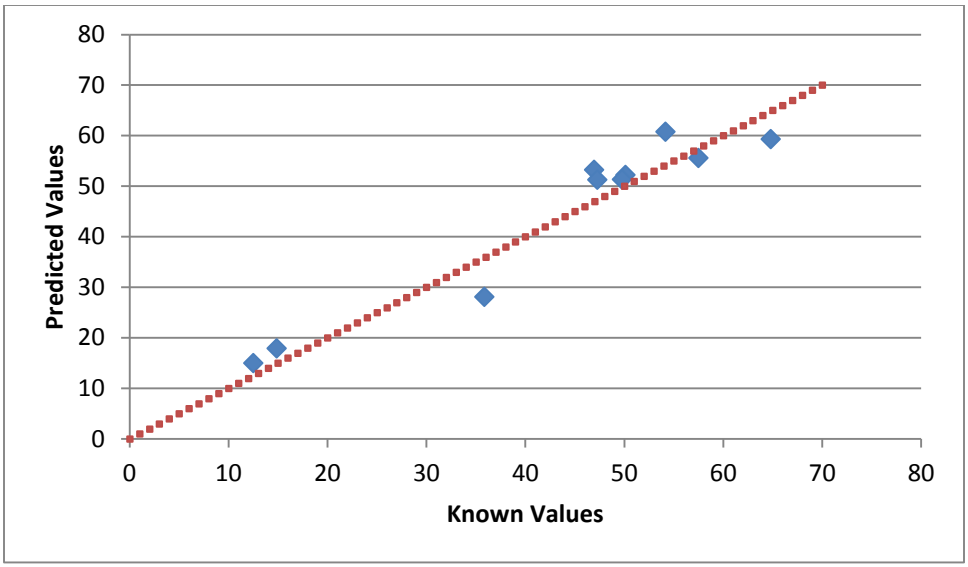


*Figure 4.46.* $SiO_2$ Split Training, Derivative Model Predictions

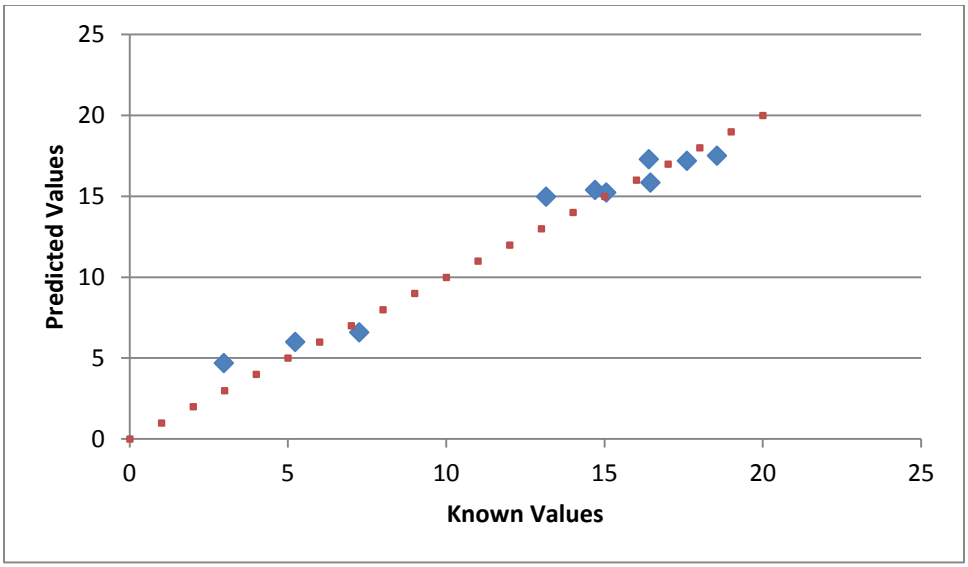


*Figure 4.47.* $Al_2O_3$ Split Training, Derivative Model Predictions

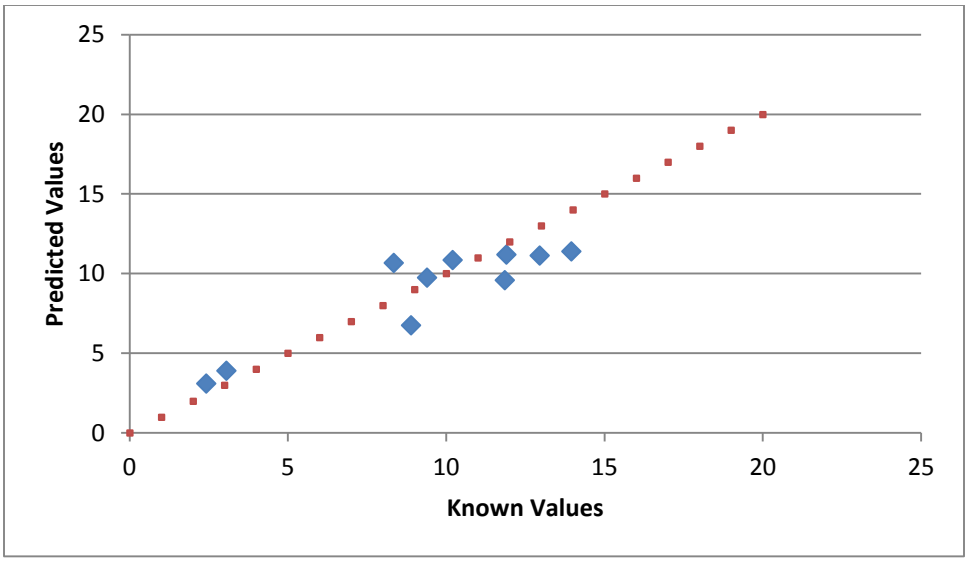


*Figure 4.48.* $Fe_2O_3$ Split Training, Derivative Model Predictions

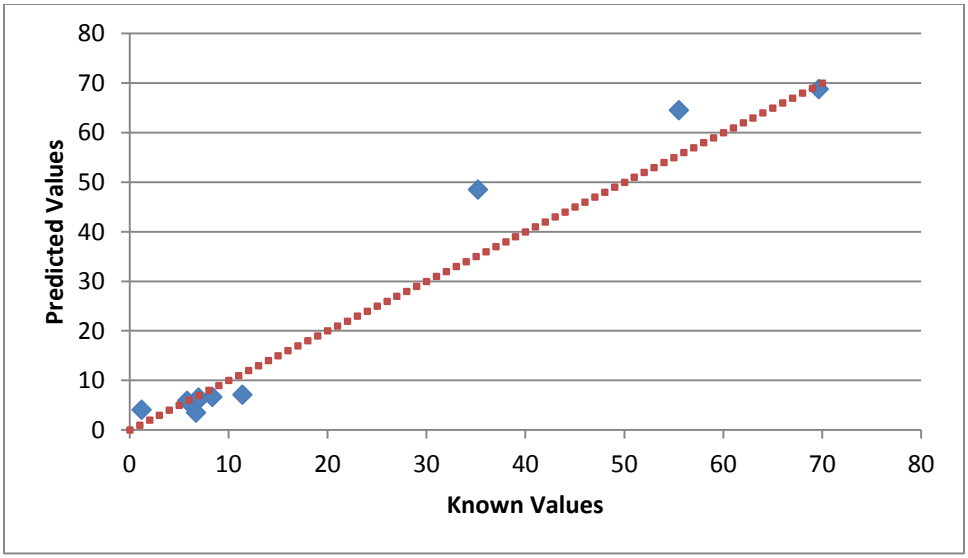


*Figure 4.49.* CaO Split Training, Derivative Model Predictions

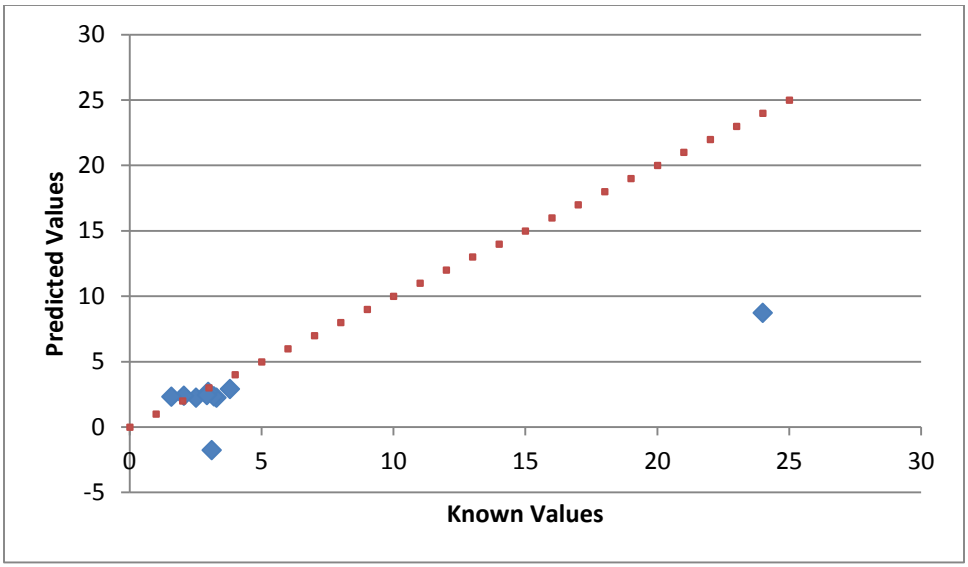


*Figure 4.50.* MgO Split Training, Derivative Model Predictions

Following these results, using a combination of the split training model and 0:1 Y-Scaling was determined to be the optimal strategy for this application, and would be used consistently moving forward.

**4.2.9 Finalizing calibration strategy.** Once the model calibration strategy had been selected, the other data pre-processing steps were revisited before the strategy was finalized. Three alternate model were developed and tested; one considering models which selected a number of PLS components as the number required before the next two consecutive PLS components would both explain less than an additional 1% variation in the known composition values, one which did not use center clipping to remove negative light intensity values, and one which performed the Y-Scaling separately for the carbonate and non-carbonate models, as opposed to considering the overall data set in its entirety, as had been done previously.

While the first alternate model performed reasonably well in terms of accuracy, this strategy would have caused 5 PLS components to be used for the carbonate rock model while 26 would be used for the non-carbonate rock model, which is likely excessive. As this alternate model did not perform significantly better than the previous strategy, future models would continue to select the number of PLS components based on the first component which would explain less than 1% additional variation.

The second alternate model strategy was rejected almost immediately because the amount of variation explained by each PLS component using this strategy had an unusual distribution; which if the normal method was applied would cause 0 PLS components to be selected which is not an acceptable number. While a number may have been selected manually, the distribution of explained variation was more uniform than previous models, as opposed to the normal depreciating trend, and an unreasonable number would be required for the model to explain more than a small fraction of the overall variation in the data set.

Models calibrated via the third strategy performed very similarly to the original case, with the exception of the Glen Mills Gneiss sample, which experienced significant changes in accuracy and distribution of predictions. At this time, the original method wherein Y-Scaling is applied to the overall data set and not for each individual model was determined to be marginally superior, however this conclusion will be confirmed using models calibrated with a larger number of samples.

### 4.3 Determining Optimal Testing Set Size

Once an optimal model calibration strategy had been selected, efforts moved on to selecting an appropriate testing set size for finding accurate predictions. At this time, predictions were developed from the results of LIBS tests at 5 points each on 5 samples for a given type of stone, for a total of 25 separate predictions, which were then averaged together. To determine a reasonable sample size for accurate predictions, the average predictions for each type of stone were determined using a number of test spectra ranging from 1 to 25. Averages were determined using both a simple list of predictions moving from top to bottom, and using the average of 1 to 5 points across all 5 samples. A sample size was then selected such that the addition of more testing data would have little relative effect on the average. With few exceptions, prediction averages stabilized by about 10 to 15 predictions, which was selected as a minimum recommended sample size, however a larger sample size may be used, if desired, or if one encounters a particularly inhomogeneous sample. The two averaging strategies also revealed that the number of samples tested was generally of greater overall importance to prediction accuracy than the number of locations tested per sample, as was expected. However, given the variability of predictions from some types of stone; likely less homogeneous stones, it is recommended that at least 2 to 3 locations per sample be tested.

### 4.4 Development of a User-Friendly Program

Once an optimal model calibration strategy and a testing sample size had been selected, the research team began working on developing a user-friendly program for calibrating and testing models; allowing for future development, and for making more

rapid predictions from existing models. An overview of the program concept, and operation of the Graphical User Interface (GUI) is described below. As the program run time can require several seconds to several minutes depending on the computer capabilities, the size of data sets, and the format under which data sets were saved, the user will be provided with progress messages at each step so that it is clear that the program is running correctly. The program will be set to one of two modes; calibration or testing; each of which is intended to require as few user inputs as possible. All programming and the development of the GUI was completed in MatLAB.

**4.4.1 Calibration mode.** While in Calibration Mode, the model input field will by faded out, as it does not apply to this mode. The user will use a browser to select a file containing the input X and corresponding Y data, which will have been arranged previously into a standard format by a separate program. The user will then have the option to specify the number of PLS components for each of the broad base, carbonate, and non-carbonate models, or allow the program to select an appropriate number automatically according to a standard procedure outlined below. The user then simply presses the 'Run' button on the GUI.

***4.4.1.1 Calibration – automatic component selection.*** If the user wishes the program to select a number of PLS components automatically, the program will apply all of the finalized pre-processing steps; removal of negative values, normalization of spectra, and Y-Scaling, to the raw data sets. It will then attempt to calibrate the model with 25 PLS components, including the optional cross-validation function. It will then search the second row of the 'PCTVAR' output matrix until it finds a PLS component which explains less than 1% additional variation in the known values, and will store a

number equaling one less than this count. It will then recalibrate the model using that number of PLS components. The program will then divide the data sets into samples known to contain more or less than 15% CaO; which was selected as a reasonable value given past results as a simple division between carbonate and non-carbonate rocks. Note that this value may be changed, if necessary. The program then repeats the calibration for each of the two specialized models, and the user is prompted to save the 3 models as a singular file which can then be easily selected for testing purposes.

***4.4.1.2 Calibration – manual component selection.*** If the user chooses to manually specify a number of PLS components, the program will run normally, but use the input numbers of PLS components instead of selecting one automatically whenever a number of PLS components is required, and the program will store the 'PCTVAR' matrix produced for each model. Once all three models are calibrated, the program will display all three of the 'PCTVAR' matrices along with the total amount of variation in known values explained, and the user will be prompted to either rerun the program using different numbers of PLS components, or simply save the produced models.

**4.4.2 Testing mode.** While in Testing Mode, the options to use automatic or manual PLS component selection are faded out, as they are not necessary for this mode. The user is provided with browsers to select a file or folder containing unknown sample input LIBS data, and a file containing the previously calibrated models. The user then simply needs to press the 'Run' button on the GUI to obtain a predicted chemical composition for the unknown sample.

When run, the program will automatically compile the input sample data, and apply all pre-processing steps, as previously, to adjust the raw data to a useable form. The program will then perform the normal matrix operations required to produce an output (see Appendix A), and apply the reverse of the Y-Scaling adjustments, as per the maximum and minimum composition values stored in the model file. The program will then identify whether the sample is a carbonate or non-carbonate rock based on this initial prediction, and then utilize the appropriate model to make a more accurate prediction through the same method. Next, the program will determine an average and standard deviation for each compound from the predicted values. These values are then displayed for the user and the user is prompted to input a confidence percentile, which will cause the program to calculate a corresponding appropriate confidence interval for each predicted value. When it has done so and displayed these intervals, or if the user does not require a confidence interval, the user will be prompted to save the predictions.

# Chapter 5

# Conclusions

## 5.1 Summary of Findings

Throughout this study, Laser-Induced Breakdown Spectroscopy was used to obtain characteristic light spectra corresponding to various types of aggregate stones collected from various quarries and sources in New Jersey and surrounding states. X-Ray Fluorescence tests were performed by the New Jersey Department of Transportation to obtain the chemical compositions of each stone, assuming all elements to be bound in oxides, and Partial Least Squares Regression analysis was used to develop predictive models using these known values corresponding to each collected spectrum of light.

Throughout this research, a variety of tests were conducted and system timing and laser energy emission were optimized. The final, and most reliable timing was determined to use a flashlamp-Q-switch delay of 400 μs and a spectrometer delay of 6.3 μs for the Quantel, Brilliant B laser used for lab testing. Alternative testing setups were considered, including using a higher energy laser pulse in conjunction with a beam splitter, and/or using radiofrequency (RF) heating to extend the useful life of the plasma glow resulting from a laser pulse striking a sample. It was determined that the beam splitter arrangement resulted in a less focused laser beam striking the sample, leading to less consistent results, and the RF enhancement system was not determined to produce significant improvement in test results, and would be too cumbersome to be implemented in the field. For these reasons neither of these alternatives was selected for continued use. It was determined that by collecting test data as the sum of the light emitted following

many laser pulses, variability in test data due to randomness in the system became less significant, and this strategy continued to be used.

Various combinations of data pre-processing techniques were used in attempts to identify the strategy which would produce the most accurate and reliable predictive model. While applying center clipping or other baseline subtraction techniques was not found to significantly improve model accuracy, it continued to be used to remove negative light intensity values caused by signal noise. The selected optimal data pre-processing strategy was found to be the following:

- Center Clipping with a threshold of 0 was applied to remove negative values caused by signal noise from the data.
- Each collected spectrum was intensity-normalized such that the sum of all light intensity values was 1.
- Known chemical composition values were scaled to values between 0 and 1 so that the calibration algorithm would consider each compound with equal priority. The reverse adjustments were then applied to values predicted by the model.

The adjusted spectra were then used to develop predictive models using PLSR. The models were calibrated using a number of PLS components such that less than 1% of the total variation in the known values would be explained by adding another. After considering a combination of data pre-processing and model calibration strategies, it was determined that the most accurate and reliable results would be obtained by first using a broad-base model developed through this technique to determine whether a sample is a carbonate or non-carbonate rock, before applying a model calibrated using only samples

within that sub-set, but otherwise calibrated the same way; using the same spectra data pre-processing as above. This split model training strategy results in two independent models which consider a more narrow range of possibilities, allowing each to be more specialized and accurate overall, and reducing the influence of chemical matrix effects within each. This combined split training and Y-Scaling method was found to produce very similar values when compared to X-Ray Fluorescence results.

### 5.2 Recommendations and Feasibility

This research shows that using LIBS as a means of in-situ analysis of aggregate chemical composition is feasible, and it should be feasible to interpret these results for quality control of aggregate mineralogy. While this alternative testing method is not intended to replace traditional testing methods, it can be used for rapid analyses in the field to obtain reasonably accurate and consistent results without significantly disrupting construction timelines. Such a system may be transported without the need for specialized equipment beyond a hatchback truck or similar vehicle, and field testing will begin in the near future while the research team finalizes the logistics of the system's transport and maintenance. Based on these findings, the research team recommends that such a system be implemented for initially small-scale use so as to monitor for remaining issues with the system, and increase use if no major issues are encountered.

Given the results of the model development throughout this research, it became evident that using a variety of stone types to calibrate the predictive models generally improved accuracy overall. It is however entirely possible that an aggregate stone encountered will be significantly different than samples used to calibrate the model, and

this model will not be expected to perform well with such samples. Given this and past experience, the research team recommends improving and updating the model over time as new samples with known compositions become available. To better facilitate continued development, the research team has developed a simple, user-friendly program so that new data could be added to the data sets used to calibrate the model, and revised models can be rapidly developed with minimal user inputs. This program also facilitates testing unknown sample data rapidly, with minimal user inputs so as to improve the speed at which accurate predictions can be obtained.

### 5.3 Future Work

- Continue refining predictive models as new samples become available.
- Develop a standard method of interpreting chemical composition predictions in terms of aggregate mineralogy.
- Complete field testing setup, confirm validity of existing models for use with data collected by this new system, and conduct field tests.
- Finalize system transport methods.
- Determine required particle morphological characteristics.
- Consider various imaging techniques for bulk analysis of aggregate stone samples in the field.
- Select the most appropriate method and develop models (if necessary) to determine morphological traits using this method.
- Consider the feasibility of using this method in the field as a means of in-situ quality control.

- Develop a user manual and train NJDOT staff in the use of mineralogical and morphological quality control systems and models.

## References


[1] F. L. Roberts, P. S. Kandhal, E. R. Brown, D.-Y. Lee and T. W. Kennedy, Hot Mix Asphalt Materials, Mixture Design, and Construction, 2nd ed., Lanham, Mayland: NAPA Educational Foundation, 1996.

[2] NJDOT, "New Jersey Department of Transportation Standard Specifications for Road and Bridge Construction," 2007. [Online]. Available: http://www.state.nj.us/transportation/eng/specs/2007/Division.shtml.

[3] P. Kandhal and E. Bishara, "Evaluation of Limestone Aggregates in Asphalt Wearing Courses," National Center for Asphalt Technology, Auburn University, Alabama, 1992.

[4] ASTM, "ASTM D3042-09: Standard Test Method for Insoluble Residue in Carbonate Aggregates," ASTM International, West Conshohocken, PA, 2009.

[5] K. Miskovsky, "Enrichment of Fine Mica Originating From Rock Aggregate Production and Its Influence on the Mechanical Properties of Bituminous Mixtures," *Journal of Materials Engineering and Performance, Vol 13 (5)*, pp. 607-611, 2004.

[6] E. Johansson, "Free Mica in Crushed Rock Aggregates," Luleå University of Technology, Department of Civil, Mining and Environmental Engineering, Division of Mining and Geotechnical Engineering, Sweden, 2008.

[7] AASHTO T112, "AASHTO T 112: Clay Lumps and Friable Particles in Aggregate".

[8] FHWA, "Superpave Mixture Design Guide," US Department of Transportation, Washington, D.C, 2001.

[9] FHWA, "Chapter 2 Alkali-Silica Reaction," July 2006. [Online]. Available: http://www.fhwa.dot.gov/publications/research/infrastructure/pavements/pccp/06073/chapt2.cfm.

[10] W. Chesner and N. McMillan, "Automated Laser Spectrographic Pattern Matching for Aggregate Identification," Highway IDEA Program, 2012.

[11] S. Nelson, "Mineral Chemistry," 2013. [Online]. Available: http://www.tulane.edu/~sanelson/eens211/mineral_chemistry.htm.

[12] R. E. Wolf, "What is ICP-MS?," March 2005. [Online]. Available: http://crustal.usgs.gov/laboratories/icpms/intro.html.

[13] K. Wirth and A. Barth, "X-Ray Fluorescence (XRF)," 11 December 2013. [Online]. Available: http://serc.carleton.edu/research_education/geochemsheets/techniques/XRF.html.

[14] J. Goodge, "Electron probe micro-analyzer (EPMA)," 23 July 2012. [Online]. Available: http://serc.carleton.edu/research_education/geochemsheets/techniques/EPMA.html.

[15] D. A. Cremers and L. J. Radziemski, "Handbook of Laser-Induced Breakdown Spectroscopy," John Wiley & Sons, Ltd., 2006.

[16] W. e. a. Pierce, "Automated Laser Spectrographic Pattern Matching For Aggregate Identification," 2006.

[17] W. Pierce, S. M. Christian, M. J. Myers and J. D. Myers, "Field-Testing for Environmental Pollutants Using Briefcase Sized Portable LIBS System," in *3rd International Conference on Laser Induced Plasma Spectroscopy and Applications*, 2004.

[18] G. Globle, "White Paper: How Lasers Function," 5 February 2008. [Online]. Available: http://www.maximumpc.com/article/white_paper_how_lasers_function.

[19] R. Paschotta, "Q-Switching," October 2008. [Online]. Available: http://www.rp-photonics.com/q_switching.html.

[20] R. Paschotta, "Q-Switched Lasers," October 2008. [Online]. Available: http://www.rp-photonics.com/encyclopedia_cite.html?article=Q-switched%20lasers.

[21] E. e. a. Tognoni, "Calibration-Free Laser-Induced Breakdown Spectroscopy: State of the art," *Spectrochimica Acta Part B, Vol. 65*, pp. 1-14, 2009.

[22] C. Pasquini, J. Cortez, L. M. C. Silva and F. B. Gonzaga, "Laser induced breakdown spectroscopy," *Journal of the Brazilian Chemical Society, Vol 18, No. 3*, pp. 463-512, 2007.

[23] E. Morgan, "LIBS Detects Explosives at a Distance," 2007. [Online]. Available: http://www.rsc.org/Publishing/ChemTech/Volume/2007/12/LIBS_detects_explosives_at_a_distance.asp.

[24] A. e. a. Taffe, "Development of a portable LIBS-device for quality assurance in concrete repair," *Concrete Repair, Rehabilitation and Retrofitting II,* 2009.

[25] A. e. a. Mansoori, "Quantitative analysis of cement powder by laser induced breakdown spectroscopy," *Optics and Lasers in Engineering, Vol. 49, Issue 3,* pp. 318-323, 2011.

[26] H. Xia and M. C. M. Bakker, "Online Sensor System Based on Laser Induced Breakdown Spectroscopy in Quality Inspection of Demolition Concrete," in *27th International Conference on Solid Waste Technology and Management,* 2012.

[27] A. e. a. De Giacomo, "Experimental and theoretical comparison of single-pulse and double-pulse laser induced breakdown spectroscopy on metallic samples," *Spectrochimica Acta Part B, Vol. 63,* pp. 805-816, 2008.

[28] Y. Liu, M. Baudelet and M. Richardson, "Elemental analysis by microwave-assisted laser-induced breakdown spectroscopy: Evaluation on ceramics," *Journal of Analytical Atomic Spectroscopy,* pp. 1316-1323, 2010.

[29] M. Tampo, M. Miyabe, K. Akaoka, M. Oba, H. Ohba, Y. Maruyama and I. Wakaida, "Enhancement of intensity in microwave-assisted laser-induced breakdown spectroscopy for remote analysis of nuclear fuel recycling," *Journal of Analytical Atomic Spectrometry, Vol. 29,* pp. 886-892, 2014.

[30] F. Rosenblatt, "The Perceptron: A Probabilistic Model for Information Storage and Organization in the Brain," *Psychological Review, 65,* pp. 386-408, 1958.

[31] A. e. a. Koujelev, "Laser-induced breakdown spectroscopy with artificial neural network processing for material identification," *Planetary and Space Science, Vol. 58,* pp. 682-690, 2010.

[32] K. Pearson, "On Lines and Planes of Closest Fit to Systems od Points in Space," *Philosophical Magazine, 2,* pp. 559-572, 1901.

[33] H. Hotelling, "Analysis of a Complex of Statistical Variables into Principal Components," *Journal of Educational Psychology, 24,* pp. 417-441 and 498-520, 1933.

[34] R. De Maesschalck, "Decision criteria for soft independent modelling of class analogy applied to near infrared data," *Chemometrics and Intelligent Laboratory Systems, Vol. 47,* pp. 65-77, 1998.

[35] S. Wold, M. Sjöström and L. Eriksson, "PLS-Regression: a Basic Tool of Chemometrics," *Chemometrics and Intelligent Laboratory Systems, Vol. 58, Issue 2*, pp. 109-130, 2001.

[36] J. M. e. a. Tucker, "Optimization of laser-induced breakdown spectroscopy for rapid geochemical analysis," *Chemical Geology, Vol. 277, Issues 1-2*, pp. 137-148, 2010.

## Appendix A

## PLSR Algorithm and Simple Example

plsregress function as per MATLAB 2014 (Copyright 2007-2010 The MathWorks, Inc.)

```
function [Xloadings,Yloadings,Xscores,Yscores, ...
          beta,pctVar,mse,stats] = plsregress(X,Y,ncomp,varargin)
%PLSREGRESS Partial least squares regression.
%   [XLOADINGS,YLOADINGS] = PLSREGRESS(X,Y,NCOMP) computes a partial least
%   squares regression of Y on X, using NCOMP PLS components or latent
%   factors, and returns the predictor and response loadings.  X is an N-by-P
%   matrix of predictor variables, with rows corresponding to observations,
%   columns to variables.  Y is an N-by-M response matrix.  XLOADINGS is a
%   P-by-NCOMP matrix of predictor loadings, where each row of XLOADINGS
%   contains coefficients that define a linear combination of PLS components
%   that approximate the original predictor variables.  YLOADINGS is an
%   M-by-NCOMP matrix of response loadings, where each row of YLOADINGS
%   contains coefficients that define a linear combination of PLS components
%   that approximate the original response variables.
%
%   [XLOADINGS,YLOADINGS,XSCORES] = PLSREGRESS(X,Y,NCOMP) returns the
%   predictor scores, i.e., the PLS components that are linear combinations of
%   the variables in X.  XSCORES is an N-by-NCOMP orthonormal matrix with rows
%   corresponding to observations, columns to components.
%
%   [XLOADINGS,YLOADINGS,XSCORES,YSCORES] = PLSREGRESS(X,Y,NCOMP)
%   returns the response scores, i.e., the linear combinations of the
%   responses with which the PLS components XSCORES have maximum covariance.
%   YSCORES is an N-by-NCOMP matrix with rows corresponding to observations,
%   columns to components.  YSCORES is neither orthogonal nor normalized.
%
%   PLSREGRESS uses the SIMPLS algorithm, and first centers X and Y by
%   subtracting off column means to get centered variables X0 and Y0.
%   However, it does not rescale the columns.  To perform partial least
%   squares regression with standardized variables, use ZSCORE to normalize X
%   and Y.
%
%   If NCOMP is omitted, its default value is MIN(SIZE(X,1)-1, SIZE(X,2)).
%
%   The relationships between the scores, loadings, and centered variables X0
%   and Y0 are
%
%     XLOADINGS = (XSCORES\X0)' = X0'*XSCORES,
%     YLOADINGS = (XSCORES\Y0)' = Y0'*XSCORES,
%
%   i.e., XLOADINGS and YLOADINGS are the coefficients from regressing X0 and
%   Y0 on XSCORES, and XSCORES*XLOADINGS' and XSCORES*YLOADINGS' are the PLS
%   approximations to X0 and Y0.  PLSREGRESS initially computes YSCORES as
%
%     YSCORES = Y0*YLOADINGS = Y0*Y0'*XSCORES,
%
%   however, by convention, PLSREGRESS then orthogonalizes each column of
```

```
%   YSCORES with respect to preceding columns of XSCORES, so that
%   XSCORES'*YSCORES is lower triangular.
%
%   [XL,YL,XS,YS,BETA] = PLSREGRESS(X,Y,NCOMP,...) returns the PLS regression
%   coefficients BETA.  BETA is a (P+1)-by-M matrix, containing intercept
%   terms in the first row, i.e., Y = [ONES(N,1) X]*BETA + Yresiduals, and
%   Y0 = X0*BETA(2:END,:) + Yresiduals.
%
%   [XL,YL,XS,YS,BETA,PCTVAR] = PLSREGRESS(X,Y,NCOMP) returns a 2-by-NCOMP
%   matrix PCTVAR containing the percentage of variance explained by the
%   model.  The first row of PCTVAR contains the percentage of variance
%   explained in X by each PLS component and the second row contains the
%   percentage of variance explained in Y.
%
%   [XL,YL,XS,YS,BETA,PCTVAR,MSE] = PLSREGRESS(X,Y,NCOMP) returns a
%   2-by-(NCOMP+1) matrix MSE containing estimated mean squared errors for
%   PLS models with 0:NCOMP components.  The first row of MSE contains mean
%   squared errors for the predictor variables in X and the second row
%   contains mean squared errors for the response variable(s) in Y.
%
%   [XL,YL,XS,YS,BETA,PCTVAR,MSE] = PLSREGRESS(...,'PARAM1',val1,...) allows
%   you to specify optional parameter name/value pairs to control the
%   calculation of MSE.  Parameters are:
%
%     'CV'      The method used to compute MSE.  When 'CV' is a positive
%               integer K, PLSREGRESS uses K-fold cross-validation.  Set
%               'CV' to a cross-validation partition, created using
%               CVPARTITION, to use other forms of cross-validation.  When
%               'CV' is 'resubstitution', PLSREGRESS uses X and Y both to
%               fit the model and to estimate the mean squared errors,
%               without cross-validation.  The default is 'resubstitution'.
%
%     'MCReps'  A positive integer indicating the number of Monte-Carlo
%               repetitions for cross-validation.  The default value is 1.
%               'MCReps' must be 1 if 'CV' is 'resubstitution'.
%
%     'Options' A structure that specifies options that govern how PLSREGRESS
%               performs cross-validation computations. This argument can be
%               created by a call to STATSET. PLSREGRESS uses the following
%               fields of the structure:
%                  'UseParallel'
%                  'UseSubstreams'
%                  'Streams'
%               For information on these fields see PARALLELSTATS.
%               NOTE: If supplied, 'Streams' must be of length one.
%
%
%   [XL,YL,XS,YS,BETA,PCTVAR,MSE,STATS] = PLSREGRESS(X,Y,NCOMP,...) returns a
%   structure that contains the following fields:
%      W           P-by-NCOMP matrix of PLS weights, i.e., XSCORES = X0*W
%      T2          The T^2 statistic for each point in XSCORES
%      Xresiduals  The predictor residuals, i.e. X0 - XSCORES*XLOADINGS'
%      Yresiduals  The response residuals, i.e. Y0 - XSCORES*YLOADINGS'
%
%   Example: Fit a 10 component PLS regression and plot the cross-validation
%   estimate of MSE of prediction for models with up to 10 components.  Plot
```

```
%   the observed vs. the fitted response for the 10-component model.
%
%     load spectra
%     [xl,yl,xs,ys,beta,pctvar,mse] = plsregress(NIR,octane,10,'CV',10);
%     plot(0:10,mse(2,:),'-o');
%     octaneFitted = [ones(size(NIR,1),1) NIR]*beta;
%     plot(octane,octaneFitted,'o');
%
%   See also PCA, BIPLOT, CANONCORR, FACTORAN, CVPARTITION, STATSET,
%            PARALLELSTATS, RANDSTREAM.

% References:
%    [1] de Jong, S. (1993) "SIMPLS: an alternative approach to partial least squares
%        regression", Chemometrics and Intelligent Laboratory Systems, 18:251-263.
%    [2] Rosipal, R. and N. Kramer (2006) "Overview and Recent Advances in Partial
%        Least Squares", in Subspace, Latent Structure and Feature Selection:
%        Statistical and Optimization Perspectives Workshop (SLSFS 2005),
%        Revised Selected Papers (Lecture Notes in Computer Science 3940), C.
%        Saunders et al. (Eds.) pp. 34-51, Springer.

%   Copyright 2007-2010 The MathWorks, Inc.


if nargin < 2
   error(message('stats:plsregress:TooFewInputs'));
end

[n,dx] = size(X);
ny = size(Y,1);
if ny ~= n
   error(message('stats:plsregress:SizeMismatch'));
end

% Return at most maxncomp PLS components
maxncomp = min(n-1,dx);
if nargin < 3
   ncomp = maxncomp;
elseif ~isscalar(ncomp) || ~isnumeric(ncomp) || (ncomp~=round(ncomp)) || (ncomp<=0)
   error(message('stats:plsregress:BadNcomp'));
elseif ncomp > maxncomp
   error(message('stats:plsregress:MaxComponents', maxncomp));
end

names = {'cv'              'mcreps'          'options'};
dflts = {'resubstitution'      1                 []   };
[cvp,mcreps,ParOptions] = internal.stats.parseArgs(names, dflts, varargin{:});

if isnumeric(cvp) && isscalar(cvp) && (cvp==round(cvp)) && (0<cvp) && (cvp<=n)
   % ok, cvp is a kfold value. It will be passed as such to crossval.
elseif isequal(cvp,'resubstitution')
   % ok
elseif isa(cvp,'cvpartition')
   if strcmp(cvp.Type,'resubstitution')
      cvp = 'resubstitution';
```

```
    else
        % ok
    end
else
    error(message('stats:plsregress:InvalidCV'));
end

if ~(isnumeric(mcreps) && isscalar(mcreps) && (mcreps==round(mcreps)) && (0<mcreps))
    error(message('stats:plsregress:InvalidMCReps'));
elseif mcreps > 1 && isequal(cvp,'resubstitution')
    error(message('stats:plsregress:InvalidResubMCReps'));
end

% Center both predictors and response, and do PLS
meanX = mean(X,1);
meanY = mean(Y,1);
X0 = bsxfun(@minus, X, meanX);
Y0 = bsxfun(@minus, Y, meanY);

if nargout <= 2
    [Xloadings,Yloadings] = simpls(X0,Y0,ncomp);

elseif nargout <= 4
    [Xloadings,Yloadings,Xscores,Yscores] = simpls(X0,Y0,ncomp);

else
    % Compute the regression coefs, including intercept(s)
    [Xloadings,Yloadings,Xscores,Yscores,Weights] = simpls(X0,Y0,ncomp);
    beta = Weights*Yloadings';
    beta = [meanY - meanX*beta; beta];

    % Compute the percent of variance explained for X and Y
    if nargout > 5
        pctVar = [sum(abs(Xloadings).^2,1) ./ sum(sum(abs(X0).^2,1));
                  sum(abs(Yloadings).^2,1) ./ sum(sum(abs(Y0).^2,1))];
    end

    if nargout > 6
        if isequal(cvp,'resubstitution')
            % Compute MSE for models with 0:ncomp PLS components, by
            % resubstitution.  CROSSVAL can handle this, but don't waste time
            % fitting the whole model again.
            mse = zeros(2,ncomp+1,class(pctVar));
            mse(1,1) = sum(sum(abs(X0).^2, 2));
            mse(2,1) = sum(sum(abs(Y0).^2, 2));
            for i = 1:ncomp
                X0reconstructed = Xscores(:,1:i) * Xloadings(:,1:i)';
                Y0reconstructed = Xscores(:,1:i) * Yloadings(:,1:i)';
                mse(1,i+1) = sum(sum(abs(X0 - X0reconstructed).^2, 2));
                mse(2,i+1) = sum(sum(abs(Y0 - Y0reconstructed).^2, 2));
            end
            mse = mse / n;
            % We now have the reconstructed values for the full model to use in
            % the residual calculation below
```

```
        else
            % Compute MSE for models with 0:ncomp PLS components, by cross-validation
            mse = plscv(X,Y,ncomp,cvp,mcreps,ParOptions);
            if nargout > 7
                % Need these for the residual calculation below
                X0reconstructed = Xscores*Xloadings';
                Y0reconstructed = Xscores*Yloadings';
            end
        end
    end

    if nargout > 7
        % Save the PLS weights and compute the T^2 values.
        stats.W = Weights;
        stats.T2 = sum( bsxfun(@rdivide, abs(Xscores).^2, var(Xscores,[],1)) , 2);

        % Compute X and Y residuals
        stats.Xresiduals = X0 - X0reconstructed;
        stats.Yresiduals = Y0 - Y0reconstructed;
    end
end



%-----------------------------------------------------------------------------
%SIMPLS Basic SIMPLS.  Performs no error checking.
function [Xloadings,Yloadings,Xscores,Yscores,Weights] = simpls(X0,Y0,ncomp)

[n,dx] = size(X0);
dy = size(Y0,2);

% Preallocate outputs
outClass = superiorfloat(X0,Y0);
Xloadings = zeros(dx,ncomp,outClass);
Yloadings = zeros(dy,ncomp,outClass);
if nargout > 2
    Xscores = zeros(n,ncomp,outClass);
    Yscores = zeros(n,ncomp,outClass);
    if nargout > 4
        Weights = zeros(dx,ncomp,outClass);
    end
end

% An orthonormal basis for the span of the X loadings, to make the successive
% deflation X0'*Y0 simple - each new basis vector can be removed from Cov
% separately.
V = zeros(dx,ncomp);

Cov = X0'*Y0;
for i = 1:ncomp
    % Find unit length ti=X0*ri and ui=Y0*ci whose covariance, ri'*X0'*Y0*ci, is
    % jointly maximized, subject to ti'*tj=0 for j=1:(i-1).
    [ri,si,ci] = svd(Cov,'econ'); ri = ri(:,1); ci = ci(:,1); si = si(1);
    ti = X0*ri;
    normti = norm(ti); ti = ti ./ normti; % ti'*ti == 1
```

```
    Xloadings(:,i) = X0'*ti;

    qi = si*ci/normti; % = Y0'*ti
    Yloadings(:,i) = qi;

    if nargout > 2
        Xscores(:,i) = ti;
        Yscores(:,i) = Y0*qi; % = Y0*(Y0'*ti), and proportional to Y0*ci
        if nargout > 4
            Weights(:,i) = ri ./ normti; % rescaled to make ri'*X0'*X0*ri == ti'*ti == 1
        end
    end

    % Update the orthonormal basis with modified Gram Schmidt (more stable),
    % repeated twice (ditto).
    vi = Xloadings(:,i);
    for repeat = 1:2
        for j = 1:i-1
            vj = V(:,j);
            vi = vi - (vj'*vi)*vj;
        end
    end
    vi = vi ./ norm(vi);
    V(:,i) = vi;

    % Deflate Cov, i.e. project onto the ortho-complement of the X loadings.
    % First remove projections along the current basis vector, then remove any
    % component along previous basis vectors that's crept in as noise from
    % previous deflations.
    Cov = Cov - vi*(vi'*Cov);
    Vi = V(:,1:i);
    Cov = Cov - Vi*(Vi'*Cov);
end

if nargout > 2
    % By convention, orthogonalize the Y scores w.r.t. the preceding Xscores,
    % i.e. XSCORES'*YSCORES will be lower triangular.  This gives, in effect, only
    % the "new" contribution to the Y scores for each PLS component.  It is also
    % consistent with the PLS-1/PLS-2 algorithms, where the Y scores are computed
    % as linear combinations of a successively-deflated Y0.  Use modified
    % Gram-Schmidt, repeated twice.
    for i = 1:ncomp
        ui = Yscores(:,i);
        for repeat = 1:2
            for j = 1:i-1
                tj = Xscores(:,j);
                ui = ui - (tj'*ui)*tj;
            end
        end
        Yscores(:,i) = ui;
    end
end
```

```
%-------------------------------------------------------------------------
%PLSCV Efficient cross-validation for X and Y mean squared error in PLS.
function mse = plscv(X,Y,ncomp,cvp,mcreps,ParOptions)

[n,dx] = size(X);

% Return error for as many components as asked for; some columns may be NaN
% if ncomp is too large for CV.
mse = NaN(2,ncomp+1);

% The CV training sets are smaller than the full data; may not be able to fit as
% many PLS components.  Do the best we can.
if isa(cvp,'cvpartition')
   cvpType = 'partition';
   maxncomp = min(min(cvp.TrainSize)-1,dx);
   nTest = sum(cvp.TestSize);
else
   cvpType = 'Kfold';
%    maxncomp = min(min( floor((n*(cvp-1)/cvp)-1), dx));
   maxncomp = min( floor((n*(cvp-1)/cvp)-1), dx);
   nTest = n;
end
if ncomp > maxncomp
   warning(message('stats:plsregress:MaxComponentsCV', maxncomp));
   ncomp = maxncomp;
end

% Cross-validate sum of squared errors for models with 1:ncomp components,
% simultaneously.  Sum the SSEs over CV sets, and compute the mean squared
% error
CVfun = @(Xtr,Ytr,Xtst,Ytst) sseCV(Xtr,Ytr,Xtst,Ytst,ncomp);
sumsqerr = crossval(CVfun,X,Y,cvpType,cvp,'mcreps',mcreps,'options',ParOptions);
mse(:,1:ncomp+1) = reshape(sum(sumsqerr,1)/(nTest*mcreps), [2,ncomp+1]);



%-------------------------------------------------------------------------
%SSECV Sum of squared errors for cross-validation
function sumsqerr = sseCV(Xtrain,Ytrain,Xtest,Ytest,ncomp)

XmeanTrain = mean(Xtrain);
YmeanTrain = mean(Ytrain);
X0train = bsxfun(@minus, Xtrain, XmeanTrain);
Y0train = bsxfun(@minus, Ytrain, YmeanTrain);

% Get and center the test data
X0test = bsxfun(@minus, Xtest, XmeanTrain);
Y0test = bsxfun(@minus, Ytest, YmeanTrain);

% Fit the full model, models with 1:(ncomp-1) components are nested within
[Xloadings,Yloadings,~,~,Weights] = simpls(X0train,Y0train,ncomp);
XscoresTest = X0test * Weights;

% Return error for as many components as the asked for.
outClass = superiorfloat(Xtrain,Ytrain);
```

```
sumsqerr = zeros(2,ncomp+1,outClass); % this will get reshaped to a row by CROSSVAL

% Sum of squared errors for the null model
sumsqerr(1,1) = sum(sum(abs(X0test).^2, 2));
sumsqerr(2,1) = sum(sum(abs(Y0test).^2, 2));

% Compute sum of squared errors for models with 1:ncomp components
for i = 1:ncomp
   X0reconstructed = XscoresTest(:,1:i) * Xloadings(:,1:i)';
   sumsqerr(1,i+1) = sum(sum(abs(X0test - X0reconstructed).^2, 2));

   Y0reconstructed = XscoresTest(:,1:i) * Yloadings(:,1:i)';
   sumsqerr(2,i+1) = sum(sum(abs(Y0test - Y0reconstructed).^2, 2));
end
```

Simpls algorithm example:

For sake of demonstration a simple example is provided. The input matrices X and Y are shown below. The matrices are composed of 9 rows and 2 columns each. The X and Y matrix must have the same number of rows, indicating a matching number of independent data sets in X and number of dependent sets in Y. The number of columns does not need to be identical; each column in X corresponds to a particular measured quantity, while each column in Y corresponds to a particular dependent trait or value.

| **Example X** | |
|---|---|
| 195 | 45 |
| 185 | 30 |
| 156 | 90 |
| 181 | 45 |
| 164 | 30 |
| 158 | 0 |
| 185 | 15 |
| 186 | 105 |
| 187 | 45 |

| Example Y | |
|---|---|
| 95 | 44 |
| 73 | 43 |
| 63 | 36 |
| 80 | 45 |
| 70 | 40 |
| 55 | 38 |
| 89 | 44 |
| 78 | 45 |
| 91 | 43 |

Prior to running the simpls algorithm, the variance must be determined for each feature or trait. This is done by simply determining the average of the values in each separate column for both X and Y and subtracting this value from each number in the corresponding column. In the example, the averages of the values in the first and second column of X are 177.44 and 45.00, respectively, while the averages of the values in the first and second columns of Y are 77.11 and 42.00, respectively. The new matrices are referred to as $X_0$ and $Y_0$. $X_0$ and $Y_0$ for the above example are as below.

| Example $X_0$ | |
|---|---|
| 17.56 | 0 |
| 7.56 | -15.00 |
| -21.44 | 45.00 |
| 3.56 | 0 |
| -13.44 | -15.00 |
| -19.44 | -45.00 |
| 7.56 | -30.00 |
| 8.56 | 60.00 |
| 9.56 | 0 |

| Example $Y_0$ | |
|---|---|
| 17.89 | 2.00 |
| -4.11 | 1.00 |
| -14.11 | -6.00 |
| 2.89 | 3.00 |
| -7.11 | -2.00 |
| -22.11 | -4.00 |
| 11.89 | 2.00 |
| 0.89 | 3.00 |
| 13.89 | 1.00 |

The major purpose of this procedure is to decompose the X and Y matrices into the products of two matrices each; the scores and loadings matrices, plus an error matrix each.

The X loadings matrix will have a number of rows equal to the number of columns in X (in this case 2) and a number of columns equal to the number of PLS components used. This number may be selected based on results of previous models (as long as it is a positive integer) or may use the default maximum number of components allowable, which is the lesser of the number of columns in X or one less than the number of rows in X. For this example, the maximum number of PLS components will be used (2 for this case), although generally one should attempt to use the least PLS components possible which will still explain sufficient variation in known data. The Y loadings matrix will have a number of rows equal to the number of columns in Y (2) and a number of columns equal to the number of PLS components to be used (2).

The X and Y scores matrices will have a number of rows equal to the number of rows in X and Y (9), and a number of columns equal to the number of PLS components to be used (2).

As this procedure is typically done via a computer program or function, it is generally advisable to pre-allocate the size and memory for these matrices in advance.

An orthonormal basis matrix, V, with a number of rows equal to the number of columns in X and a number of columns equal to the number of PLS components to be used throughout this procedure, will be used and space should be pre-allocated. In this case it will be a 2x2 matrix.

A starting Covariance matrix is then determined as the product of the transpose of the $X_0$ matrix and the $Y_0$ matrix. The covariance matrix for the example is shown below. Each orthonormal basis vector used in the procedure below will be removed from the covariance matrix separately.

| **Example Initial Covariance Matrix** | |
|---|---|
| 1351.6 | 337.0 |
| 225.0 | 45.0 |

The following steps are a cyclic process which must be repeated a number of times equal to the number of PLS components to be used. In this case, it is only necessary to go through this process twice.

The following steps will be used to determine two unit vectors, t and u, whose covariance is maximized, while the product of the transpose of the t vector and the vector formed by any previous column in the X scores matrix is 0.

For each cycle, a Single Value Decomposition is applied to the current covariance matrix, decomposing it into three matrices, r, c, and s. The values for each of these matrices for the example and the first cycle are given below.

| **Example r matrix – Cycle 1** |
|---|
| -0.987 |
| -0.162 |

| **Example s matrix – Cycle 1** |
|---|
| 1411.7 |

| **Example c matrix – Cycle 1** |
|---|
| -0.971 |
| -0.241 |

A new matrix, t (which is this cycle's contribution to the X scores matrix), is defined as the product of the $X_0$ matrix and the r matrix from the Single Value Decomposition of the Covariance matrix. The values in this matrix are then normalized to form a unit vector; each value in the vector is divided by the Euclidian distance of the original vector, which is effectively the total length of the vector within n-dimensional space. The normalized t vector is shown below. The column of the X loadings matrix corresponding to the cycle number is defined by the product of the transpose of the $X_0$ matrix and the normalized t vector, as shown below. In this first cycle, the second column has not yet been defined, and values of 0 are entered as placeholders.

| Example normalized t vector – Cycle 1 |
|---|
| -0.397 |
| -0.115 |
| 0.318 |
| -0.080 |
| 0.360 |
| 0.607 |
| -0.059 |
| -0.417 |
| -0.216 |

| Example X loadings – Cycle 1 | |
|---|---|
| -37.65 | 0 |
| -39.93 | 0 |

The corresponding column in the Y loadings matrix is defined by a vector, q, which is defined as the product of the s and c matrices, which is then normalized to the length of the original t vector, as shown below.

| Example Y loadings – Cycle 1 | |
|---|---|
| -31.39 | 0 |
| -7.79 | 0 |

The corresponding column in the X scores matrix is defined by the normalized t vector, and the corresponding column of the Y scores is defined as the product of the $Y_0$ matrix and q vector. The corresponding column in the Weights matrix, which will be used later to determine a predictive model, is defined by dividing the r matrix by the

length of the original t vector to normalize it. Each of these matrices for the first cycle is as shown below.

| **Example X scores – Cycle 1** | |
|---|---|
| -0.397 | 0 |
| -0.115 | 0 |
| 0.318 | 0 |
| -0.080 | 0 |
| 0.360 | 0 |
| 0.607 | 0 |
| -0.059 | 0 |
| -0.417 | 0 |
| -0.216 | 0 |

| **Example Y scores – Cycle 1** | |
|---|---|
| -577.27 | 0 |
| 121.30 | 0 |
| 489.80 | 0 |
| -114.07 | 0 |
| 238.86 | 0 |
| 725.42 | 0 |
| -388.88 | 0 |
| -51.27 | 0 |
| -443.89 | 0 |

| **Example Weights – Cycle 1** | |
|---|---|
| -0.0226 | 0 |
| -0.0037 | 0 |

The orthonormal basis is then revised in response to the previous additions to the above matrices using a modified Gram-Schmidt procedure. A vector, v, is defined containing the entries which were just added to the X loadings matrix, as shown below.

| **Example Initial v – Cycle 1** |
|---|
| -37.65 |
| -39.93 |

The following is then repeated twice:

For a number of times equal to one less than the number of the cycle (for the first cycle, this step is not performed), a new vector is defined as the number of the column of the orthonormal basis (V) matrix corresponding to the sub-loop and repetition of this step. The above initial v vector is then revised by subtracting the product of the transpose of the orthonormal basis vector, the v vector, and the orthonormal basis vector again. This is repeated for the appropriate number of cycles, and this full sub-cycle procedure is repeated a second time for stability.

After the above procedure has been repeated twice, the v vector is then normalized to its Euclidian distance, and this new vector then defines the column of the orthonormal basis matrix, V, corresponding to the cycle number. As the above procedure is not performed for the first cycle, the original v vector above for this example is simply normalized and input as the first column of the orthonormal basis matrix, as shown below.

| Example Normalized v – Cycle 1 |
|---|
| -0.686 |
| -0.728 |

| Orthonormal Basis, V – Cycle 1 | |
|---|---|
| -0.686 | 0 |
| -0.728 | 0 |

Finally, for each cycle, the Covariance matrix is deflated by projecting onto the ortho-complement of the X loadings. Projections from the current cycle are removed first, followed by components along previous basis vectors to reduce effects of noise left behind from previous deflations. To do this, the v vector is multiplied by the product of the transpose of the v vector and the current Covariance matrix, and this resulting matrix is subtracted from the current Covariance matrix. Then, a matrix composed of the first n columns of the orthonormal basis matrix, V, (where n is the number of the cycle) is multiplied by the product of the transpose of this same matrix and the updated Covariance matrix, and this resulting matrix is subtracted from the updated Covariance matrix. The first and second updated Covariance matrices for the first cycle, and the modified orthonormal basis matrix used in calculation are shown below. Note that the effects of noise from previous deflations are negligible, for the first several cycles.

| Covariance Matrix – Updated Once – Cycle 1 | |
|---|---|
| 603.18 | 155.94 |
| -568.72 | -147.03 |

| Modified Orthonormal Basis – Cycle 1 |
|---|
| -0.686 |
| -0.728 |

| Covariance Matrix – Updated Twice – Cycle 1 | |
|---|---|
| 603.18 | 155.94 |
| -568.72 | -147.03 |

The next cycle is then started. As it is only necessary to proceed through this cycle twice for the given example, each of the steps for the second cycle is shown below.

A Single Value Decomposition is performed on the updated Covariance matrix to yield the r, s, and c matrices below.

| Example r matrix – Cycle 2 |
|---|
| -0.728 |
| 0.686 |

| Example s matrix – Cycle 2 |
|---|
| 856.3 |

| Example c matrix – Cycle 2 |
|---|
| -0.968 |
| -0.250 |

The resulting normalized t vector, and the new X and Y loadings matrices are shown below.

| **Example normalized t vector – Cycle 2** |
|---|
| -0.184 |
| -0.228 |
| 0.670 |
| -0.037 |
| -0.0073 |
| -0.241 |
| -0.376 |
| 0.504 |
| -0.100 |

| **Example X loadings – Cycle 2** | |
|---|---|
| -37.65 | -14.16 |
| -39.93 | 86.05 |

| **Example Y loadings – Cycle 2** | |
|---|---|
| -31.39 | -11.96 |
| -7.79 | -3.09 |

The resulting new X and Y scores and Weights matrices are shown below:

| **Example X scores – Cycle 2** | |
|---|---|
| -0.397 | -0.184 |
| -0.115 | -0.228 |
| 0.318 | 0.670 |
| -0.080 | -0.037 |
| 0.360 | -0.0073 |
| 0.607 | -0.241 |
| -0.059 | -0.376 |
| -0.417 | 0.504 |
| -0.216 | -0.100 |

| **Example Y scores – Cycle 2** | |
|---|---|
| -577.27 | -220.06 |
| 121.30 | 46.06 |
| 489.80 | 187.26 |
| -114.07 | -43.81 |
| 238.86 | 91.20 |
| 725.42 | 276.73 |
| -388.88 | -148.33 |
| -51.27 | -19.90 |
| -443.89 | -169.15 |

| **Example Weights – Cycle 2** | |
|---|---|
| -0.0226 | -0.0105 |
| -0.0037 | 0.0099 |

The initial v vector for this cycle is shown below.

| **Example Initial v – Cycle 2** |
|---|
| -14.16 |
| 86.05 |

In the second cycle, the sub-cycle will only be performed once, but as always the other sub-cycle procedure will be performed twice. The orthonormal basis vector will be the same for each case because the sub-cycle is only performed once for the second cycle. The v vector after the first and second revisions is shown below.

| **Example v After First Repetition – Cycle 2** |
|---|
| -50.45 |
| 47.57 |

| **Example v After Second Repetition – Cycle 2** |
|---|
| -50.45 |
| 47.57 |

The normalized v vector for this cycle is shown below:

| **Example Normalized v – Cycle 2** |
|---|
| -0.728 |
| 0.686 |

This results in the final orthonormal basis matrix:

| **Orthonormal Basis, V – Cycle 2** | |
|---|---|
| -0.686 | -0.728 |
| -0.728 | 0.686 |

The Covariance matrix is then deflated for the second cycle. The updated Covariance matrix and the orthonormal basis matrix used in the calculation are shown below. Note the small values in the once updated covariance matrix, which is noise left from the previous deflation.

| **Covariance Matrix – Updated Once – Cycle 2** | |
|---|---|
| 0 | 0 |
| -0.114e-12 | -0.028e-12 |

| Modified Orthonormal Basis – Cycle 2 | |
|---|---|
| -0.686 | -0.728 |
| -0.728 | 0.686 |

| Covariance Matrix – Updated Twice – Cycle 2 | |
|---|---|
| 0 | 0 |
| 0 | 0 |

Finally, the X and Y scores matrices are adjusted such that the Y scores are orthagonalized to the previous X scores, so that the Y scores indicate only the new contribution for each corresponding PLS component. This is performed via another modified Gram-Schmidt procedure.

For a number of cycles equal to the number of number of PLS components being used, a vector, u, is defined by the values in the column of the Y scores matrix corresponding to the PLS component being considered; which is also the cycle number.

The following procedure is then repeated twice for each cycle:

For a number of sub-cycles equal to one less than the number of the cycle (for the first cycle this step is skipped), a matrix equal to the product of the transpose of the vector formed by the nth column of the X scores matrix (where n is the number of the sub-cycle), the u vector, and the vector from X scores for this sub-cycle, is subtracted from the u vector.

The Y scores matrix is then updated such that the column corresponding to the current cycle is changes to the revised u matrix. The above procedure is demonstrated below:

In the first cycle, the u matrix is not changed, so the first column of the Y scores matrix will remain unchanged, as shown below.

| **Initial u vector – Cycle 1** |
|---|
| -577.27 |
| 121.30 |
| 489.80 |
| -114.07 |
| 238.86 |
| 725.42 |
| -388.88 |
| -51.27 |
| -443.89 |

| **Modified Y scores – Cycle 1** | |
|---|---|
| -577.27 | -220.06 |
| 121.30 | 46.06 |
| 489.80 | 187.26 |
| -114.07 | -43.81 |
| 238.86 | 91.20 |
| 725.42 | 276.73 |
| -388.88 | -148.33 |
| -51.27 | -19.90 |
| -443.89 | -169.15 |

In the second cycle however, the u vector and consequently the Y scores matrix is adjusted. The initial u vector is below:

| **Initial u vector – Cycle 2** |
|---|
| -220.06 |
| 46.06 |
| 187.26 |
| -43.81 |
| 91.20 |
| 276.73 |
| -148.33 |
| -19.90 |
| -169.15 |

The vector from the X scores matrix will be the same throughout for the second cycle, and is shown below:

| **X scores vector – Cycle 2** |
|---|
| -0.397 |
| -0.115 |
| 0.318 |
| -0.080 |
| 0.360 |
| 0.607 |
| -0.059 |
| -0.417 |
| -0.216 |

The u vector after the first and second repetitions is shown below:

| **Once Modified u vector – Cycle 2** |
|---|
| -61.48 |
| 92.02 |
| 60.44 |
| -11.69 |
| -52.54 |
| 34.19 |
| -124.67 |
| 146.57 |
| -82.83 |

| **Twice Modified u vector – Cycle 2** |
|---|
| -61.48 |
| 92.02 |
| 60.44 |
| -11.69 |
| -52.54 |
| 34.19 |
| -124.67 |
| 146.57 |
| -82.83 |

The modified Y scores matrix is as shown:

| Modified Y scores – Cycle 2 | |
|---|---|
| -577.27 | -61.48 |
| 121.30 | 92.02 |
| 489.80 | 60.44 |
| -114.07 | -11.69 |
| 238.86 | -52.54 |
| 725.42 | 34.19 |
| -388.88 | -124.67 |
| -51.27 | 146.57 |
| -443.89 | -82.83 |

This procedure yields the final X and Y scores, final X and Y loadings, and Weights matrices. Predictions can be made by multiplying a new X data set by the beta matrix.

The beta matrix is determined by the following procedure:

An initial beta matrix is defined as the product of the Weights matrix and the transpose of the Y loadings matrix, as shown below:

| Beta Matrix | |
|---|---|
| 0.8355 | 0.2085 |
| -0.0015 | -0.0016 |

The beta matrix is then modified to add a row at the top of the matrix describing the intercepts. The intercepts row is calculated by subtracting the product of the vector

formed by the X column averages and the original beta matrix from the vector formed from the Y column averages. The resulting modified beta matrix is as shown:

| **Final Beta Matrix with Intercepts** | |
|---|---|
| -71.07 | 5.09 |
| 0.8355 | 0.2085 |
| -0.0015 | -0.0016 |

Note that to make a prediction using this format for beta, it is necessary to modify an input X vector by adding an additional column on the left side containing a 1 to account for intercepts. For input X values of 160 and 120, the predicted Y values are 62.43 and 38.24. The MatLAB algorithm also includes optional sections which will automatically conduct a cross-validation analysis, if desired.

## Appendix B

## Known Sample Chemical Composition

Below is a summary of XRF results provided by the NJDOT. Note that this list only includes samples used for model calibration. Additional samples and chemical composition results have recently been received and will be incorporated into future models.

| Charge | Tilcon Quarries New York, Inc. | Baer Aggregates |
|---|---|---|
| Formation | Haverstraw, NY | Carpentersville, NJ |
| Stone | trap rock | carbonate |
| Stratigraphic Unit | Jurassic Diabase | Allentown Dolomite |
| $SiO_2$ | 46.9500 | 12.5000 |
| $Al_2O_3$ | 16.4500 | 2.9700 |
| $Fe_2O_3$ | 13.9500 | 2.4200 |
| CaO | 11.4000 | 55.5000 |
| MgO | 3.8050 | 24.0000 |
| $Na_2O$ | 3.4350 | 0.0000 |
| $P_2O_5$ | 1.5300 | 0.8705 |
| $TiO_2$ | 1.3250 | 0.1795 |
| $K_2O$ | 0.7145 | 1.3000 |
| MnO | 0.1950 | 0.0669 |
| BaO | 0.0480 | 0.0548 |
| $SO_3$ | 0.0533 | 0.0408 |
| SrO | 0.0389 | 0.0181 |
| CuO | 0.0307 | 0.0000 |
| $ZrO_2$ | 0.0243 | 0.0099 |
| ZnO | 0.0180 | 0.0000 |
| $Y_2O_3$ | 0.0049 | 0.0000 |
| $Rb_2O$ | 0.0043 | 0.0000 |
| $Ga_2O_3$ | 0.0000 | 0.0000 |
| Cl | 0.0262 | 0.0384 |
| $Cr_2O_3$ | 0.0000 | 0.0000 |
| NiO | 0.0000 | 0.0000 |
| $CeO_2$ | 0.0000 | 0.0000 |
| $Nb_2O_5$ | 0.0000 | 0.0000 |
| $Co_3O_4$ | 0.0000 | 0.0000 |
| CdO | 0.0000 | 0.0000 |
| $Ag_2O$ | 0.0000 | 0.0000 |

| Plumstead Materials, Div. of Naceville Mat. | Plumstead Materials, Div. of Naceville Mat. | Plumstead Materials, Div. of Naceville Mat. | Hanson Aggregates |
|---|---|---|---|
| Plumstead Twp., PA | Plumstead Twp., PA | Plumstead Twp., PA | Glen Mills, PA |
| Argillite (1) | Argillite (2) | Argillite (3) | gneiss |
| Lockatong Formation | Lockatong Formation | Lockatong Formation | Precambrian gabbroic gneiss |
| 50.1000 | 49.7500 | 47.2500 | 54.1500 |
| 18.5500 | 16.4000 | 17.6000 | 13.1500 |
| 10.2000 | 12.9500 | 11.9000 | 11.8500 |
| 6.9300 | 6.9550 | 8.3400 | 6.7150 |
| 2.5200 | 2.0550 | 2.9300 | 3.2950 |
| 4.5500 | 3.5850 | 3.9800 | 3.2050 |
| 1.4800 | 1.7950 | 1.5700 | 2.1850 |
| 1.1650 | 1.3450 | 1.1700 | 1.9000 |
| 3.6450 | 4.0150 | 4.1700 | 2.2150 |
| 0.1860 | 0.2345 | 0.2195 | 0.1780 |
| 0.1195 | 0.2235 | 0.1830 | 0.1565 |
| 0.3090 | 0.4225 | 0.4395 | 0.7265 |
| 0.0464 | 0.0702 | 0.0719 | 0.0542 |
| 0.0000 | 0.0000 | 0.0000 | 0.0097 |
| 0.0401 | 0.0635 | 0.0367 | 0.0752 |
| 0.0257 | 0.0330 | 0.0289 | 0.0305 |
| 0.0127 | 0.0200 | 0.0166 | 0.0150 |
| 0.0242 | 0.0379 | 0.0348 | 0.0057 |
| 0.0032 | 0.0000 | 0.0000 | 0.0000 |
| 0.0415 | 0.0314 | 0.0457 | 0.0685 |
| 0.0000 | 0.0000 | 0.0168 | 0.0000 |
| 0.0000 | 0.0000 | 0.0000 | 0.0000 |
| 0.0335 | 0.0408 | 0.0359 | 0.0000 |
| 0.0020 | 0.0000 | 0.0024 | 0.0000 |
| 0.0000 | 0.0000 | 0.0000 | 0.0000 |
| 0.0000 | 0.0000 | 0.0000 | 0.0000 |
| 0.0000 | 0.0000 | 0.0000 | 0.0000 |

| Lehigh Asphalt Paving & Construction Co. | Atkinson Materials (H&K Group) | Eastern Concrete Materials, Inc. | S.W. Barrick & Sons |
|---|---|---|---|
| Andreas, PA | Paupack Twp., PA | Hamburg,NJ | Woodsboro,MD |
| carbonate | quartzite | gneiss | carbonate |
| Helderburg Formation | Catskill Formation | Quartz-oligocase gneiss | Grove limestone |
| 35.8500 | 64.8000 | 57.5000 | 14.8500 |
| 7.2500 | 15.0500 | 14.7000 | 5.2300 |
| 8.8850 | 9.3900 | 8.3400 | 3.0550 |
| 35.2000 | 1.2100 | 5.7950 | 69.6500 |
| 3.1950 | 1.5750 | 2.9750 | 3.1100 |
| 0.7750 | 0.7560 | 4.1150 | 0.0000 |
| 1.2700 | 1.6400 | 1.9000 | 0.9320 |
| 1.4100 | 0.5450 | 1.2500 | 0.5775 |
| 3.9650 | 3.7900 | 2.8600 | 1.8650 |
| 0.1240 | 0.2450 | 0.0923 | 0.0000 |
| 0.1148 | 0.1023 | 0.1160 | 0.0731 |
| 1.6000 | 0.0984 | 0.1320 | 0.4155 |
| 0.1990 | 0.0104 | 0.0729 | 0.1030 |
| 0.0000 | 0.0000 | 0.0249 | 0.0000 |
| 0.0326 | 0.0706 | 0.0358 | 0.0303 |
| 0.0143 | 0.0271 | 0.0084 | 0.0070 |
| 0.0137 | 0.0111 | 0.0111 | 0.0000 |
| 0.0291 | 0.0205 | 0.0193 | 0.0117 |
| 0.0000 | 0.0000 | 0.0000 | 0.0000 |
| 0.0420 | 0.0000 | 0.0855 | 0.0535 |
| 0.0000 | 0.0000 | 0.0000 | 0.0000 |
| 0.0000 | 0.0000 | 0.0000 | 0.0000 |
| 0.0000 | 0.0000 | 0.0000 | 0.0000 |
| 0.0000 | 0.0023 | 0.0038 | 0.0000 |
| 0.0000 | 0.0000 | 0.0000 | 0.0000 |
| 0.0000 | 0.0000 | 0.0000 | 0.0000 |
| 0.0000 | 0.0000 | 0.0000 | 0.0000 |